CDF/ANAL/EXOTIC/CDFR/9136
Version 4.0
January 24, 2008

Search for the Standard Model Higgs Boson Production in Association with $W^{\pm}$ Boson using $\int \mathcal{L}dt$ = 1.9 fb^{-1}

Jay Dittmann[1], Pedro Fernandez[7], Martin Frank[1], Richard Hughes[2], Shinhong Kim[6], Nils Krumnack[1], Kevin Lannon[2], Tatsuya Masubuchi[6], Yoshikazu Nagai[6], Jason Nielsen[5], Thomas Mullar[8], Thomas Peiffer[8], Jason Slaunwhite[2], Anyes Taffard[3], Jeannine Wagner-Kuhr[8], Wolfgang Wagner[8], Brian Winer[2], Weiming Yao[4]

[1]*Baylor University*
[2]*Ohio State University*
[3]*UC Irvine*
[4]*LBNL*
[5]*UC Santa Cruz*
[6]*University of Tsukuba*
[7]*FNAL*
[8]*Karlsruhe*

Abstract

We present a search for Standard Model Higgs boson production in association with a $W^{\pm}$ boson. This search uses data through period 12, corresponding to an integrated luminosity of 1.9fb^{-1}. We select at least one tagged $W+2$ jet events that fall into one of three tag categories: Events with two tight SECVTX tags or events with one tight SECVTX tag plus one jet probability tag or one tight SECVTX tag. Furthermore neural network b-tagging algorithm is applied to one SECVTX tag evens to improve signal-background ratio. Discrimination between the Higgs signal and the large backgrounds in the $W+2$ jet bin is increased through the use of an artificial neural net. We see no evidence for a Higgs signal, so we set a 95% confidence level upper limit on the WH cross section times the branching ratio of the Higgs to decay to a $b\bar{b}$ pair. Using neural network discriminant gives best results

$$\sigma(p\bar{p} \to W^{\pm}H) \times BR(H \to b\bar{b}) < 1.4 \text{ to } 0.9 \text{ pb},$$

for Higgs masses from 110 GeV/c^2 to 150 GeV/c^2

1 Introduction

This note describes the search for $p\bar{p} \rightarrow WH \rightarrow \ell\nu b\bar{b}$ in events that are at least one b-tagged using the SECVTX and jet probability algorithms. The signature for this process is a W-boson decaying semileptonically to a high-p_T electron or muon and two jets containing b-quarks (see Figure 1). This signature is primarily sensitive for low Higgs masses, as shown in Figure 2. The main backgrounds for this process include $W + 2$ jet production (where the jets contain either tagged heavy flavor or mistagged light flavor), $t\bar{t}$ production, and QCD multijet production, where one jet fakes a lepton. These background processes are essentially the same as the backgrounds for the $t\bar{t}$ search in the $W+ \geq 3$ jet bin, although in the case of $t\bar{t}$ the ratio of signal to background is much higher. This search uses data collected up to May 2007, which correspond to a total integrated luminosity of 1.9fb^{-1} .

The previous WH search [1] was performed with integrated luminosity of 1.7fb^{-1} and set an upper limit on the production cross section as shown in Figure 3. These limits ranged from $\sigma(WH) \times BR(H \rightarrow b\bar{b}) < 1.4$ pb for a Higgs mass of 110 GeV/c^2 to 1.1 pb for a Higgs mass of 150 GeV/c^2. For this version of the analysis, we take the following steps to improve the sensitivity:

1. We add one SECVTX tagged category to increase signal acceptance. For the one SECVTX tagged events, neural network flavor separation is applied to decrease background contamination.

2. We improve an artificial neural network (NN) used in previous analysis to increase sensitivity.

We have investigated a number of other improvements, including adding additional acceptance through using PHX electrons and leptons identified as isolated tracks, and increasing the signal discrimination using more complicated multivariate techniques. We expect these improvements to be incorporated in the next update.

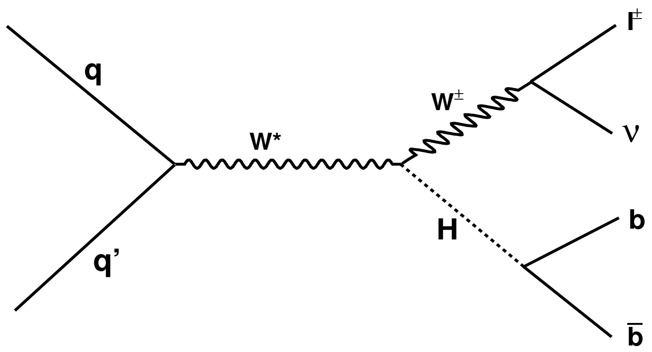

Figure 1: Feynman diagram of WH production.

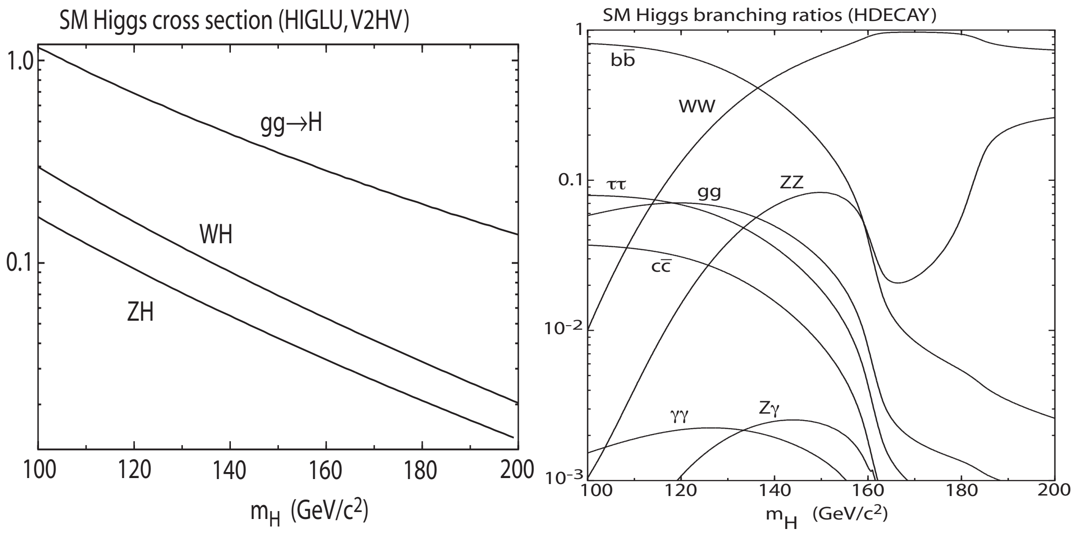

Figure 2: Standard model Higgs boson production cross section at the Tevatron and the branching ratio of Higgs boson.

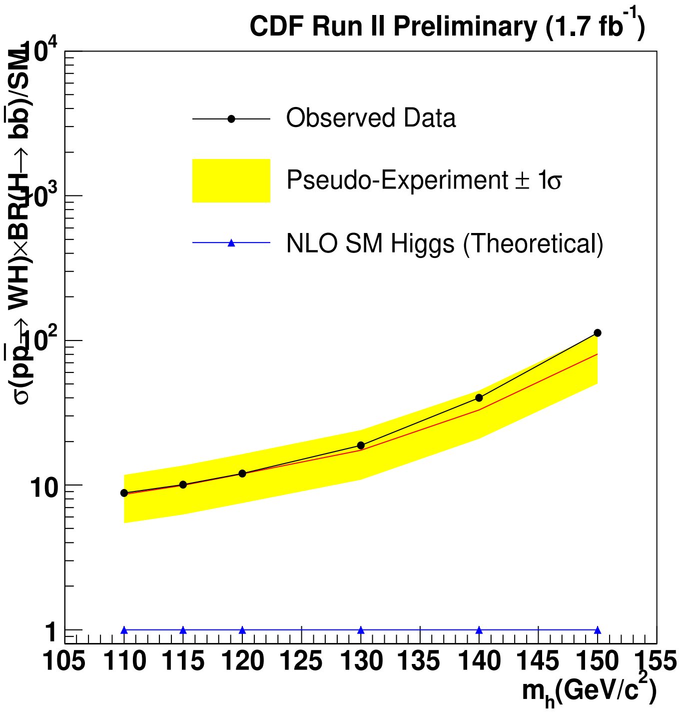

Figure 3: Upper limit on $\sigma(p\bar{p} \to WH) \times BR(H \to b\bar{b})$ obtained with integrated luminosity of 1.7fb^{-1} .

2 Data/MC samples and Luminosity Calculation

The data used for this analysis come from the high p_T electron `bhel0d, bhel0h, bhel0i, bhel0j` and muon `bhmu0d, bhmu0h, bhmu0i, bhmu0j` datasets collected through March 2007. We select events from these datasets that pass the central electron (ELECTRON_CENTRAL_18) and central muon (MUON_CMUP18 and MUON_CMX18) triggers. Due to trigger bandwidth limitations at high luminosity, several versions of the muon trigger: a luminosity-enabled version, which disables the CMX trigger until a certain luminosity is reached, a "JET10" version, which adds an additional jet requirement, and at the highest luminosities, one that combines the luminosity enable and jet requirement. The luminosity lost to the luminosity enabled CMX triggers is accounted for when the sample luminosity is calculated. Luminosities are calculated using the DQM version 18 good run list (bits [1,1,4,1]). The corresponding total integrated luminosity is $1.92\,\mathrm{fb}^{-1}$ for CEM and CMUP leptons, $1.88\,\mathrm{fb}^{-1}$ for CMX muons.

Our Higgs signal model comes from the official Higgs Discovery Group Higgs Monte Carlo (MC) samples generated with PYTHIA using the standard MC procedure outlined in CDF software version 6.1.4. These Higgs samples were generated for a range of Higgs masses (M_h = 110, 115, 120, 130, 140 and 150 GeV). Our background models are composed of a number of components. The W and Z plus light flavor and heavy flavor jet processes are modeled using ALPGEN version 2.10 showered with PYTHIA. Likewise, the single-top contribution is modeled using parton-level events generated by MadEvent and showered through PYTHIA. The rest of the background processes, including the $t\bar{t}$, WW, WZ, and ZZ processes were generated with PYTHIA. For backgrounds involving a top quark, the top mass was set to 175 GeV/c^2.

3 Event Selection

We use the same event selection criteria as in the SECVTX $t\bar{t}$ cross section measurement [2]. We require events to contain an isolated electron or muon with $E_T(p_T) > 20$ GeV as well as $\not\!\!E_T > 20$ GeV, after accounting for the muon and jet energy corrections. Jets are clustered using JETCLU with a cone size of 0.4 and are required to have $E_T > 20$ GeV after level 5 jet corrections (using `jetCorr12` jet energy correction code) and $|\eta_{Detector}| < 2.0$. Currently, we are not using any additional QCD veto, such as the standard cut on the angle between the $\not\!\!E_T$ and the leading jet. The tagged sample is defined by requiring that at least one of the jets has a positive tight SECVTX tag.

3.1 b-tagging strategies

In the previous version of this analysis, we focused double b-tagging events which have double SECVTX tagged events or one SECVTX tag plus one Jet Probablity tagged events. For this version of the analysis, we try to include the single SECVTX tagged events. Because these events still have large signal acceptance. However the background contamination is much worse than double tagged events. Therefore, we apply NN flavor separation [3] for one tagged events. Finally, events used in this search fall into one of three exclusive categories:

SECVTX tight + SECVTX tight (ST+ST): Events in this category are required to have both jets tagged by the tight operating point of SECVTX.

SECVTX tight + Jet Probability (ST+JP): Events in this category are required to have one jet tagged by the tight operating point of SECVTX and one jet to be tagged by the jet probability algorithm. To be tagged, a jet must have a jet probability of less than 5%.

SECVTX tight w/ NN tag: Events in this category are required to have exact one SECVTX tight tagged jet and its jets need to pass NN separator.

Figure 4 shows comparison between the b-tagging categories used in this version of the analysis and the previous version. Almost all tagging events of at least one SECVTX agged events is utilized in this analysis.

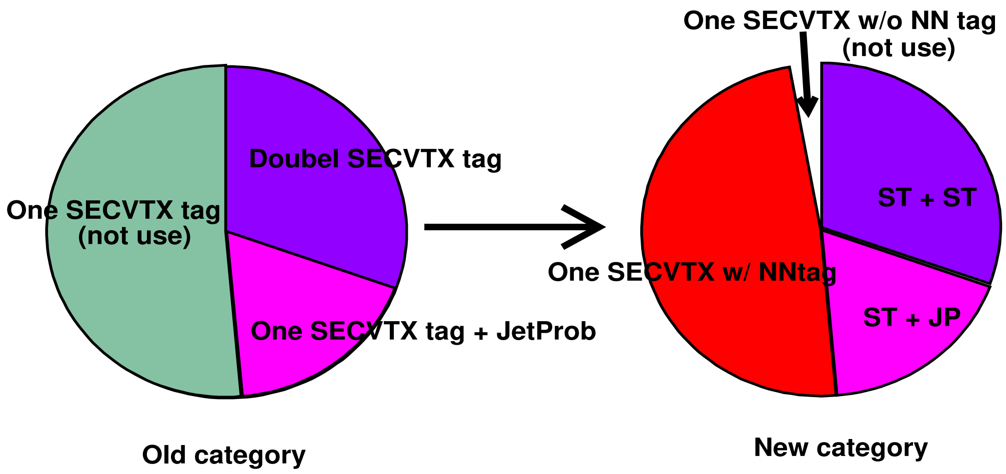

Figure 4: b-tagging category comparison between the current analysis and the previous one. Left plot shows b-tagging category in previous analysis and right plot show b-tagging category in this analysis

4 Background Estimation

In this note, we build on the method of background estimation used in $t\bar{t}$ cross section measurement[2], the so-called "Method 2". In the W+jets sample, the following background sources are considered:

Non-W QCD: A W signature is generated when one jet fakes a high p_T lepton and $\not\!\!E_T$ is generated through jet energy mismeasurement.

W + Mistags: This background occurs when one or more light flavor jets produced in association with a W boson are mistakenly identified as a heavy flavor jet by the b-tagging algorithms. Mistags are generated because of the finite resolution of the tracking, because of material interactions, or because of long-lived light flavor hadrons (Λ and K_s) that produce displaced vertices.

W+ Heavy Flavor: These processes ($W + b\bar{b}$, $W + c\bar{c}$ and $W + c$) involve the production of actual heavy flavor quarks in association with a W boson.

Top Quark Backgrounds: This background comes both from single top quark production and top quark pair production.

Other EWK Backgrounds: Additional small background contributions come from Z + jets production and diboson (WW, WZ, and ZZ) production.

The Non-W background is estimated using the "MET vs ISO" technique described below. The W + Mistag background is estimated from the data by apply a mistag parameterization, also known as the mistag matrix, to the data before tagging (pretag data). The W + Heavy Flavor background is also estimated from the pretag data using the ALPGEN + PYTHIA MC to set the relative normalization of light to heavy flavor events as well as the b-tagging efficiency for W + Heavy Flavor events (see below). The Top Quark and Other EWK backgrounds are normalized directly by their theoretical cross sections, calculated at next-to-leading order. More details can be found in the $t\bar{t}$ cross section documentation [2].

4.1 NonW (QCD fake) background

To estimate the number of events in which QCD jets fakes a lepton, we use the $\not\!\!E_T$ vs Isolation method. We divide the $\not\!\!E_T$ vs isolation plane into the following regions (see Figure 5):

- region A: Isolation > 0.2 and $\not\!\!E_T < 15$ GeV
- region B: Isolation < 0.1 and $\not\!\!E_T < 15$ GeV
- region C: Isolation > 0.2 and $\not\!\!E_T > 20$ GeV
- region D: Isolation $< 0{,}1$ and $\not\!\!E_T > 20$ GeV

Here region D is our signal region. We assume that the lepton isolation is independent of $\not\!\!E_T$, and that the tagging efficiency is the same between Region B and D. Then we define the fraction of events which are the non-W contribution:

$$f_{\text{non}-W} = \frac{N_B \times N_C}{N_A \times N_D}, \tag{1}$$

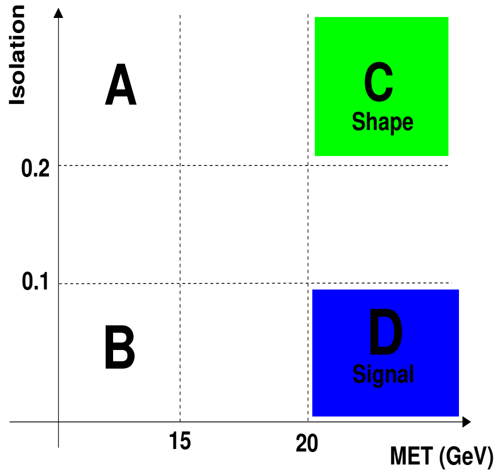

Figure 5: Each region in $\not\!\!E_T$ and L lepton isolation plane

where N_i $(i = A, B, C, D)$ are the number of pretag events in each sideband region. To obtain the non-W background for tagged events, we measure the b-tagging efficiency from region B. For this purpose, we define tagging efficiency as

$$r_B = \frac{N_B^{(\text{tagged events})}}{N_B^{(\text{taggable jets})}}, \tag{2}$$

where $N_B^{(\text{tagged jets})}$ and $N_B^{(\text{taggable jets})}$ are number of taggable and tagged jets in region B respectively. Then we obtain the non-W background in region D with the relation

$$N_D^{(\text{non}-W)} = f_{\text{non}-W} \times r_B \times N_D^{(\text{taggable jets})}. \tag{3}$$

We call this procedure the “Tag Rate Method” since it uses the tag rate in region B. It is also possible to have a estimate directly from the tagged sample, by using

$$N_D^+ = \frac{N_B^+ \times N_C^+}{N_A^+}, \tag{4}$$

where $+$ denotes positive tagged events, and we call this method as “Tagged Method” in this note.

These methods are data-based techniques, so the estimates could also contain other background processes. Subtracting the known backgrounds should result in a better non-W QCD estimate. The contributions from $t\bar{t}$ and W+jets events to each sideband region are estimated and subtracted based on theoretical cross section and ratio to D region. The non-W fractions after the correction are shown in Table 1. Systematic uncertainty of nonW fraction ,25%, are quoted from previous analysis[4],[5] and [1] as there are no reason from previous.

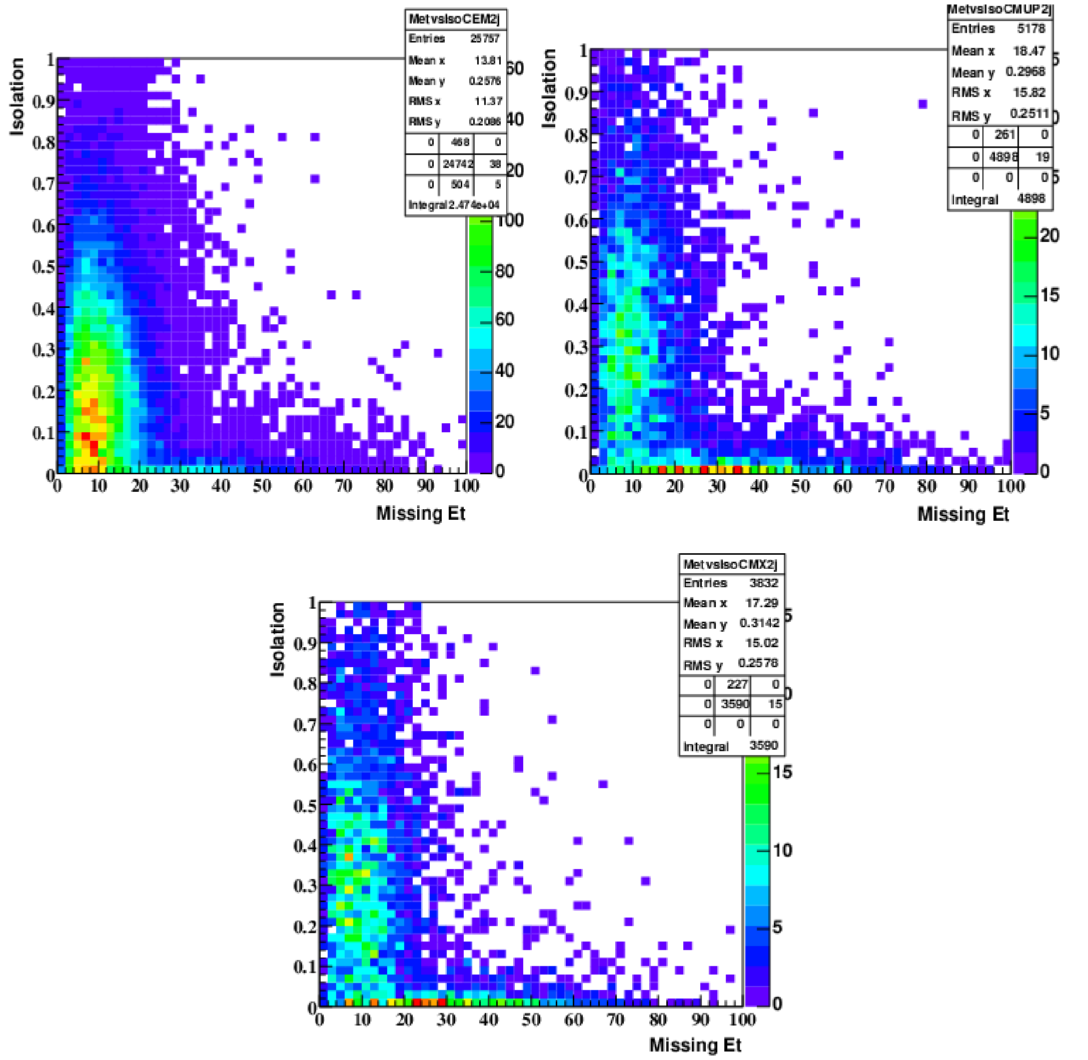

Figure 6: Observed data on $\not\!\!E_T$ vs Iso plane. From left, CEM, CMUP and CMX region. These events has exact 2 tight jets

To combine the estimates from the tag rate and tagged methods, the two sums are combined in a weighted average to get the total non-W backgrounds.

The low statistics of the double-tagged and NN tagged samples prevents us from applying this technique directly. Instead, estimates from the $\geq$ 1-tagged sample are extended into the double-tagged or NN tagged sample using the ratio of at events with at least 1 tag to events with double tag events in region A'(Isolation > 0.1 and $10 < \not\!\!E_T < 20$ GeV), B, and C'(Isolation > 0.1 and $\not\!\!E_T > 20$ GeV).

Njets	1jet	2 jet	>= 3jet
bhel0d	0.209±0.052	0.232±0.059	0.248±0.065
bhmu0d	0.055±0.014	0.071±0.018	0.090±0.025
bhel0h	0.236±0.059	0.251±0.063	0.251±0.065
bhmu0h	0.056±0.014	0.067±0.017	0.058±0.016
bhel0i	0.246±0.062	0.260±0.066	0.215±0.057
bhmu0i	0.054±0.014	0.071±0.018	0.073±0.021
bhelmi (Period 8)	0.257±0.065	0.264±0.067	0.280±0.075
bhmumi (Period 8)	0.054±0.014	0.072±0.019	0.078±0.023
bhelmi2 (Period 9)	0.258±0.065	0.291±0.074	0.256±0.069
bhmumi2 (Period 9)	0.057±0.014	0.065±0.017	0.061±0.019
bhelmi3 (Period 10)	0.275±0.069	0.277±0.070	0.308±0.081
bhmumi3 (Period 10)	0.059±0.015	0.073± 0.019	0.038±0.011
bhel0j (Period 11)	0.287±0.072	0.285± 0.072	0.84±0.075
bhmu0j (Period 11)	0.055±0.014	0.080±0.021	0.068±0.020
bhelmj2 (Period 12)	0.279±0.07	0.287± 0.073	0.285±0.077
bhmumj2 (Period 12)	0.059±0.015	0.075±0.020	0.068±0.021

Table 1: NonW fraction after correction for each dataset and each jet bin. 3 jet and more than 3 jet is merged due to statistical limitation

4.2 W + Heavy flavor

The $Wb\bar{b}$ and $Wc\bar{c}$ states are major sources of background of b-tags in the W+jets channel. They are estimated primarily from the Monte Carlo, but their overall rates are normalized to data. The contribution from true heavy flavor production in W+jet events is determined from measurements of the heavy flavor event fraction in $W+$jet events and the tagging efficiency for those events.

These heavy flavor fractions and a scaling factor for these fractions (k-factor) have been studied extensively elsewhere [2, 6] using ALPGEN v2 + PYTHIA Monte Carlo. Heavy flavor fractions measured in ALPGEN have been calibrated using a jet data sample, and it is found that a k-factor of 1.4 ± 0.4 is necessary to make the heavy flavor production in Monte Carlo match the production in data. Although we can apply most of the numbers from Ref [2] without modification, we need to calculate the tagging efficiency of the ST+JP and one SECVTX tag w/ NNtag categories ourselves. Table 2,3 show the heavy flavor tagging efficiency results for these two categories. The heavy flavor fractions and tagging efficiencies are multiplied by the number of pre-tagged events in data, after the number of pre-tagged events has been corrected for the non-W and other background contribution.

$$N_{W+HF} = f_{HF} \cdot \epsilon_{\mathrm{tag}} \cdot \left[N_{\mathrm{pretag}} \cdot (1 - f_{\mathrm{non}-W}) - N_{\mathrm{EWK}}\right], \tag{5}$$

where f_{HF} is heavy fraction, ϵ_{tag} is tagging efficiency and N_{EWK} is the expected number of $t\bar{t}$ and diboson events.

One SECVTX w/ NN tag	1jet	2 jet	3 jet	>=4 jet
WBB (1B)	27.5±1.49	28.1±1.25	26.7±1.42	26.9± 3.67
WBB (2B)		26.2±1.22	24.1±1.23	22.6±1.31
WCC (1C)	4.17±0.23	4.59±0.25	4.91±0.29	5.23±0.66
WCC (2C)		6.28±0.38	6.56±0.42	6.85±0.64

Table 2: Heavy flavor tagging efficiency calculated from ALPGEN v2 W+jets MC for one SECVTX w/ NNtag category.

SECVTX + Jet Probability(5%)	2 jet	3 jet	>=4 jet
WBB (2B)	10.1±1.2	11.1±1.3	12.4±1.5
WCC (2C)	1.6±0.2	2.3±0.3	3.2±0.4

Table 3: Heavy flavor tagging efficiency calculated from ALPGEN v2 W+jets MC for double b-tagging categories.

4.3 Mistag

The rate of W + mistag, or falsely tagged, jets is derived from a sample of events collected with a jet-based trigger with no heavy flavor requirement. The mistag rate is obtained using negative tags, which are tags that appear to travel back toward the primary vertex. The mistag rate obtained from negative tags is parameterized in bins of η, jet E_T, track multiplicity within a jet, $\sum E_T$ of the event, number of z vertices, and the z vertex position [7]. The mistag rate derived from negative tags is corrected for the effects of heavy flavor in the jet sample, long-lived light flavor vertices, and vertices caused by material interactions in the silicon detector. This correction is parameterized as a function of E_T to reduce its systematic uncertainty [8].

Tag rate probabilities for events with at least one SECVTX tag are obtained by summing over all of the taggable jets in pretag events and exact one tag events. For double tagged events, we apply a similar procedure to events with exactly one tight SECVTX tag, summing tag rate probabilities for all taggable jets except the tagged one. The total mistag normalization is obtained by adding up all the mistag probability event sums for the pretag events. Figure 7 illustrates our mistag background calculation scheme.

The uncertainty on the mistag estimate includes the statistical errors from the matrix itself, accounting for correlations between jets which fall in the same bin of the mistag matrices, and an additional 5.9% error from all systematic uncertainties [7]. Although the mistag matrix was derived using the 1.12fb^{-1} sample, it has been shown that it is acceptable to apply this at least through period 12 data as long as the systematic uncertainties are increased by 1.8% to cover possible discrepancies.

For jet probability, mistag matrix is applied like SECVTX tag. This matrix is parametrized in E_T ,η, ϕ of jet, Number of track, sumE_T , z vertex position.

For NN b-tagging, we apply rejection factor 0.65±0.05 to one SECVTX tagged events estimated in CDF note [3]

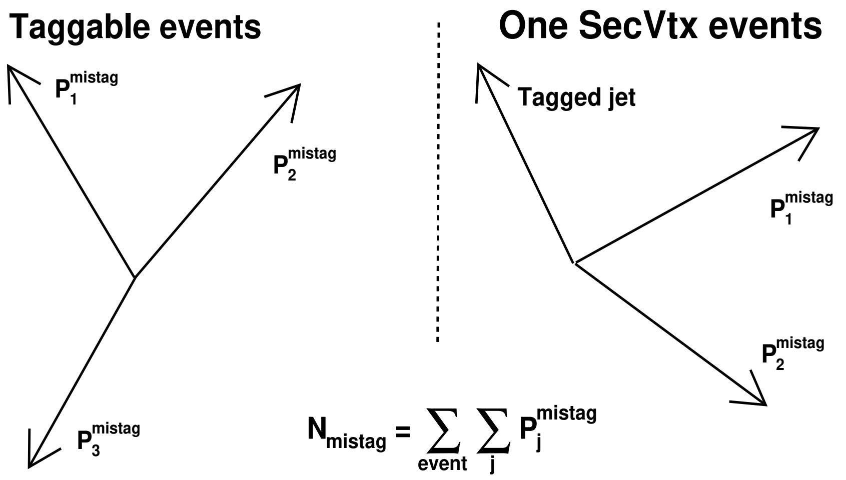

Figure 7: Mistag calculation in each tag

4.4 MC derived background

The normalization of the diboson, $t\bar{t}$ and single top backgrounds are based on the theoretical cross sections (listed in Table 4), the measured luminosity and the acceptance and b-tagging efficiency derived from MC. The MC acceptance is corrected for lepton identification, trigger efficiencies and z vertex cut. The tagging efficiency is always scaled by the MC/data scale factor of 0.95± 0.05 for SECVTX and 0.85±0.07 for jet probability. For NN b-tag, the tagging efficiency is scaled by the factor 0.97±0.02. The expected number of events is obtained by the equation

$$N = \int \mathcal{L}dt \times \epsilon \times \sigma, \tag{6}$$

where ϵ is the total detection efficiency corrected by all of the scale factors.

4.5 Background summary

We have described the contributions of individual background sources to the final background estimate. The summary table of the background estimates are shown in Tables.5-**??** and number of expected events and observed data as a function of jet multiplicity plots are shown in Figure 8-**??**

Theoretical Cross Sections	
WW	12.4 ± 0.25 pb
WZ	3.96 ± 0.06 pb
ZZ	1.58 ± 0.05 pb
Single Top s-channel	0.88 ± 0.11 pb
Single Top t-channel	1.98 ± 0.25 pb
$Z \rightarrow \tau\tau$	265 ± 30.0 pb
$t\bar{t}$	$6.7\ ^{+0.7}_{-0.9}$ pb

Table 4: Theoretical cross sections and errors for the electroweak and single top backgrounds, along with the theoretical cross section for $t\bar{t}$ at ($m_t = 175$GeV/c^2). The cross section of $Z^0 \rightarrow \tau\tau$ is obtained from direct CDF measurement.

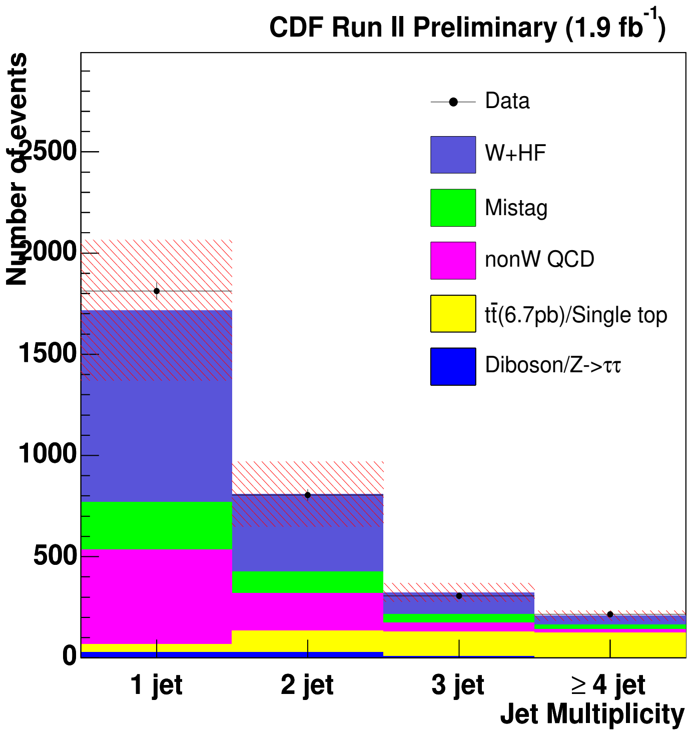

Figure 8: The number of observed one SECVTX tag w/ NN tagged events and background estimation summary as a function of jet multiplicity. Black points show observed events and each color means each estimated background. Red hash means background uncertainties.

Njet	1jet	2jet	3jet	>=4jet
Pretag Events	196160	32242	5496	1494
Mistag	236.7±19.36	107.1±9.38	41.84±3.839	20.97±1.91
$Wb\bar{b}$	431.7±182.4	215.6±92.34	61.78±24.68	26.14±10.43
$Wc\bar{c}$	514.4±154.7	167±62.14	45.4±15.31	17.71±6.86
$t\bar{t}$(6.7pb)	11.85±1.82	60.68±9.30	111±17.03	122.4±18.76
Single top(s-ch)	7.09±1.03	14.38±2.09	3.91±0.57	0.97±0.14
Single top(t-ch)	23.31±3.41	29.57±4.33	6.24±0.91	1.11±0.16
WW	7.21±0.89	15.45±1.91	4.61±0.57	1.03±0.13
WZ	5.52±0.59	7.59±0.81	1.76±0.19	0.48±0.05
ZZ	0.17±0.02	0.31±0.03	0.14±0.01	0.07±0.01
$Z->\tau\tau$	14.58±2.25	7.27±1.12	2.39±0.37	0.71±0.11
nonW QCD	465±83.21	184.7±33.04	44.83±8.57	17.03±3.67
Total Bkg	1717.6±347.89	809.61±159.38	323.92±45.45	208.57±26.24
WH signal (120 GeV)	Control region	1.82±0.15	Control region	Control region
Observed Events	1812	805	306	215

Table 5: Background summary table for one tag w/ NNtag category

Njet	2jet	3jet	>=4jet
Pretag Events	32242	5496	1494
Mistag	3.88±0.35	2.41±0.24	1.62± 0.14
$Wb\bar{b}$	37.93±16.92	14.05±5.49	7.39± 2.93
$Wc\bar{c}$	2.88±1.25	1.52±0.61	1.15± 0.47
$t\bar{t}$(6.7pb)	19.05±2.92	54.67±8.38	94.93± 14.56
Single top(s-ch)	6.90±1.00	2.28±0.33	0.61± 0.088
Single top(t-ch)	1.60±0.23	1.43±0.21	0.50± 0.07
WW	0.17±0.02	0.15±0.02	0.16± 0.02
WZ	2.41±0.26	0.68±0.07	0.16± 0.02
ZZ	0.06±0.01	0.06±0.01	0.02±0.001
$Z->\tau\tau$	0.25±0.04	0.19±0.03	0.06±0.01
nonW QCD	5.50±1.00	2.56±0.48	1.02± 0.22
Total Bkg	80.62±18.75	79.99±10.92	107.63± 15.15
WH signal (120 GeV)	0.94±0.11	Control region	Control region
Observed Events	83	88	118

Table 6: Background summary table for double SECVTX tag category

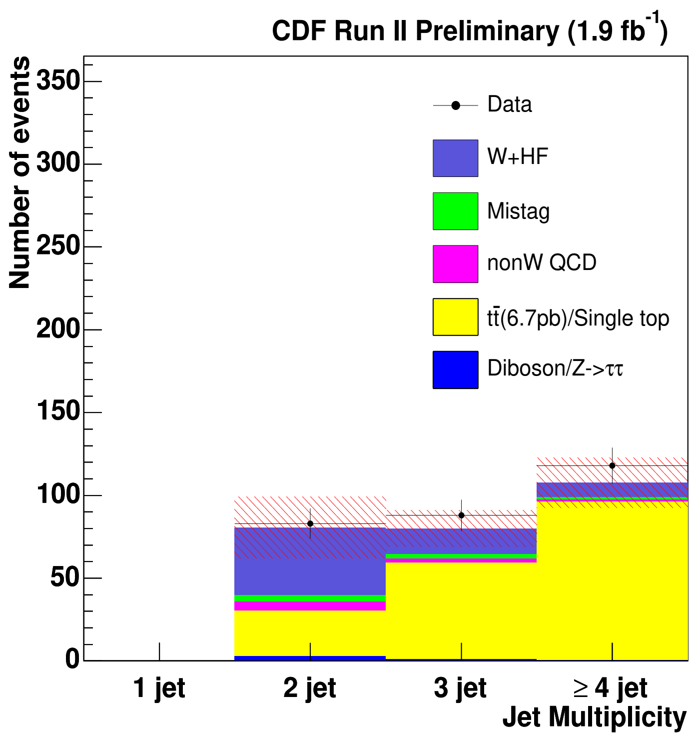

Figure 9: The number of observed double SECVTX tagged events and background estimation summary as a function of jet multiplicity. Black points show observed events and each color means each estimated background. Red hash means background uncertainties.

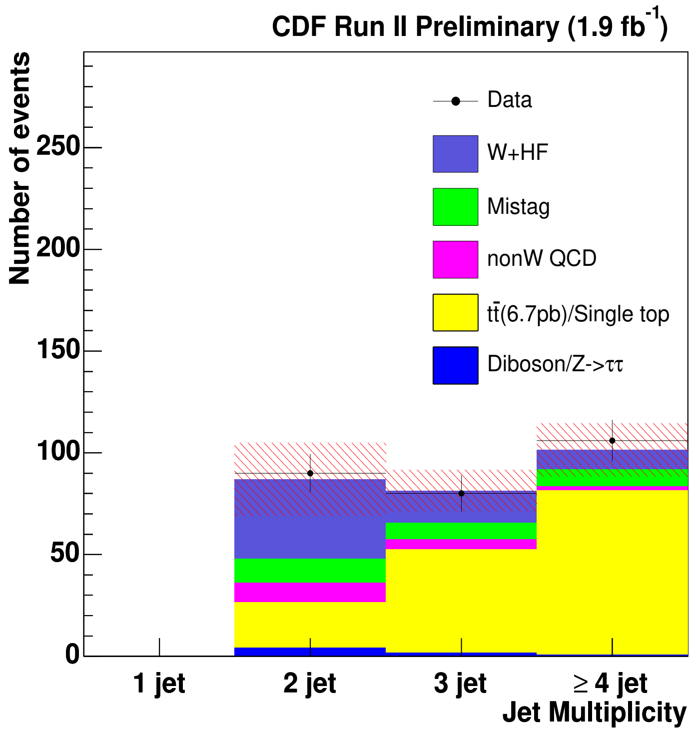

Figure 10: The number of observed one SECVTX and one Jet probability tagged events and background estimation summary as a function of jet multiplicity. Black points show observed events and each color means each estimated background. Red hash means background uncertainties.

Njet	2jet	3jet	>=4jet
Pretag Events	32242	5496	1494
Mistag	11.73±0.92	8.11±0.64	8.39±0.58
$Wb\bar{b}$	31.15±14.03	11.47±4.55	6.55±2.63
$Wc\bar{c}$	7.87±3.43	4.38±1.76	3.09±1.27
$t\bar{t}$(6.7pb)	15.56±2.39	47.48±7.28	79.81±12.24
Single top(s-ch)	5.14±0.75	1.90±0.27	0.53±0.07
Single top(t-ch)	1.87±0.27	1.49±0.22	0.44±0.06
WW	0.93±0.11	0.63±0.08	0.47±0.06
WZ	1.84±0.20	0.59±0.06	0.19±0.02
ZZ	0.08±0.01	0.04±0.003	0.02±0.002
$Z- > \tau\tau$	1.29±0.20	0.53±0.08	0.20±0.03
nonW QCD	9.55±1.73	4.87±0.93	1.80±0.40
Total Bkg	86.99±17.99	81.46±10.22	101.49±13.08
WH signal (120 GeV)	0.74±0.09	Control region	Control region
Observed Events	90	80	106

Table 7: Background summary table for one SECVTX tag + Jet Probability tag category

5 Higgs Signal Acceptance

5.1 Introduction

To calculate the expected number of signal $N_{WH\to l\nu b\bar{b}}$, the following equation is used:

$$N_{WH\to l\nu b\bar{b}} = \epsilon_{WH\to l\nu b\bar{b}} \cdot \mathcal{L} \cdot \sigma(p\bar{p} \to WH) \cdot Br(H \to b\bar{b}), \tag{7}$$

where, $\epsilon_{H\to l\nu b\bar{b}}$ is detection efficiency for signal, $\mathcal{L}$ is the integrated luminosity, $\sigma(p\bar{p} \to WH)$ is WH production cross section in proton antiproton collisions and $BR(H \to b\bar{b})$ is branching ratio for Higgs decaying to $b\bar{b}$. The detection efficiency for signal events is defined as:

$$\epsilon_{WH\to l\nu b\bar{b}} = \epsilon_{Z0} \cdot \epsilon_{trig} \cdot \epsilon_{leptonid} \cdot \epsilon^{MC}_{WH\to l\nu b\bar{b}} \cdot \left(\sum_{l'=e,\mu,\tau} BR(W \to l'\nu) \right), \tag{8}$$

where $\epsilon^{MC}_{WH\to l\nu b\bar{b}}$ is the fraction of signal events (with $|z_0| < 60$cm) which pass the kinematic and b-tagging requirements. The effect of the b-tagging scale factor in this fraction is included by randomly selecting tagged jets to discard. The quantity ϵ_{Z0} is efficiency of the $|z_0| < 60$ cm cut, and is measured in data. The trigger efficiencies for high p_T leptons, ϵ_{trig}, are also measured in data using back-up triggers with looser requirements [12, 14]. The lepton id and reconstruction efficiencies measured in Monte Carlo are corrected by scale factors, $\epsilon_{leptonid}$ derived from data [13, 14]. Finally, $Br(W \to l'\nu)$ is the branching ratio for leptonic (e, μ) W decay. Each of these factors and their systematic errors are treated separately for each data period and the results are combined weighted by the luminosity of each data period. For the later data periods, where numbers may not have been finalized, preliminary results have been taken from the slides of talks given in the Joint Physics meeting [15].

Samples of PYTHIA $WH \to l'\nu b\bar{b}$ Monte Carlo with Higgs boson masses of m_H = 110, 115, 120, 130, 140 and 150 GeV/c^2 are used to estimate $\epsilon^{MC}_{WH\to l\nu b\bar{b}}$. The run range of these MC samples covers up to period 8 run range, and we estimate the signal expectations for each period independently due to the different acceptances. As we don't have MC samples corresponding to period 9 or later, we assume that periods 9-12 acceptance is same as period 8 and scale up the contribution from period 8 to account for the luminosities in periods 9-12.

Finally, we combine the numbers from each run period, weighted by the appropriate luminosity, to obtain our final acceptance number. Figure 11 show the overall acceptance for each b-tagging condition including all systematic effects as a function of Higgs mass. The acceptance increases linearly from 0.91±0.05% to 1.01±0.06% as a function of Higgs mass for one SECVTX tight tag w/ NN tag. The acceptances for tight SECVTX double-tagged selection are from 0.42±0.04% to 0.51±0.05%. For the tight SECVTX tag + jet probability category, the acceptance are from 0.36±0.04% to 0.43±0.05%, even though these categories are exclusive sample to double SECVTX tag category. Table 9 shows the acceptance for a number of Higgs masses for the various tagging categories. Systematic uncertainties are discussed in detail in the following subsection.

The expected number of WH signal events is estimated from the calculated acceptance at each mass. The expectation for each event selection is shown in Tables 10. In these tables

	110 GeV	115 GeV	120 GeV	130 GeV	140 GeV	150 GeV
Cross section (pb)	0.21	0.18	0.15	0.12	0.09	0.07
Branching ratio (%)	0.77	0.73	0.68	0.52	0.34	0.17

Table 8: The production cross section and branching ratio for each mass points

	Acceptance (%)					
b-tagging category	110 GeV	115 GeV	120 GeV	130 GeV	140 GeV	150 GeV
Pretag	3.04±0.08	3.15±0.08	3.25±0.08	3.34±0.08	3.45±0.09	3.48±0.09
At least one tag	1.8±0.09	1.86±0.09	1.91±0.09	2.01±0.10	2.08±0.10	2.1±0.10
One tag w/o NNtag	1.02±0.03	1.05±0.03	1.05±0.03	1.08±0.04	1.14±0.04	1.16±0.04
One tag w/ NNtag	0.91±0.05	0.93±0.05	0.93±0.05	0.97±0.05	1.01±0.06	1.01±0.06
ST + ST	0.42±0.04	0.44±0.05	0.48±0.05	0.51±0.05	0.51±0.05	0.51±0.05
ST + JP	0.36±0.04	0.38±0.04	0.38±0.04	0.42±0.04	0.43±0.05	0.43±0.05

Table 9: WH signal acceptance table in W+2jet events for each tag category and each mass samples. Systematic error is included in uncertainties. Each tagging category is exclusive to other categories

	Expected Higgs events					
b-tagging category	110 GeV	115 GeV	120 GeV	130 GeV	140 GeV	150 GeV
Pretag	9.41±0.61	7.92±0.52	6.35±0.41	3.99±0.26	2.02±0.13	0.78±0.05
At least one tag	5.57±0.43	4.69±0.36	3.73±0.29	2.4±0.19	1.22±0.09	0.47±0.04
One tag w/o NNtag	3.16±0.22	2.64±0.18	2.05±0.14	1.29±0.09	0.67±0.05	0.26±0.02
One tag w/ NNtag	2.81±0.23	2.35±0.19	1.82±0.15	1.15±0.09	0.59±0.05	0.23±0.02
ST + ST	1.31±0.16	1.11±0.14	0.94±0.11	0.61±0.07	0.30±0.04	0.11±0.01
ST + JP	1.11±0.13	0.94±0.11	0.74±0.09	0.50±0.06	0.25±0.03	0.10±0.01

Table 10: WH signal expected table calculated with integrated luminosity 1.9 fb^{-1} in W+2jet events for each tag category and each mass samples. Systematic error is included in uncertainties. Each tagging category is exclusive to other categories

expected events are calculated from 2 jet bin only. The WH production cross section and branching ratio (Figure 2) on the Higgs Working Group page [10] are used. The values shown in Table 8.

5.2 Systematic Uncertainties on Acceptance

The systematic uncertainties on the acceptance include uncertainties on the jet energy scale, initial and final state radiation, lepton ID and trigger efficiencies and the b-tagging scale factor. To obtain the systematic uncertainty from jet energy scale, we use the Higgs sample

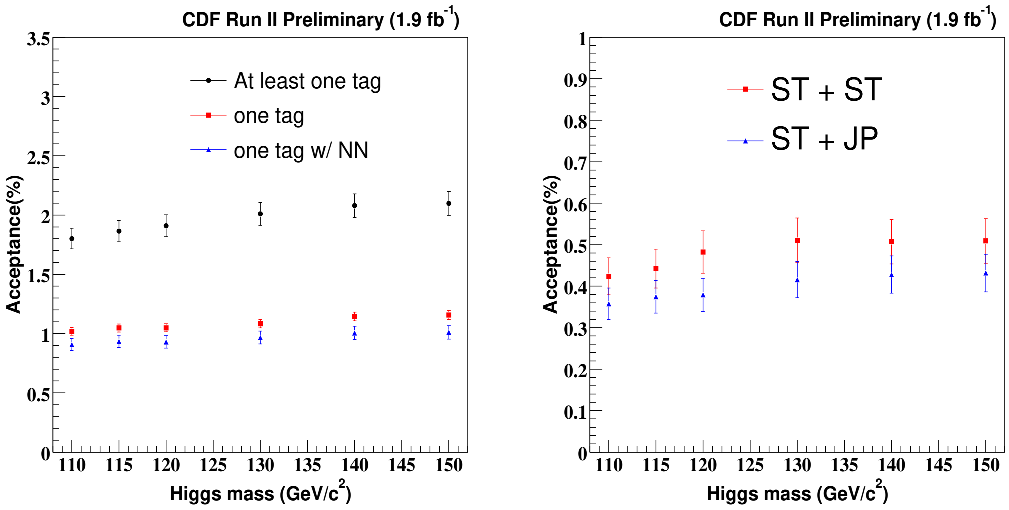

Figure 11: Signal acceptance as a function of Higgs mass. Left plot shows the at least one tag and exactly one tag category (w/ NN tag). Right plot shows the double tag categories.

for a mass of 120 GeV. The jet energies in the WH MC samples are shifted by $\pm 1\sigma$ and the difference from the nominal acceptance is taken as the systematic uncertainty. The estimated value in one SECVTX tag w/ NNtag, double SECVTX tag and one SECVTX tag plus Jet Probability tag is 2.3%, 2.5% and 2.8% using only 2 jet bin, respectively.

Lepton ID and trigger systematics are estimated in [12, 13, 14, 15]. These systematics uncertainties are calculated for each run range and combined using a luminosity weighted average. $\sim 2\%$ is assigned as Lepton ID systematic uncertainty. The uncertainty for the trigger efficiency is estimated to be less than one percent.

ISR and FSR systematic uncertainty are estimated by changing the parameters related to ISR and FSR from default values to half and double. Half of difference between the two samples is taken as the systematic uncertainly. The estimated values in one SECVTX tag w/ NNtag, ST+ST, ST+JP stage are 2.1%, 4.5% and 2.7% and 2.0%, 2.7% and 2.9% ,respectively (include MC statistics). and the combination of these uncertainties 2.9%, 5.2% and 4.0% is taken as ISR/FSR total systematic uncertainty.

PDFs uncertainties are evaluated using the standard re-weighting method recommended by Joint Physics [15]. The estimated value in one SECVTX tag w/ NN tag, ST+ST and ST+JP stage is 1.2%, 2.1% and 1.5%, respectively.

The b-tagging scale factor uncertainty comes from the High p_T b-tagging group. Propagating this uncertainty through our analysis, we estimate an acceptance uncertainty of 5.6%, 10.6% and 10.5% for one SECVTX tag w/ NN tag, double SECVTX tag and one SECVTX plus Jet Probablity. Total systematic uncertainties are listed in Table.11 for each b-tagging category.

Luminosity uncertainties are also included in calculating Higgs signal events. This un-

b-tagging category	LeptonID	Trigger	ISR/FSR	JES	PDF	b-tagging	Total
One tag w/ NN tag	$\sim 2\%$	$< 1\%$	2.9%	2.3%	1.2%	3.5%	5.6%
ST + ST	$\sim 2\%$	$< 1\%$	5.2%	2.5%	2.1%	8.4%	10.6%
ST + JP	$\sim 2\%$	$< 1\%$	4.0%	2.8%	1.5%	9.1%	10.5%

Table 11: Systematic uncertainties for each tagging category

certainty assign 6%.

Note: Previous versions of this analysis suggest that the acceptance systematics are much larger than the shape systematics. Therefore, at this time, we've focused on the acceptance systematics. In the near future, we will check this assumption by evaluating shape systematics.

6 Neural Network Discriminant

To further improve signal to background discrimination after event selection, we employ an artificial Neural Network (NN) trained on a variety of kinematic variables to distinguish WH from backgrounds. We use the RootJetnet interface to the Jetnet neural network program.

To optimize the NN, we use an iterative procedure to determine the configuration which best discriminates signal and background, and which uses a minimal number of input discriminants. The $1fb^{-1}$ ZH analysis [17] used the same optimization procedure. This is done by first determining the best one-variable NN from a list of seventy-six possible choices. The optimization algorithm keeps this variable as the first input, the loops over all other the variables to determine the best two-variable NN. The best N-variable network is finally selected once the N+1-variable network shows less than a 0.5% improvement. The criteria for comparing networks is the testing error defined, according to the standard Jetnet conventions, as the average of the squared distances between the NN output and the intended target (zero for background and one for signal).

In the training, only the WH signal, and the $W + b\bar{b}$,$t\bar{t}$, and t-channel single top background samples are used, since these samples capture the main classes of kinematic shapes. Ten thousand events from each class (signal plus three backgrounds) are used to form the training sample. An equal number of events are reserved for testing. To increase the statistics for training, events are only required to pass the pretag selection criteria.

We optimized the NN structure on signal sample with $M_H = 120$ GeV. We used the optimal structure of input variables to train sepearte neural networks for Higgs masses of 110, 115, 120, 130, 140, and 150. Re-training networks with the same structure and different signal masses keeps the neural net sensitivity constant as a function of higgs mass. We expect that this constant increase in sensitivity versus mass is also an optimal increase. Further studies could investigate whether other combinations of input variables becomes more powerful at different Higgs masses.

Our final Neural Network configuration has six input variables, eleven hidden nodes, and one output node. The inputs variables are given below

M_{jj+}**:** This variable is the invariant mass calculated from the two tight jets using Level-5 jet corrections. Furthermore, if there are additional loose jets present ($E_{T,L5} < 12$ GeV and $|\eta| < 2.4$), the loose jet that is closest to one of the two tight jets is included in this invariant mass calculation, if the separation between that loose jet and one of the tight jets is $\Delta R < 0.9$.

$\sum E_T$**(Loose Jets):** This variable is the scalar sum of the loose jet transverse energy (with Level-5 corrections).

p_T **Imbalance:** This variable expresses the difference between the scalar sum of the transverse momenta of all measured objects and the $\not\!\!E_T$. Specifically, it is calculated as $P_T(jet_1) + P_T(jet_2) + P_T(lep) - \not\!\!E_T$.

$M_{l\nu j}^{min}$**:** This is the invariant mass of the lepton, $\not\!\!E_T$, and one of the two jets, where the jet is chosen to give the minimum invariant mass. For this quantity, the p_z of the neutrino is ignored.

ΔR**(lepton-**ν_{max}**):** This is the ΔR separation between the lepton and the neutrino, where the p_z of the neutrino is taken from by choosing the solutions from the quadratic equations for the W mass constraint with the largest $|p_z|$.

$P_T(W + H)$**:** This is the total transverse momentum of the W plus two jets system, $P_T(\vec{lep} + \vec{\nu} + \vec{jet}_1 + \vec{jet}_2)$.

Figure 12 shows unit normalized shape comparison plots between the NN inputs. Figure 13 shows the shape comparison between the NN outputs.

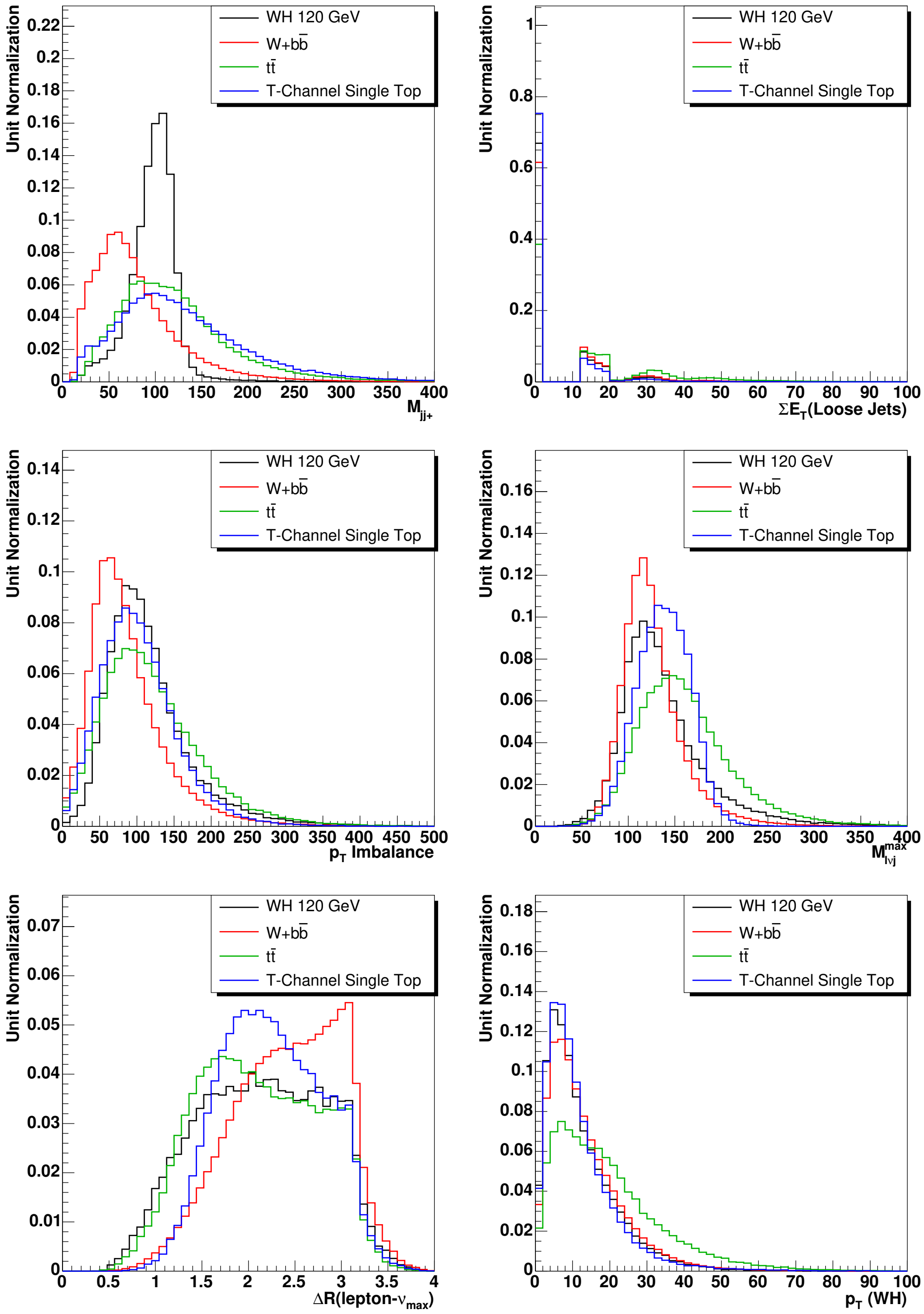

Figure 12: Comparison of NN input variable kinematics for signal (M_H = 120 GeV) and the backgrounds used in training. Each histogram is normalized to unit area.

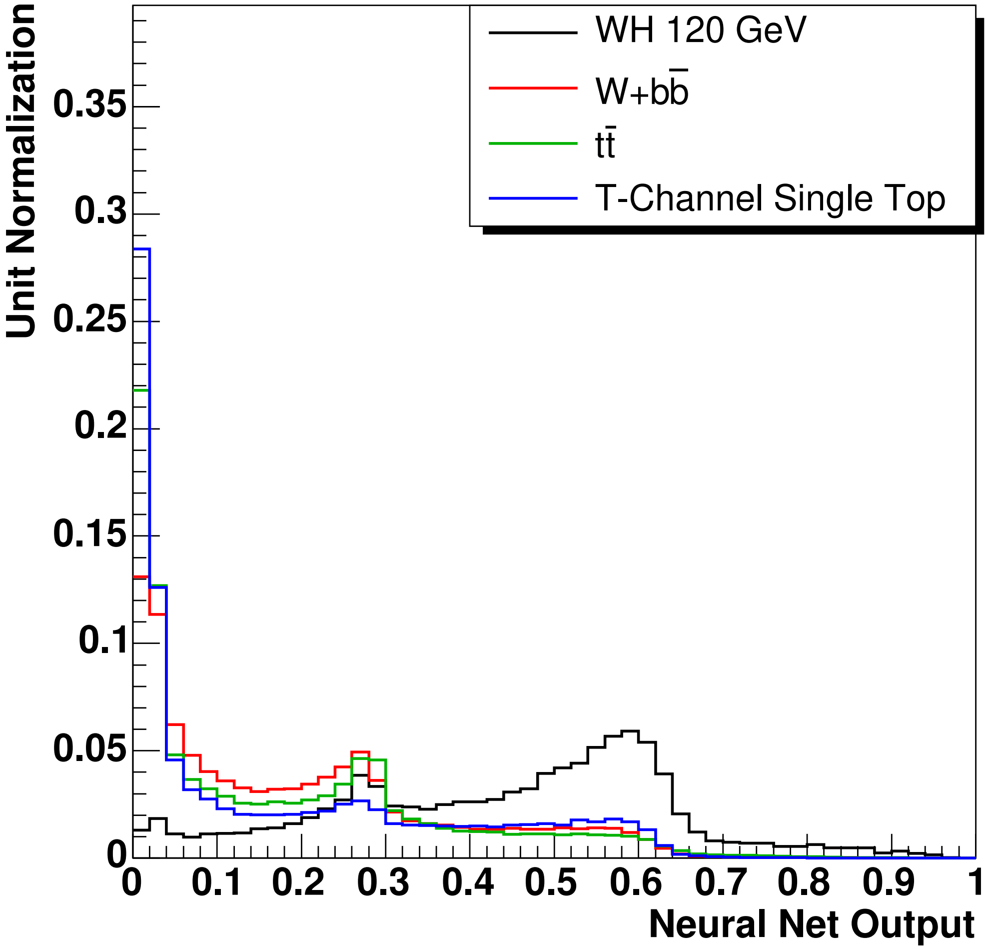

Figure 13: Comparison of NN output for signal ($M_H = 120$ GeV) and the backgrounds used in training. Each histogram normalized to unit area.

7 Kinematic shape

We check the kinematics for each tagging category to make sure that the background compositions are well understood between data and Monte Carlo. The non-W shape is derived directly from data using C region ($\not\!\!E_T >$20 GeV and lepton isolation $>$ 0.1). The W+jets shape is determined from Monte Carlo using ALPGEN_v2 and is normalized to the data after subtracting other backgrounds in pretag. The mistag shape is obtained from the data events before tagging, but weighted by the mistag matrix. The rest of the backgrounds, such as $t\bar{t}$, single top and diboson, are derived from Monte Carlo simulation with a top mass of 175 GeV/c^2. We add signal shape for each tagging category after scaling to able to see signal shape.

7.1 pretag

Figures 14-19 show the fundamental observed and expected shapes of lepton, Missing energy and two jets and correlation between these variables in the pretag sample in the W+2jet bin. As we mentioned, the background estimation is normalized to the number of events observed in the data. These plots show good agreement between the data and the background prediction.

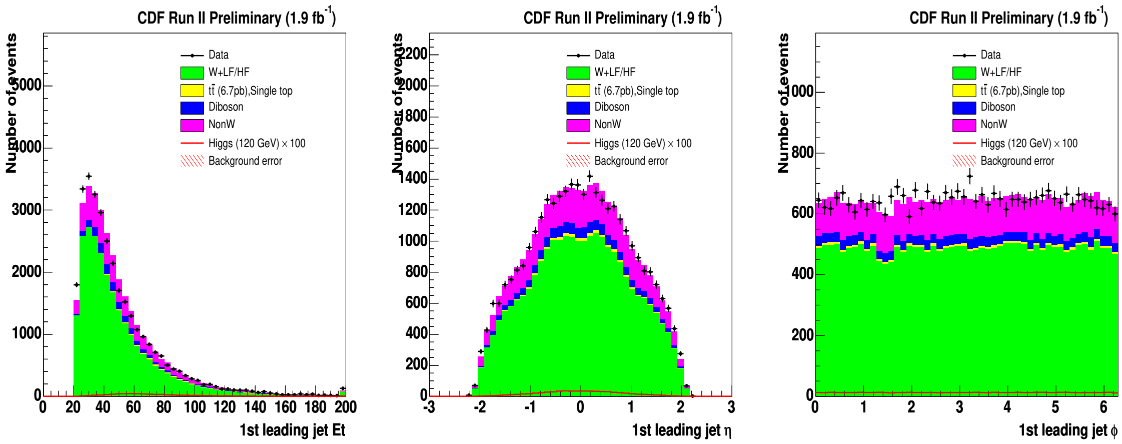

Figure 14: The first leading jet E_T, η and ϕ kinematic distributions in the pretag events. The W+jets background is normalized to the data after subtracting other backgrounds.

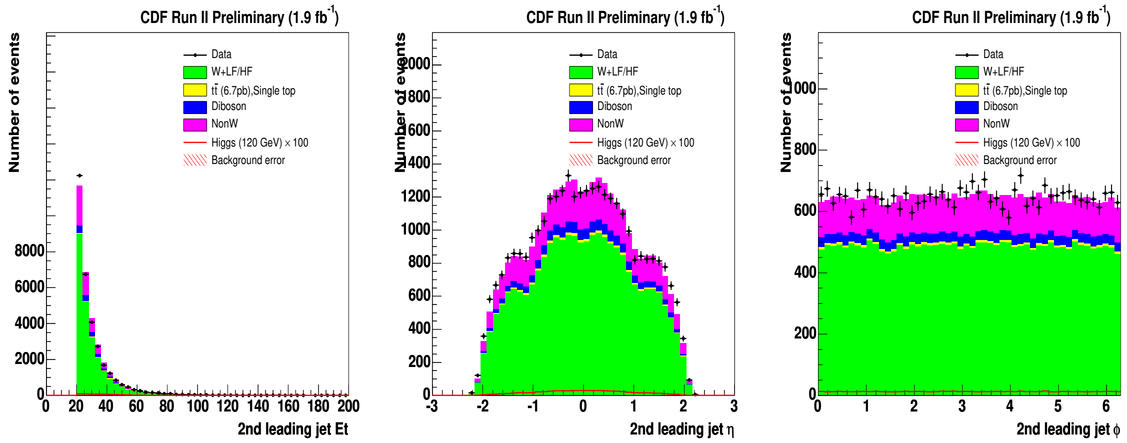

Figure 15: The second leading jet E_T, η and ϕ kinematic distributions in the pretag events. The W+jets background is normalized to the data after subtracting other backgrounds.

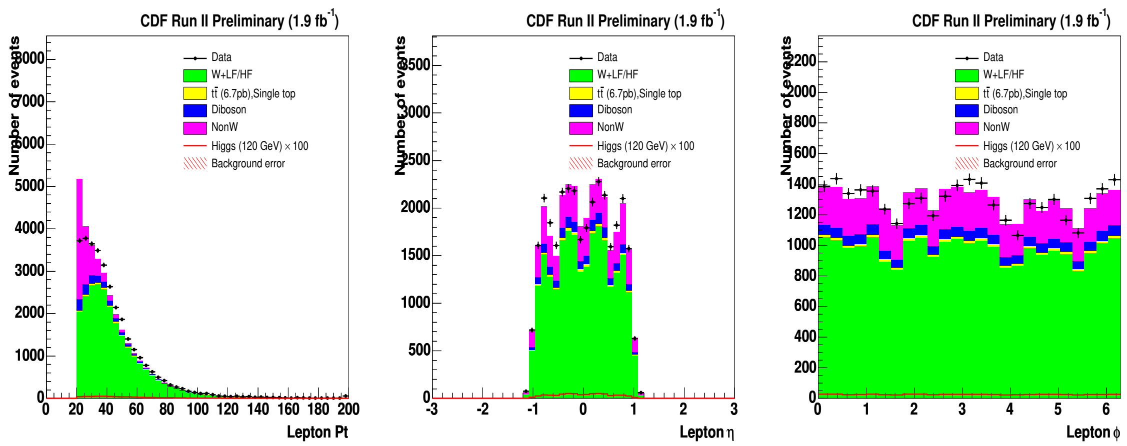

Figure 16: The lepton P_T, η and ϕ kinematic distributions in the pretag events. The W+jets background is normalized to the data after subtracting other backgrounds.

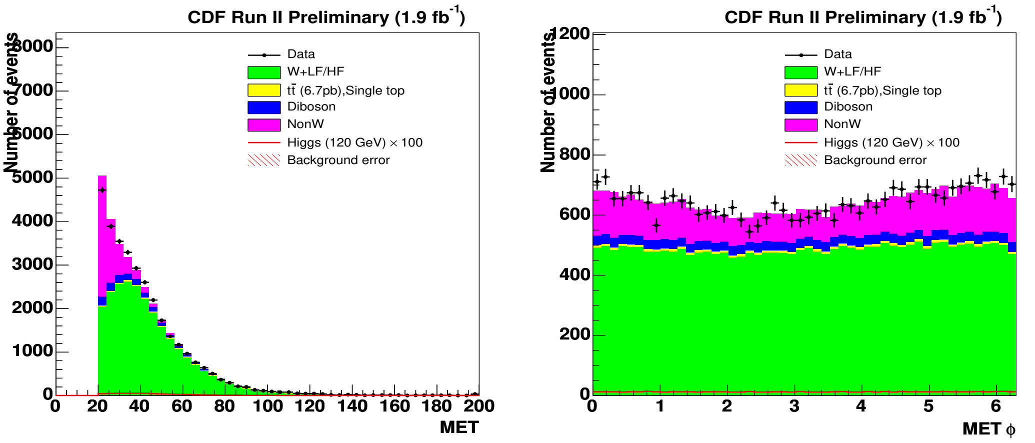

Figure 17: The $\not{E}_T$ and ϕ kinematic distributions in the pretag events. The W+jets background is normalized to the data after subtracting other backgrounds.

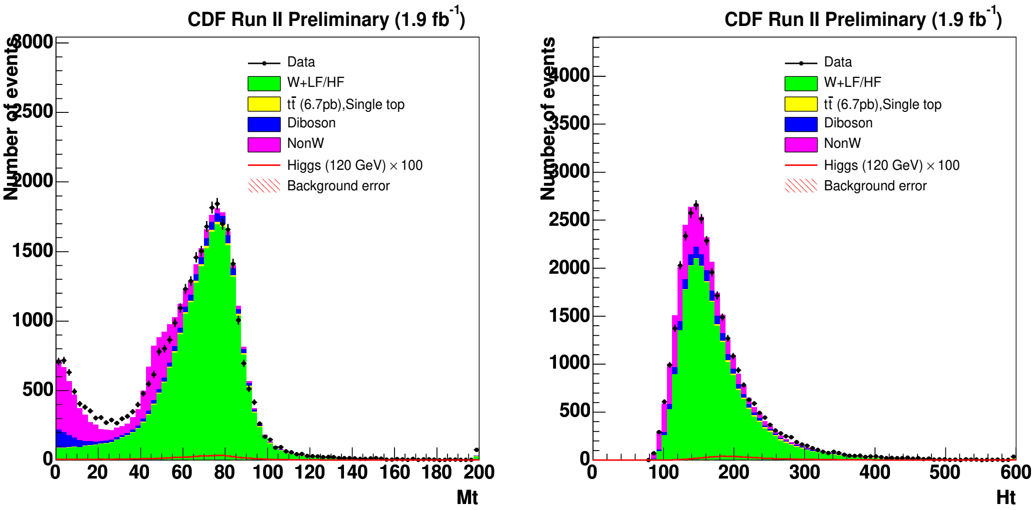

Figure 18: The reconstructed W transverse mass and Ht distributions in the pretag events. The W+jets background is normalized to the data after subtracting other backgrounds.

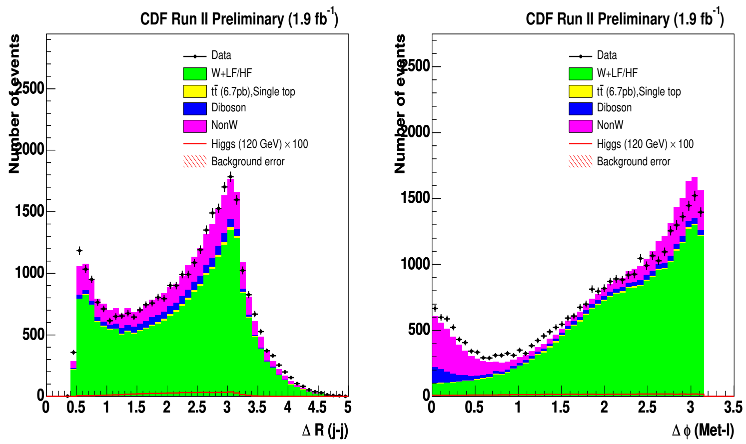

Figure 19: The observed and expected ΔR between dijet and $\Delta\phi$ between $\not\!\!E_T$ and lepton in the pretag events. The W+jets background is normalized to the data after subtracting other backgrounds.

7.2 One SECVTX tag w/ NNtag

Figures 20-25 show similar plots for events with at least one tight SECVTX tag in W+2jet bin where the backgrounds are normalized according to their Method 2 expectations and the Method 2 uncertainties are shown.

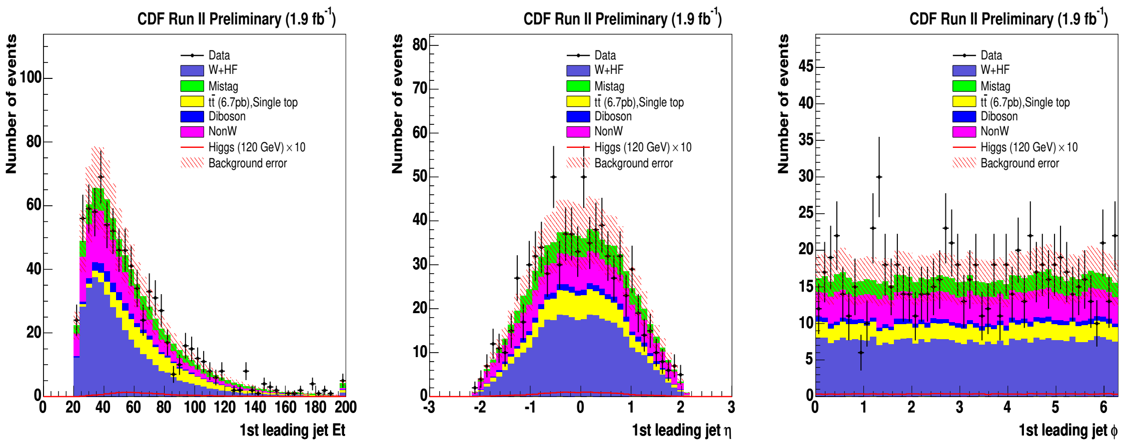

Figure 20: First leading jet E_T, η and ϕ kinematic plots in one SECVTX w/ NN tagged events. Background uncertainty is shown in red hash.

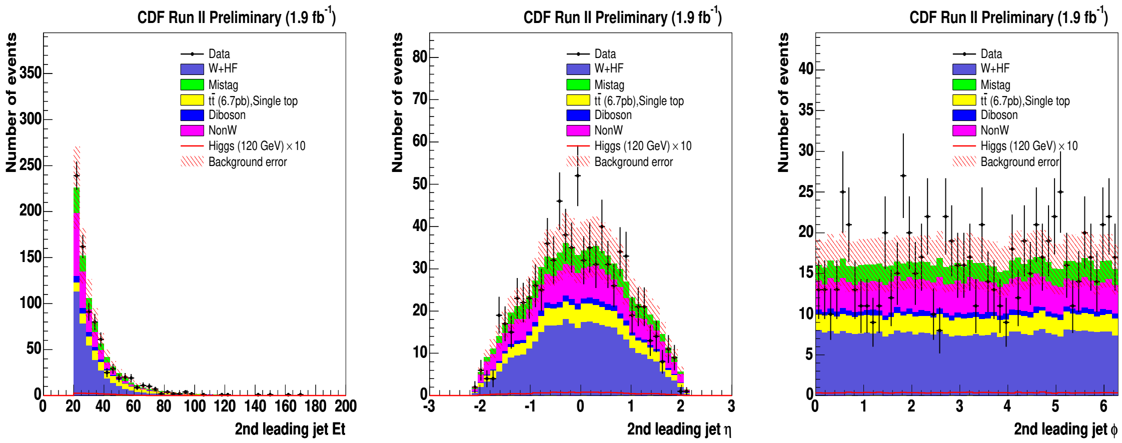

Figure 21: Second leading jet E_T, η and ϕ kinematic plots in one SECVTX w/ NN tagged events. Background uncertainty is shown in red hash.

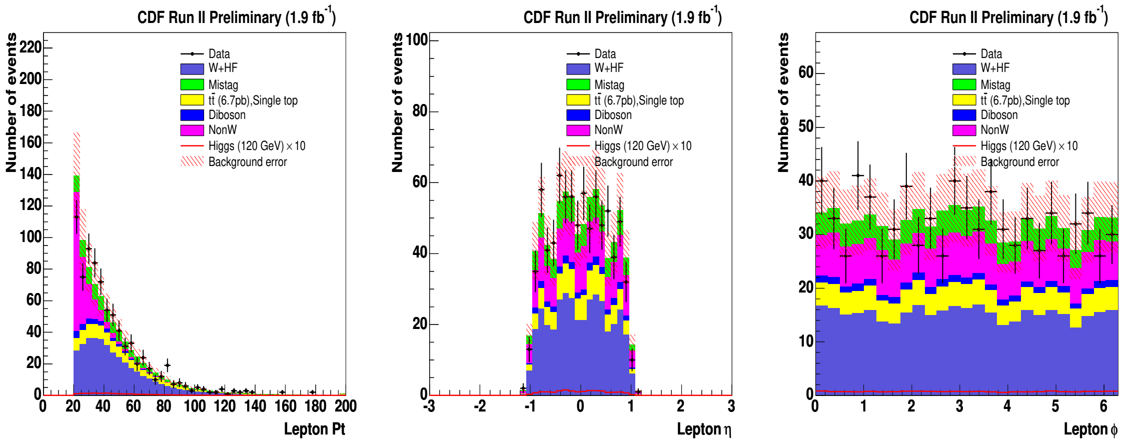

Figure 22: Lepton P_T, η and ϕ kinematic plots in one SECVTX w/ NN tagged events. Background uncertainty is shown in red hash.

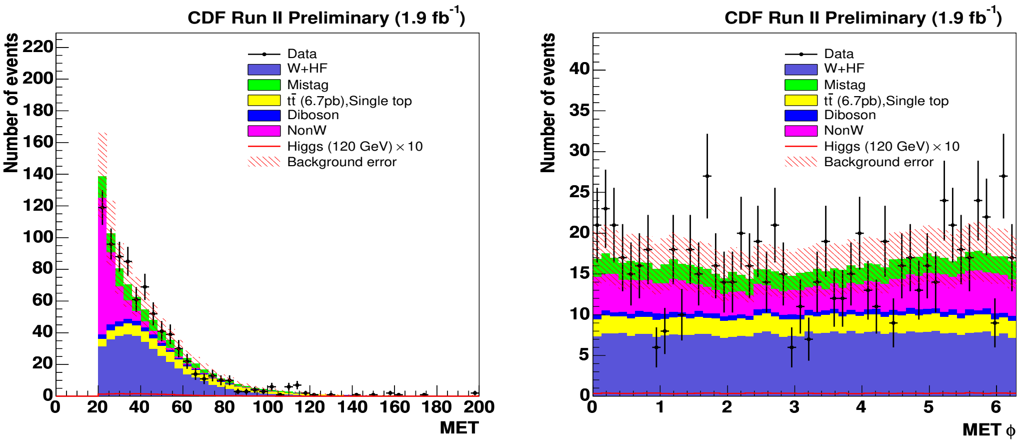

Figure 23: $\not{E}_T$ and ϕ kinematic plots in one SECVTX w/ NN tagged events. Background uncertainty is shown in red hash.

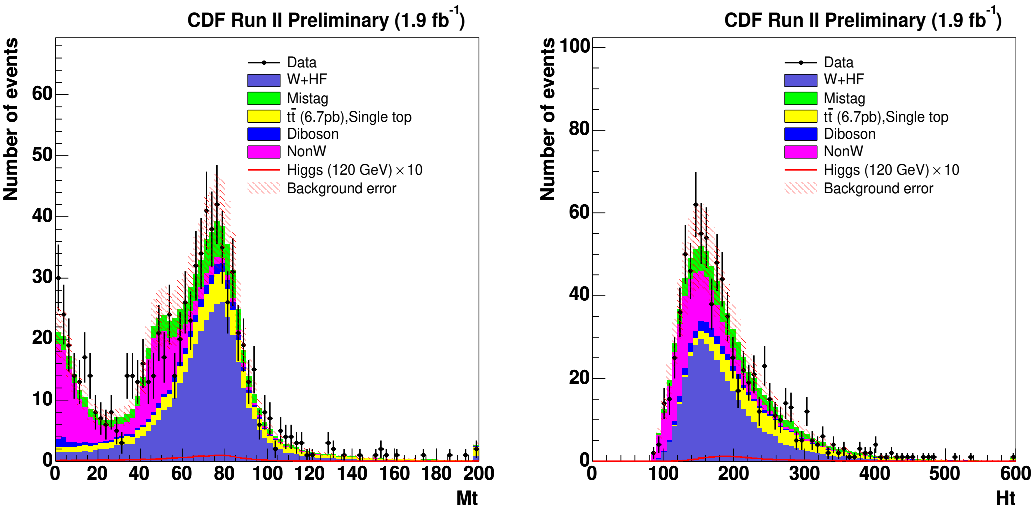

Figure 24: Transverse mass of W and Ht plots in one SECVTX w/ NN tagged events. Background uncertainty is shown in red hash.

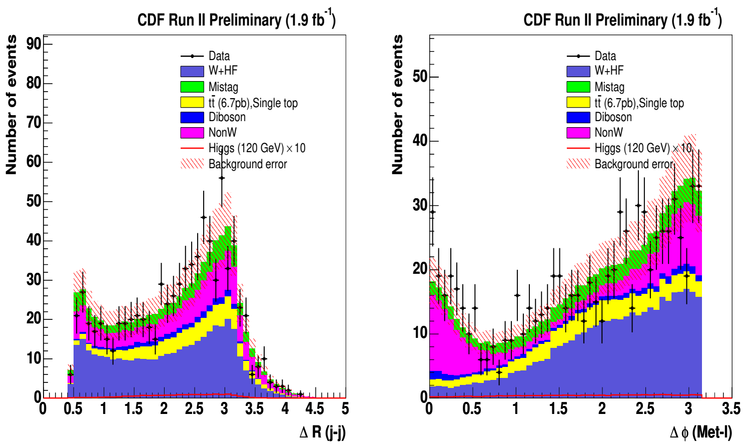

Figure 25: From left, ΔR between dijet and $\Delta\phi$ between $\not\!\!E_T$ and lepton in one SECVTX w/ NN tagged events. Background uncertainty is shown in red hash.

7.3 Double SecVtx tag

Figures 26-31 show the observed and expected kinematic distributions in the double SecVtx tagged events in W+2jet bin. Again, our data and the background model agree within the statistical uncertainty on the data.

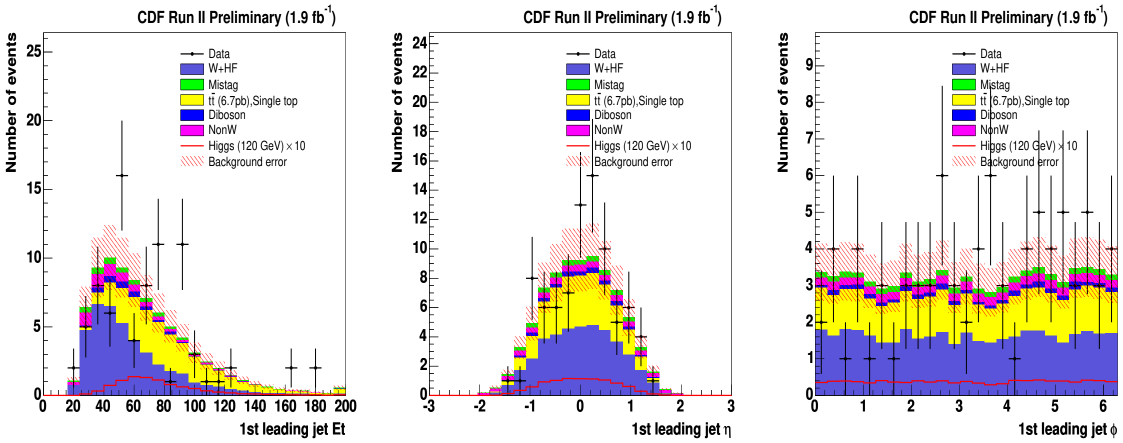

Figure 26: First leading jet E_T, η and ϕ kinematic plots in double SecVtx tagged events. Background uncertainty is shown in red hash

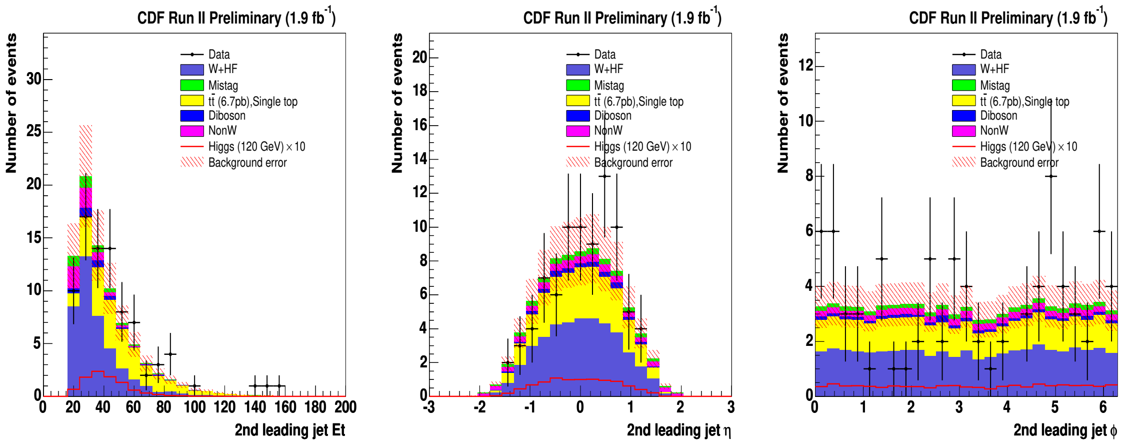

Figure 27: Second leading jet E_T, η and ϕ kinematic plots in double SecVtx tagged events. Background uncertainty is shown in red hash.

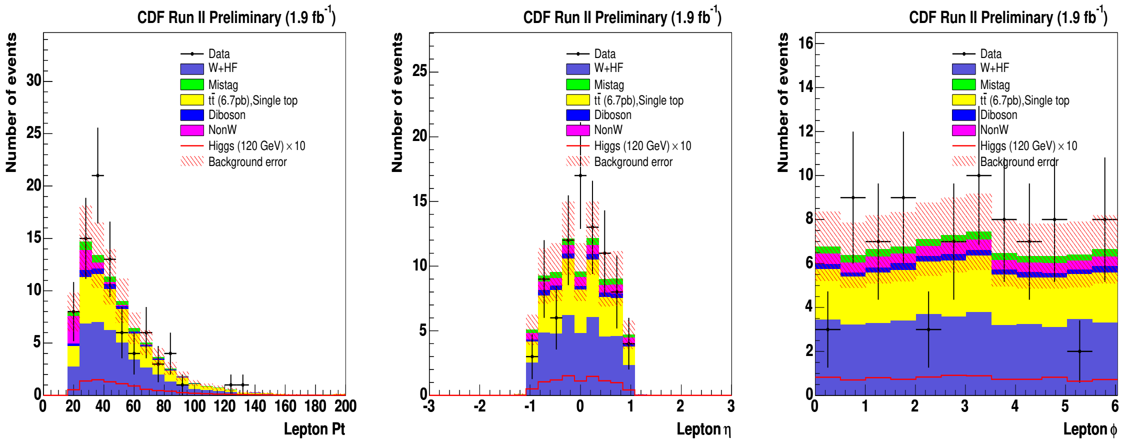

Figure 28: Lepton P_T, η and ϕ kinematic plots in double SecVtx tagged events. Background uncertainty is shown in red hash.

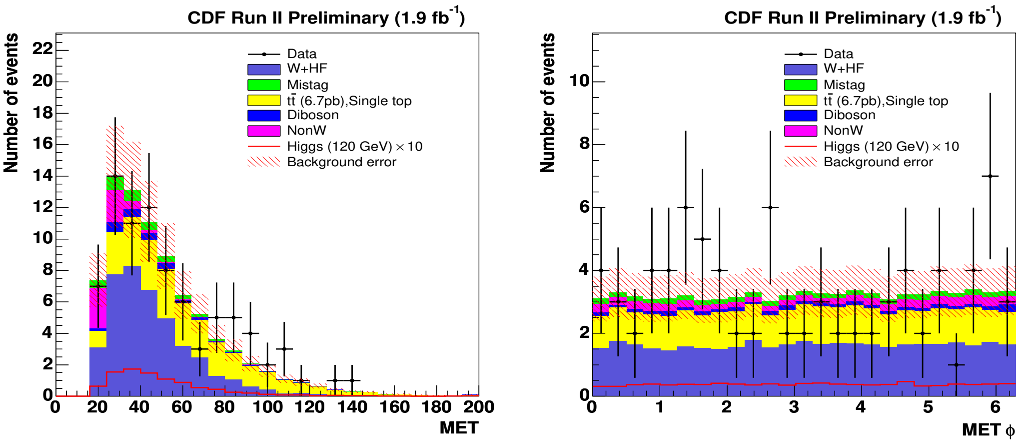

Figure 29: $\not\!\!E_T$ and ϕ kinematic plots in double SecVtx tagged events. Background uncertainty is shown in red hash.

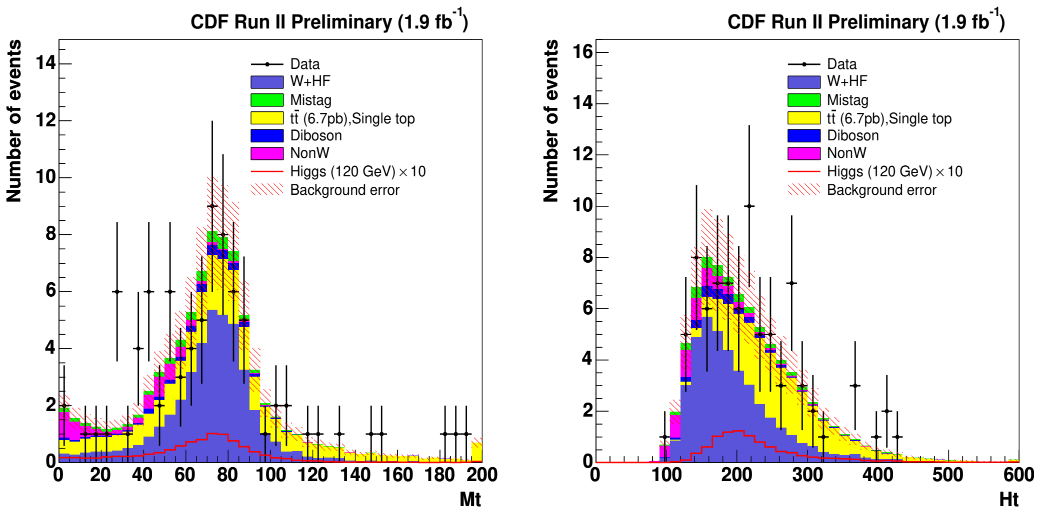

Figure 30: Transverse mass of W and Ht plots in double SecVtx tagged events. Background uncertainty is shown in red hash.

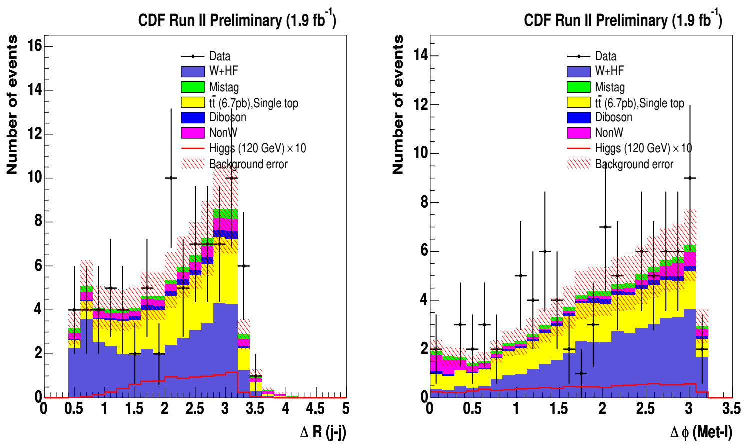

Figure 31: From left,ΔR between dijet and $\Delta\phi$ between $\not{E}_T$ and lepton in double SecVtx tagged events. Background uncertainty is shown in red hash.

7.4 One SecVtx tag and One Jet probability tag

Figures 32-37 show the observed and expected kinematic shapes in the double tagged events with one SECVTX tag + one jet probability tag in W+2jet bin. Again, the agreement between the two is excellent although the statics are not great.

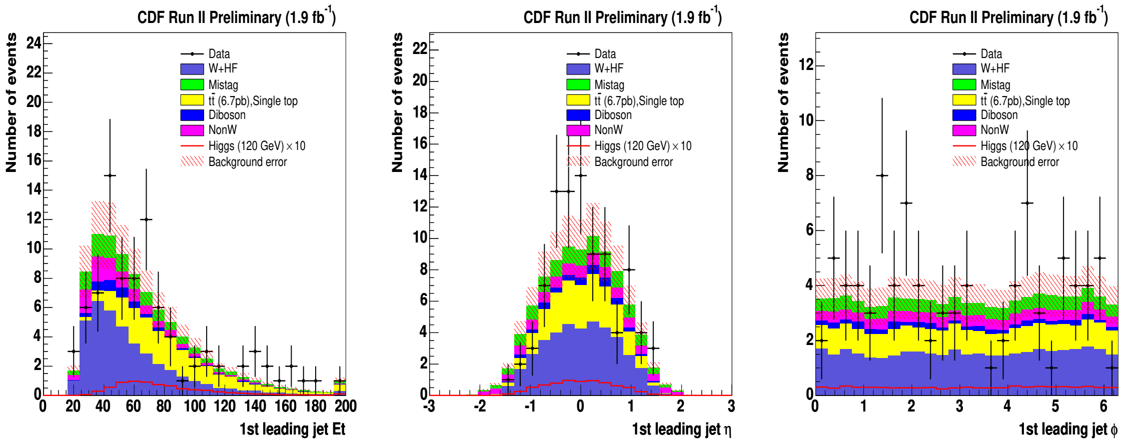

Figure 32: First leading jet E_T, η and ϕ kinematic plots in one SecVtx tag and one Jet probability tag events. Background uncertainty is shown in red hash.

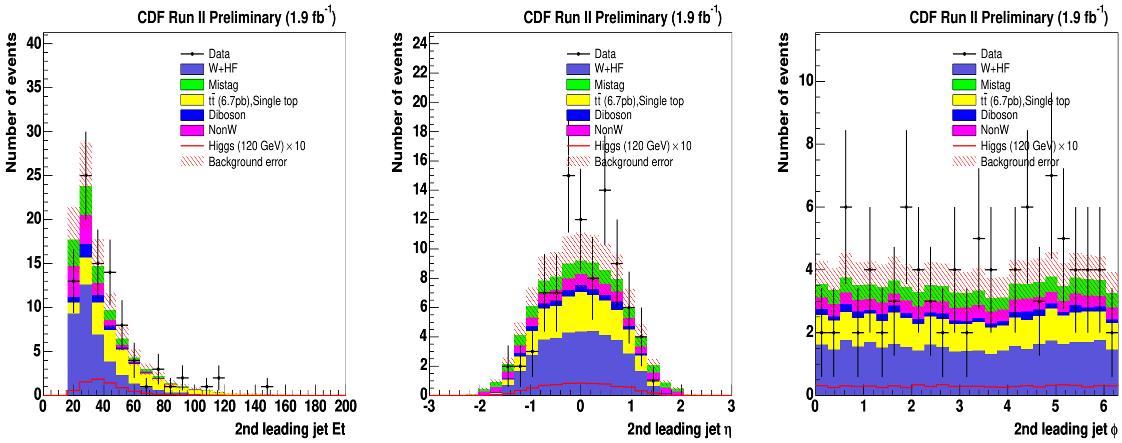

Figure 33: Second leading jet E_T, η and ϕ kinematic plots in one SecVtx tag and one Jet probability tag events. Background uncertainty is shown in red hash.

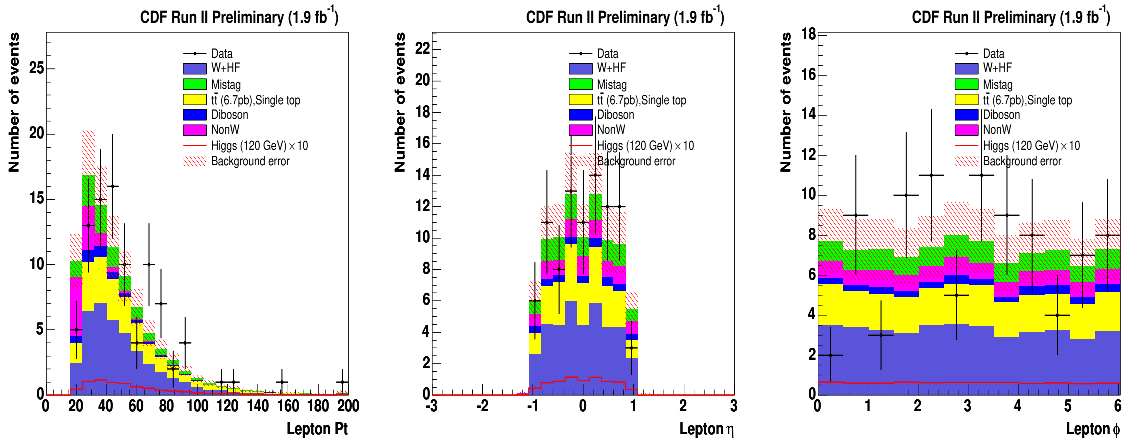

Figure 34: Lepton P_T, η and ϕ kinematic plots in one SecVtx tag and one Jet probability tag events. Background uncertainty is shown in red hash.

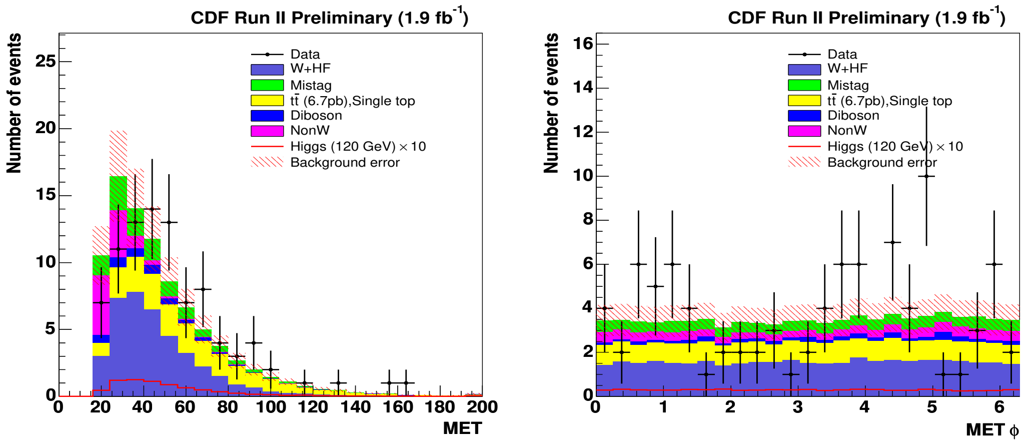

Figure 35: $\not{E}_T$ and ϕ kinematic plots in one SecVtx tag and one Jet probability tag events. Background uncertainty is shown in red hash.

8 NN kinematic shape

Figures 38-45 shows the NN input variables and output shape for each tagging category. First we check whether the all NN input variables are modeled reasonably and consistent with observed data for each tagging categories. As described in Section 6, the Higgs signal ideally produces a high NN output value while the backgrounds produce low values. Finally NN output distribution for each tagging category is shown to search for the Standard Model Higgs boson.

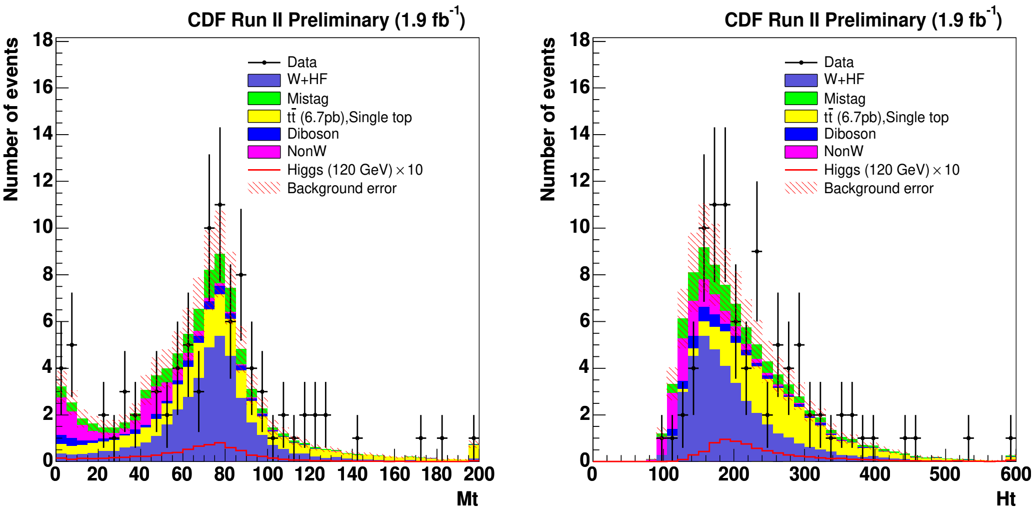

Figure 36: Transverse mass of W and Ht plots in one SecVtx tag and one Jet probability tag events. Background uncertainty is shown in red hash.

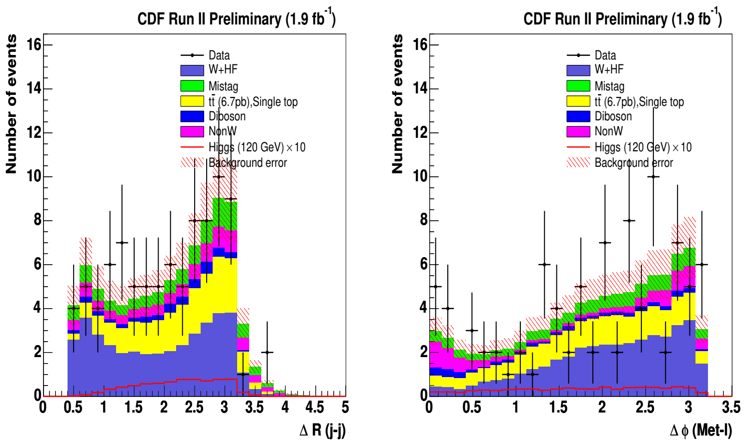

Figure 37: From left, ΔR between dijet and $\Delta\phi$ between $\not{E}_T$ and lepton in one SecVtx tag and one Jet probability tag events. Background uncertainty is shown in red hash.

8.1 pretag

Figures 38 show the NN input variables, Met Imbalance, Pt of W+2jet system, dijet mass added close loose jet contribution, invariant mass of W + 1jet system, ΔR between $\not{E}_T$ and lepton and sum loose jet E_T distribution. The total background number is normalized to data using W+jets events in pretag events. Figure 39 shows the NN output distributions calculated from six NN input variables. The expected background shape is consistent with observed background shape.

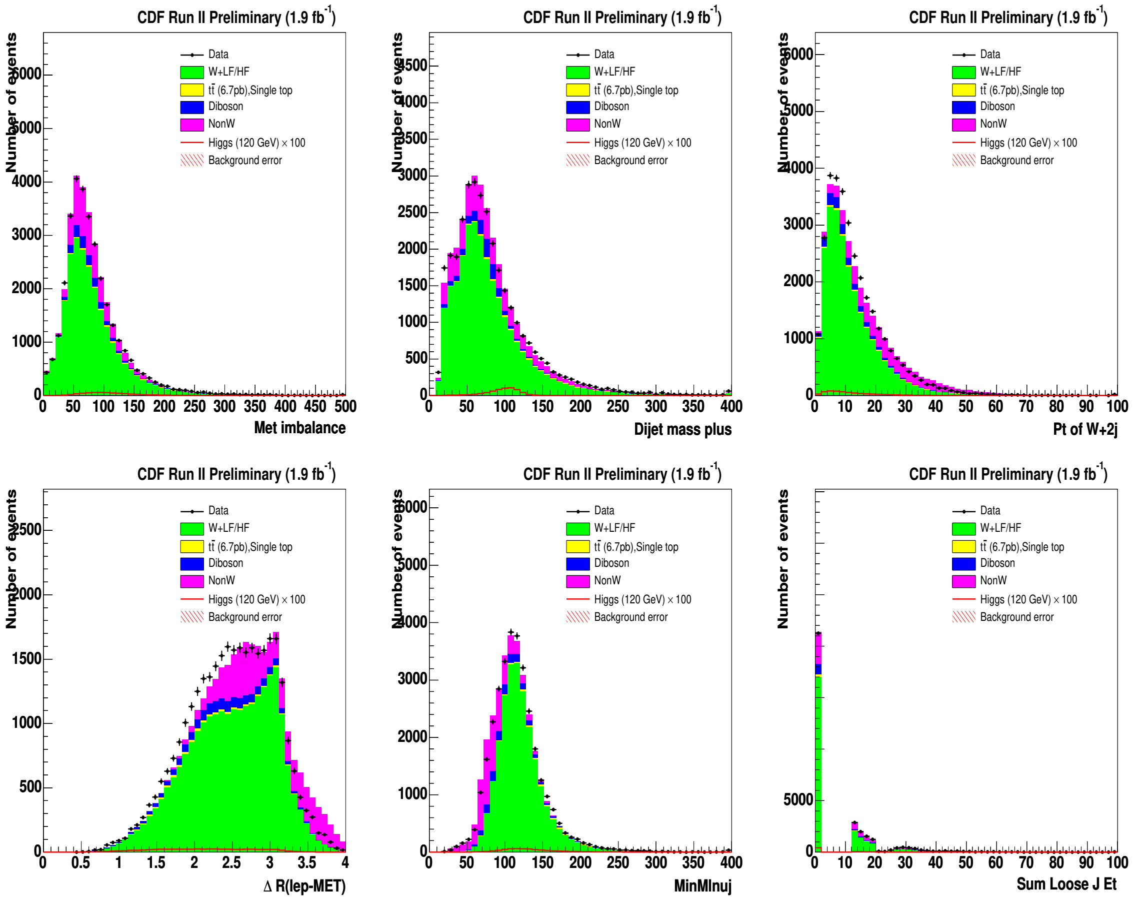

Figure 38: The observed and expected NN input variables, Met Imbalance and Dijet plus closest loose jet mass reconstructed by Jet energy correction L5, Pt of W+2jet system, ΔR between $\not{E}_T$ and lepton, invariant mass of W + 1jet system and sum of loose jet E_T in the pretag events. The W+jets background is normalized to the data after subtracting other backgrounds.

8.2 one tag w/ NNtag

Figures 40 show the NN input variables, Met Imbalance, Pt of W+2jet system, dijet mass added close loose jet contribution, invariant mass of W + 1jet system, ΔR between $\not{E}_T$ and lepton and sum loose jet E_T distribution for one SECVTX tag w/ NN tagged events. Figure 41 shows the NN output distributions calculated from six NN input variables. The expected background shape is consistent with observed background shape.

8.3 Double SECVTX tag

Figures 42 show the NN input variables, Met Imbalance, Pt of W+2jet system, dijet mass added close loose jet contribution, invariant mass of W + 1jet system, ΔR between $\not{E}_T$

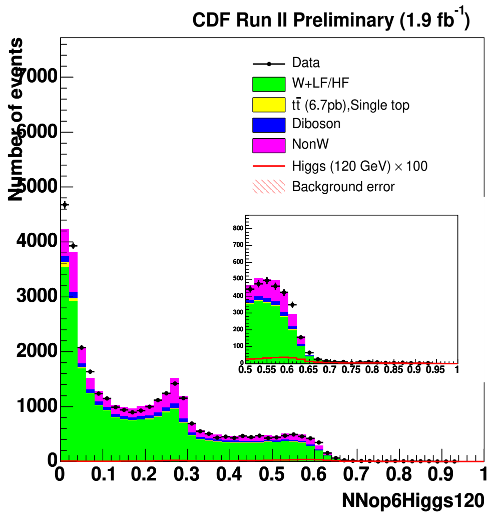

Figure 39: NN output shape calculated from six input variables for pretag events. Higgs signal should produce high NN output values.

and lepton and sum loose jet E_T distribution for double SECVTX tagged events. Figure 43 shows the NN output distributions calculated from six NN input variables. The expected background shape is consistent with observed background shape.

8.4 One SECVTX plus Jet Probability tag

Figures 44 show the NN input variables, Met Imbalance, Pt of W+2jet system, dijet mass added close loose jet contribution, invariant mass of W + 1jet system, ΔR between $\not{E}_T$ and lepton and sum loose jet E_T distribution for one SECVTX tagged plus Jet Probability tagged events. Figure 45 shows the NN output distributions calculated from six NN input variables. The expected background shape is consistent with observed background shape.

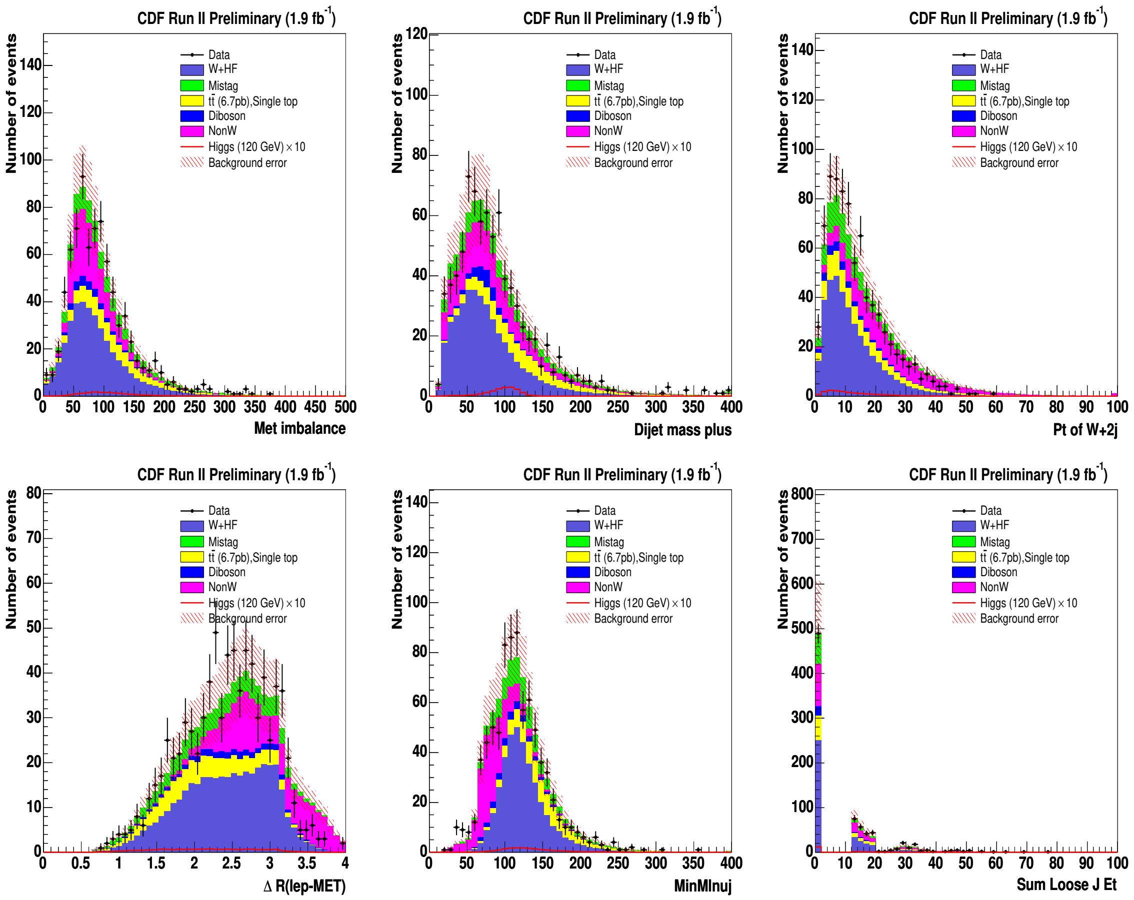

Figure 40: The observed and expected NN input variables, Met Imbalance and Dijet plus closest loose jet mass reconstructed by Jet energy correction L5, Pt of W+2jet system, ΔR between $\not\!\!E_T$ and lepton, invariant mass of W + 1jet system and sum of loose jet E_T in one SECVTX w/ NN tag.

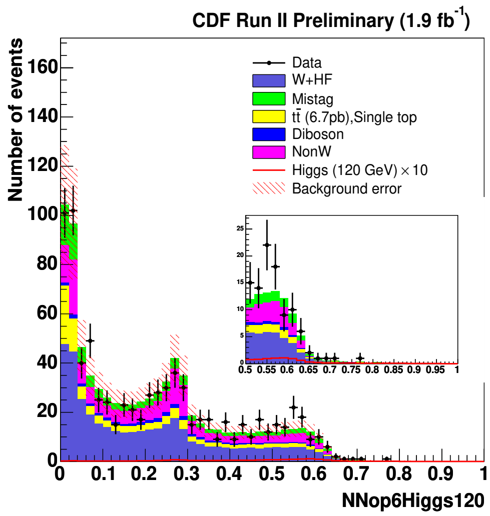

Figure 41: NN output shape calculated from six input variables for one SECVTX w/ NNtag category. This NN output shape is calculated for proper signal mass points. Higgs signal should produce high NN output values.

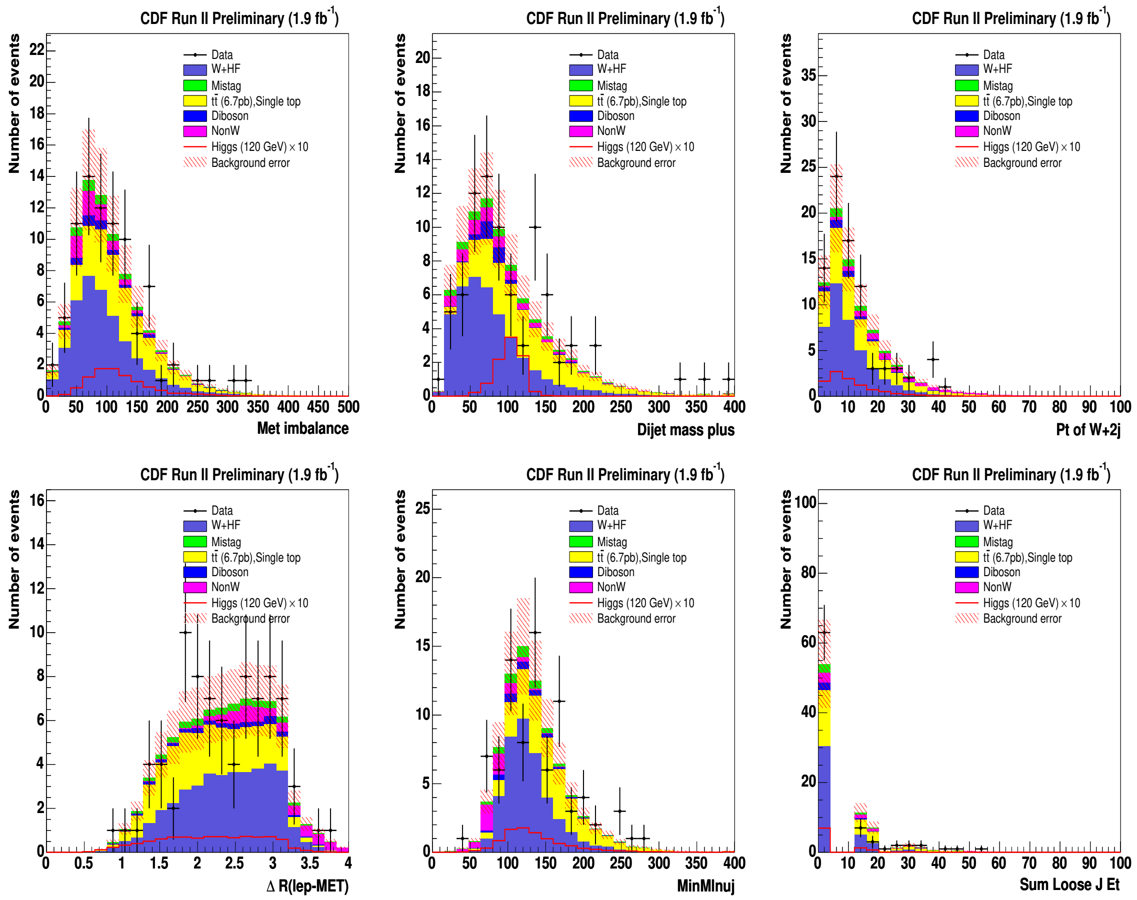

Figure 42: The observed and expected NN input variables, Met Imbalance and Dijet plus closest loose jet mass reconstructed by Jet energy correction L5, Pt of W+2jet system, ΔR between $\not\!\!E_T$ and lepton, invariant mass of W + 1jet system and sum of loose jet E_T in double SECVTX tag.

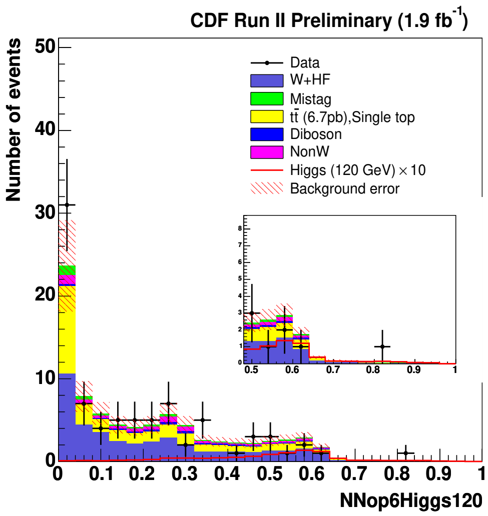

Figure 43: NN output shape calculated from six input variables for double SECVTX tag category. This NN output shape is calculated for proper signal mass points. Higgs signal should produce high NN output values.

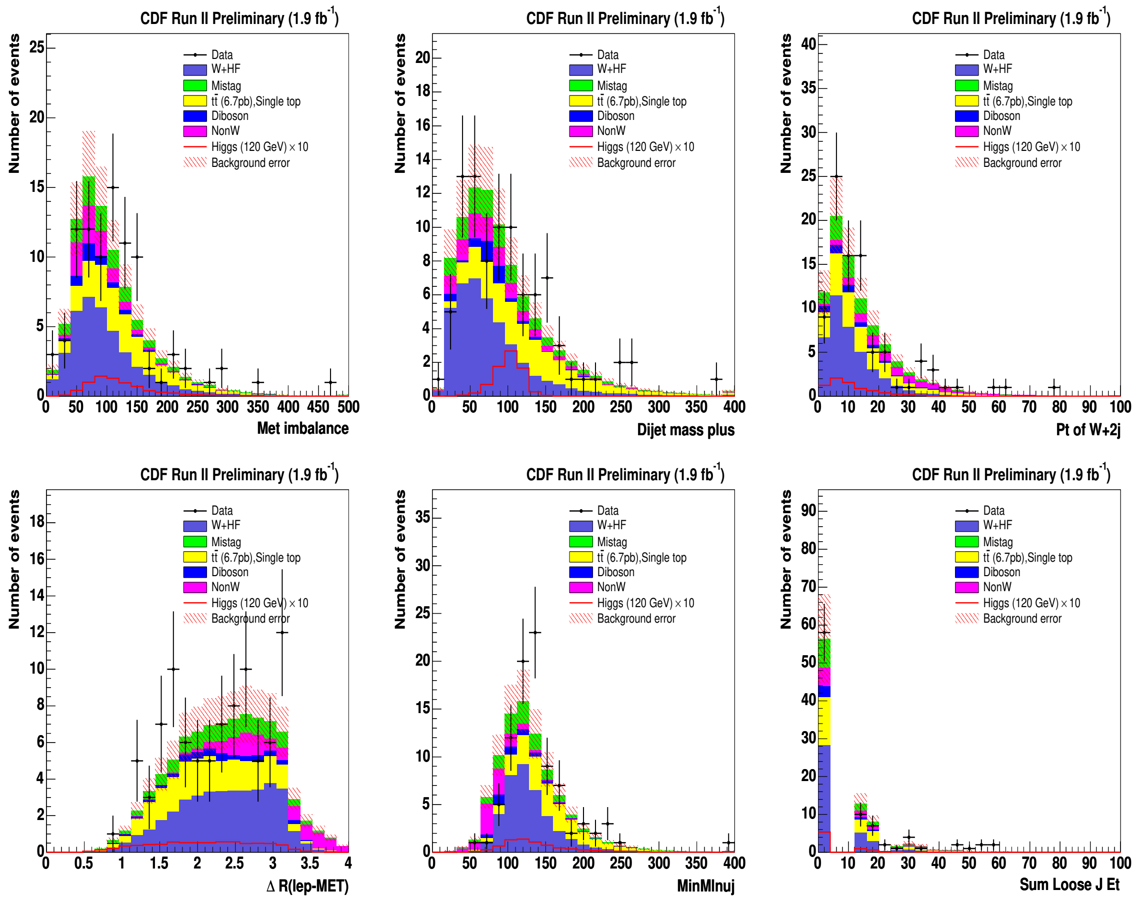

Figure 44: The observed and expected NN input variables, Met Imbalance and Dijet plus closest loose jet mass reconstructed by Jet energy correction L5, Pt of W+2jet system, ΔR between $\not{E}_T$ and lepton, invariant mass of W + 1jet system and sum of loose jet E_T in one SECVTX plus Jet Probability tag.

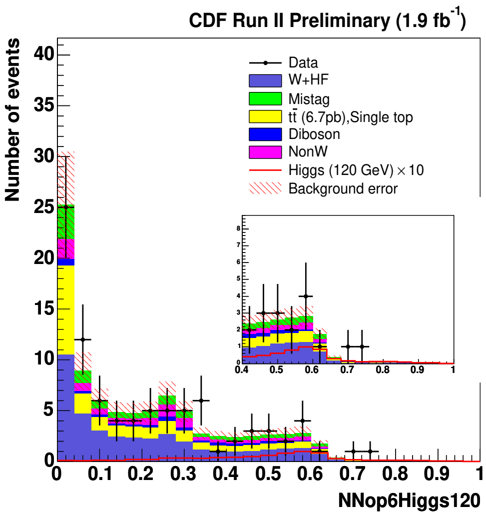

Figure 45: NN output shape calculated from six input variables for one SECVTX plus Jet Probability tag category. This NN output shape is calculated for proper signal mass points. Higgs signal should produce high NN output values.

9 Sensitivity and 95% C.L. upper limit: Dijet Invariant Mass

Since there is no significant excess of events in the data compared to the background expectation, we fit the NN output distribution and extract the expected 95% C.L. upper limit for various b-tagging strategies using pseudo-experiments based on the background expectations.

9.1 Binned Likelihood Technique

We set an upper limit on the production cross section times branching ratio of $p\bar{p} \rightarrow WH$ as a function of m_h by using the number of events in the $W^{\pm} + 2$ jets sample. Since there are no peaks observed from NN ouput distribution, we assume that the $W^{\pm} + 2$ jets and dijet mass distributions in the data consist of QCD (mistags, $W^{\pm} + b\bar{b}$, $W^{\pm} + c\bar{c}$, $W^{\pm} + c$ Z+jets and diboson), TOP ($t\bar{t}$ and single top) and WH higgs signal events. A 1-dimensional binned maximum likelihood technique is used to obtain the limit on the cross section of signal process as in the previous analysis. The expected number of events (μ_i) in each mass bin is

$$\mu_i = f_i^{QCD} \cdot N^{QCD} + f_i^{TOP} \cdot N^{TOP} + f_i^{WH \rightarrow l\nu b\bar{b}} \cdot (\varepsilon \cdot \mathcal{L} \cdot \sigma_{WH \rightarrow l\nu b\bar{b}}),$$

where f_i^{QCD}, f_i^{TOP} and $f_i^{WH \rightarrow l\nu b\bar{b}}$ are the expected fraction of events in a given mass bin predicted by Monte Carlo. N^{QCD}, N^{TOP}, ε, $\mathcal{L}$ and $\sigma_{WH \rightarrow l\nu b\bar{b}}$ are the expected number of QCD and TOP events, the detection efficiency, the luminosity and the unknown $WH \rightarrow l\nu b\bar{b}$ cross section respectively. In pseudo-experiment, to make the pseudo-data, we fluctuate the number of expected QCD and Top with Gaussian with the estimated total uncertainty independently. Then the corresponding likelihood is

$$L(\sigma \times BR) = \iiint \prod_{i=bin} \frac{\mu_i^{N_i} \cdot e^{-\mu_i}}{N_i!} G(N_{QCD}, \sigma_{N_{QCD}}) G(N_{TOP}, \sigma_{N_{TOP}}) G(N_{WH}, \sigma_{N_{WH}}) dN_{QCD} dN_{TOP} dN_{WH}, \quad (9)$$

We define the expected limit by taking the median value of the iterated pseudo-experiment. We try to calculate the expected limit with each b-tag condition (double SECVTX tag, one SECVTX tag + Jet probability tag and one SECVTX tag w/ NN tag and two double tag combiend limit and limit combined all three tagging categories). The limit of "combined all tagging categories" are obtained by combining the three likelihood of L($\sigma|$ ST+ST), L($\sigma|$ST+JP) and L($\sigma|$ one tag w/ NNtag) as

$$L(\sigma) = L(\sigma|\text{ST+ST}) \times L(\sigma|\text{ST+JP}) \times L(\sigma|\text{1tag w/ NNtag})$$

where the correlation between b-tag categories is taken into account properly. The systematic uncertainty up to the pretag acceptance, luminosity uncertainty and uncertainty of SECVTX b-tag scale factor and Jet probability scale factor are considered to be 100% correlated between the three selection criteria.

Mass/b-tagging category	ST + ST	ST + JP	One SECVTX w/ NNtag
110 GeV	1.73 (10.7)	2.28 (14.1)	3.23 (19.9)
115 GeV	1.73 (13.1)	2.23 (16.2)	3.08 (23.4)
120 GeV	1.48 (14.5)	1.98 (19.4)	2.58 (25.2)
130 GeV	1.28 (20.4)	1.68 (26.8)	2.38 (38.1)
140 GeV	1.18 (38.4)	1.53 (49.8)	1.93 (62.9)
150 GeV	1.13 (95.9)	1.38 (117.0)	1.68 (142.8)

Table 12: This table shows upper limit using NN shape fitting for each mass point and each tagging category. The values in parentheses mean upper limit normalized to SM expectation

Mass/b-tagging category	ST +ST & ST + JP	1tag & 2tag
110 GeV	1.33 (8.2)	1.23 (7.6)
115 GeV	1.28 (9.7)	1.18 (8.9)
120 GeV	1.18 (11.5)	1.03 (10.0)
130 GeV	0.98 (15.6)	0.88 (14.0)
140 GeV	0.93 (30.2)	0.78 (25.3)
150 GeV	0.83 (70.3)	0.73 (61.8)

Table 13: This table shows combined upper limit using NN shape fitting for each mass point. The values in parentheses mean upper limit normalized to SM expectation

9.2 Expected Limit Result

We check the expected upper limit and decide the best limit a priori. Figure 46 shows upper limit on the production cross section times branching ratio. Figure 47 shows upper limit normalized to SM cross section times branching ratio. Double SECVTX events has the best sensitivity in each one tagging category. Finally the best upper limit is obtained from the combined 1tag and 2 tag. Table 12 shows the expected limit obtained from selected tagging category for each Higgs mass. Table 13 shows the expected limit obtained from combination of selected tagging category for each Higgs mass. According to table, the gain by including 1tag w/ NN tag is 10% level.

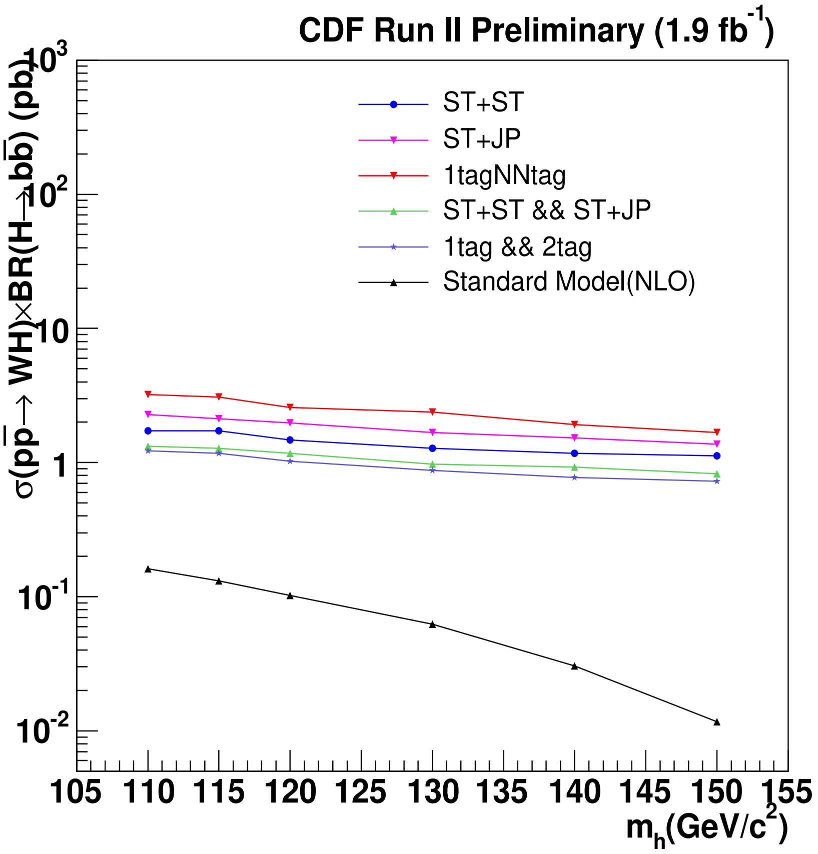

Figure 46: The 95% C.L. upper limit using the dijet invariant mass only estimated from pseudo experiments. Each color means each b-tagging strategy.

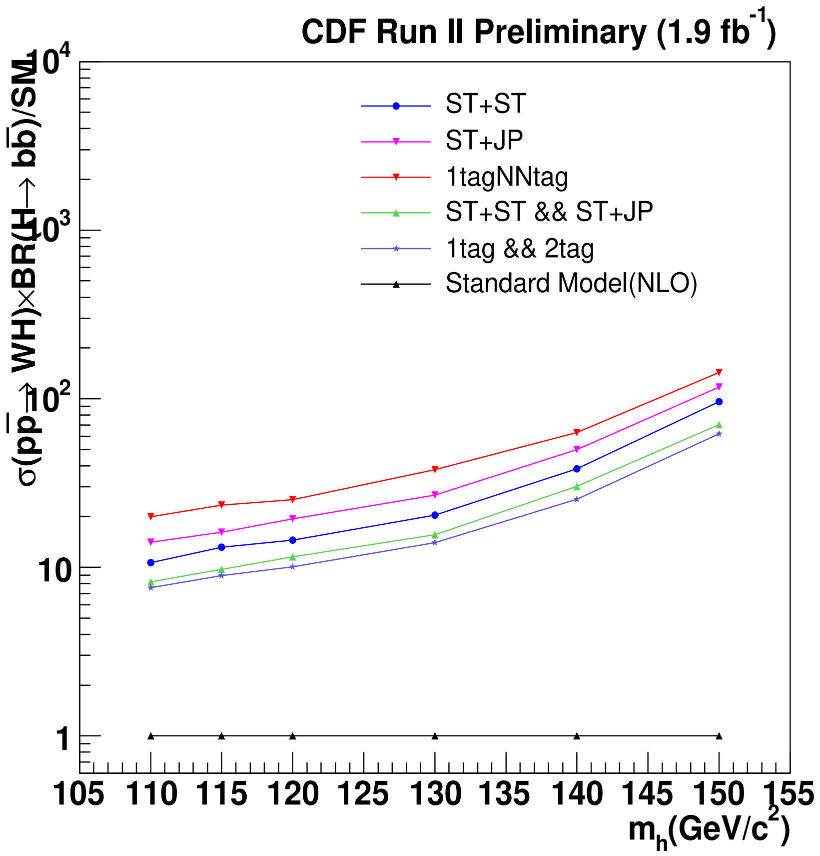

Figure 47: The ratio of 95% C.L. upper limit using the dijet invariant mass only to SM expectation. These values are estimated from pseudo experiments for each b-tagging strategy.

Figures 48-52 show distribution of 95% C.L. upper limit results from one thousand pseudo-experiments. The median of these distribution is quoted as the central value for the expected limit and the RMS provides the 1 σ uncertainty band.

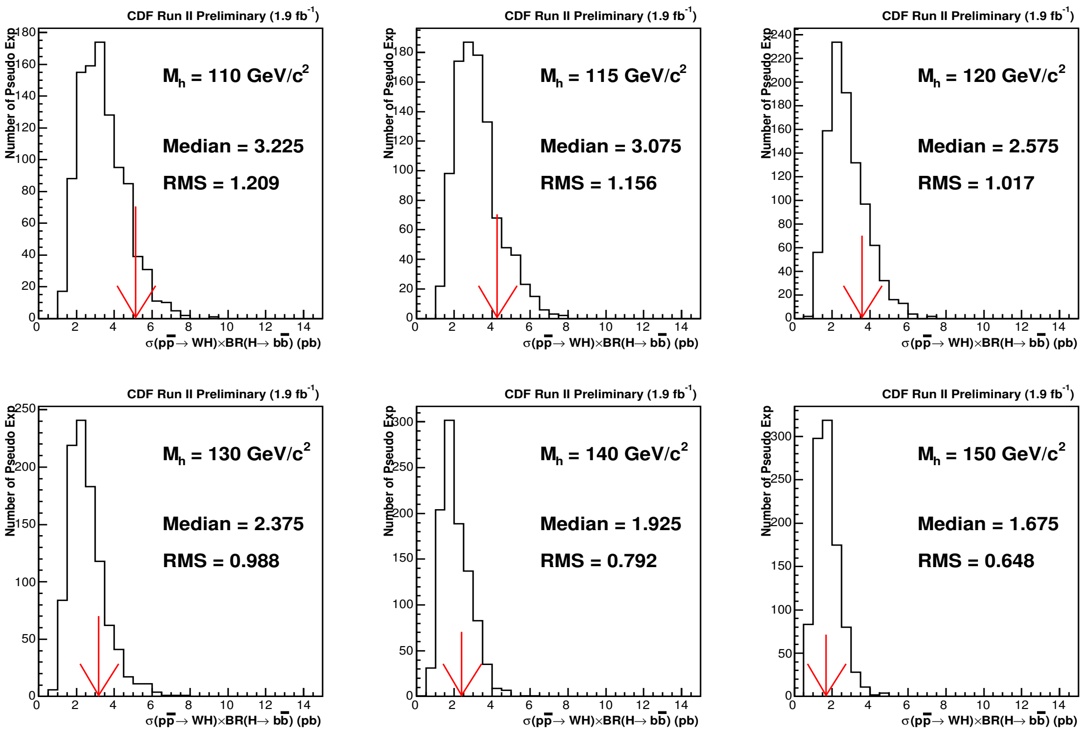

Figure 48: The results using NN output for one SECVTX tag w/ NNtag with one thousand pseudo experiments for each Higgs mass. The results show 95% C.L. upper limit for each pseudo experiment. The red arrow means the observed upper limit.

9.3 Observed limit

9.4 Neural Network Observed Limits

Figure 53 shows observed 95% C.L upper limit combined 1tag and 2tag for WH production cross section. Our observed limit is reasonable compared to pseudo experiment results. Figure 54 shows observed 95% C.L. upper limit for each tag cateogry. The observed limit for each tag category are good agreement to expected limit. In Table 15, the absolute and normalized by SM value of Observed limit values are shown.

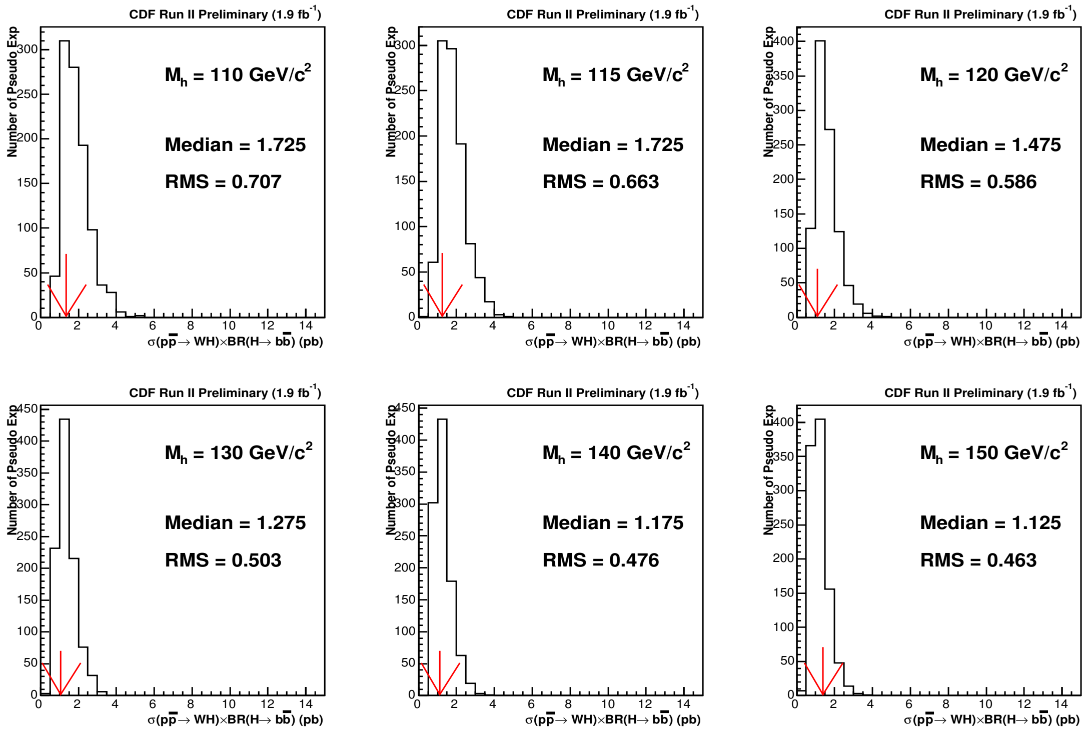

Figure 49: The results using NN output for double SECVTX tag with one thousand pseudo experiments for each Higgs mass. The results show 95% C.L. upper limit for each pseudo experiment. The red arrow means the observed upper limit.

Mass/b-tagging category	ST + ST	ST + JP	one tag w/ NNtag
110 GeV	1.43 (8.8)	2.18 (13.5)	5.13 (31.7)
115 GeV	1.33 (10.1)	2.48 (18.8)	4.28 (32.5)
120 GeV	1.13 (11.0)	2.18 (21.3)	3.63 (35.5)
130 GeV	1.08 (17.2)	2.23 (35.6)	3.18 (50.9)
140 GeV	1.18 (38.4)	1.78 (58.0)	2.43 (79.2)
150 GeV	1.43 (121.5)	1.63 (138.5)	1.73 (147.1)

Table 14: This table shows observed upper limit using NN shape fit for each mass point and each tagging category. The values in parentheses mean upper limit normalized to SM expectation

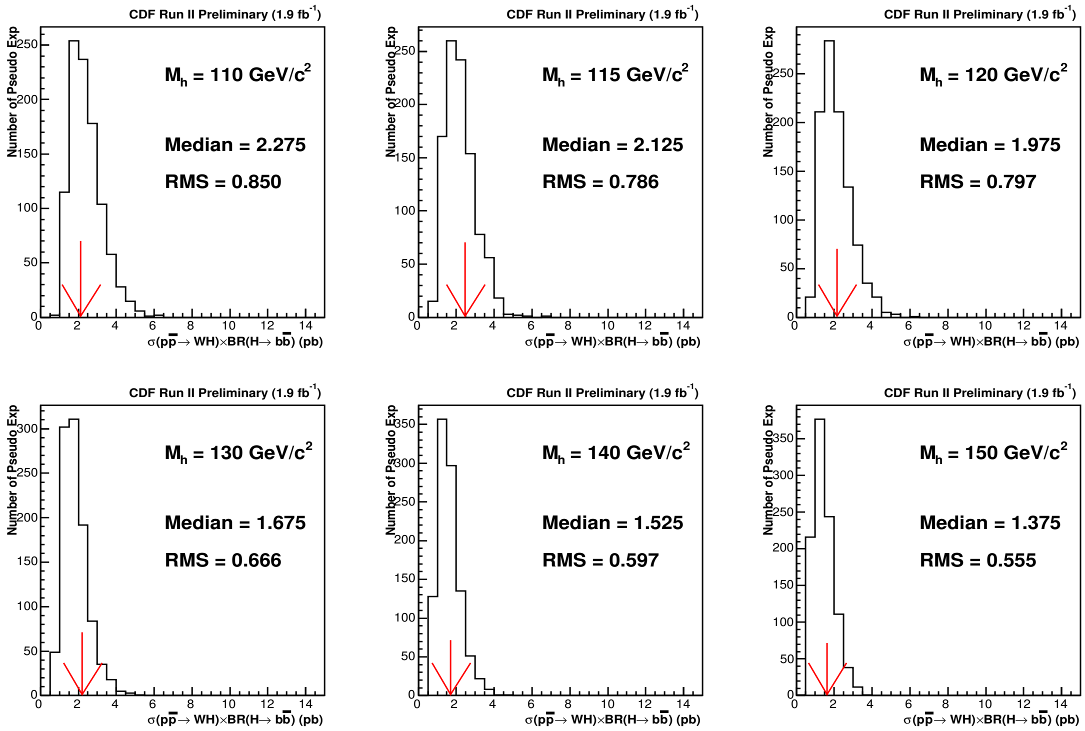

Figure 50: The results using NN output for one SECVTX tag plus Jet Probability tag with one thousand pseudo experiments for each Higgs mass. The results show 95% C.L. upper limit for each pseudo experiment. The red arrow means the observed upper limit.

Mass/b-tagging category	ST +ST & ST + JP	1tag & 2tag
110 GeV	1.13 (7.0)	1.38 (8.5)
115 GeV	1.23 (9.3)	1.28 (9.7)
120 GeV	0.98 (9.6)	1.08 (10.5)
130 GeV	0.98 (15.6)	1.08 (17.2)
140 GeV	0.98 (31.9)	0.98 (31.9)
150 GeV	1.08 (91.6)	0.93 (78.9)

Table 15: This table shows observed upper limit using NN shape fit for each mass point and each tagging category. The values in parentheses mean upper limit normalized to SM expectation

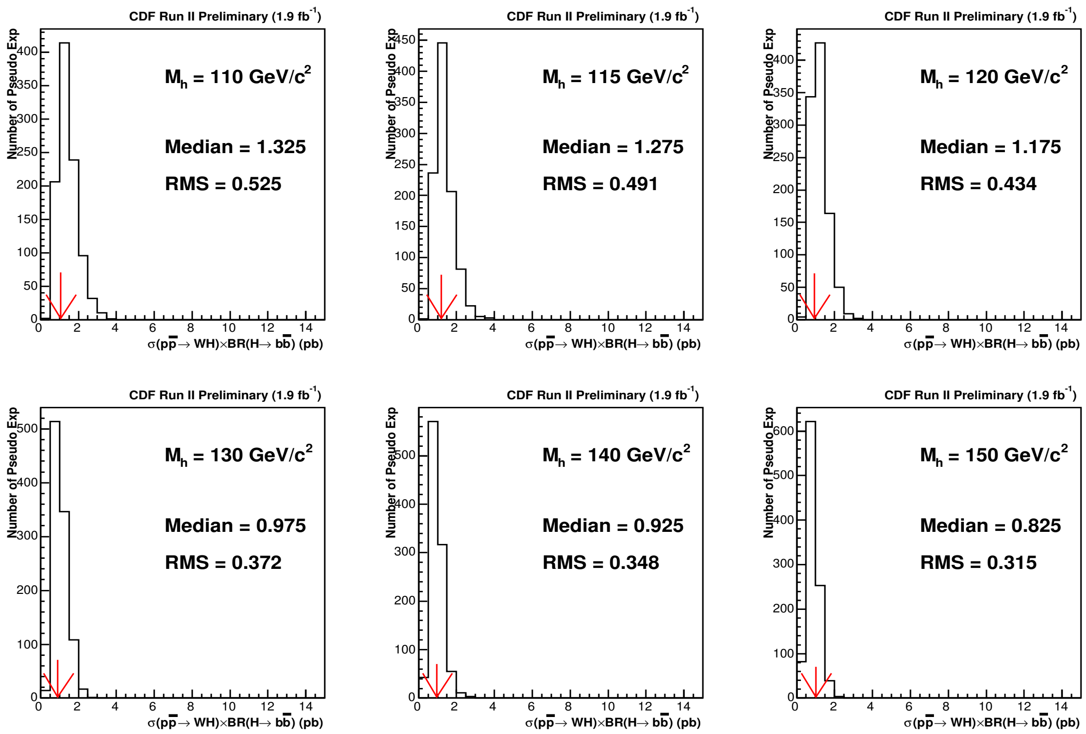

Figure 51: The results using NN output for the combination of ST+ST and ST+JP with one thousand pseudo experiments for each Higgs mass. The results show 95% C.L. upper limit for each pseudo experiment. The red arrow means the observed upper limit.

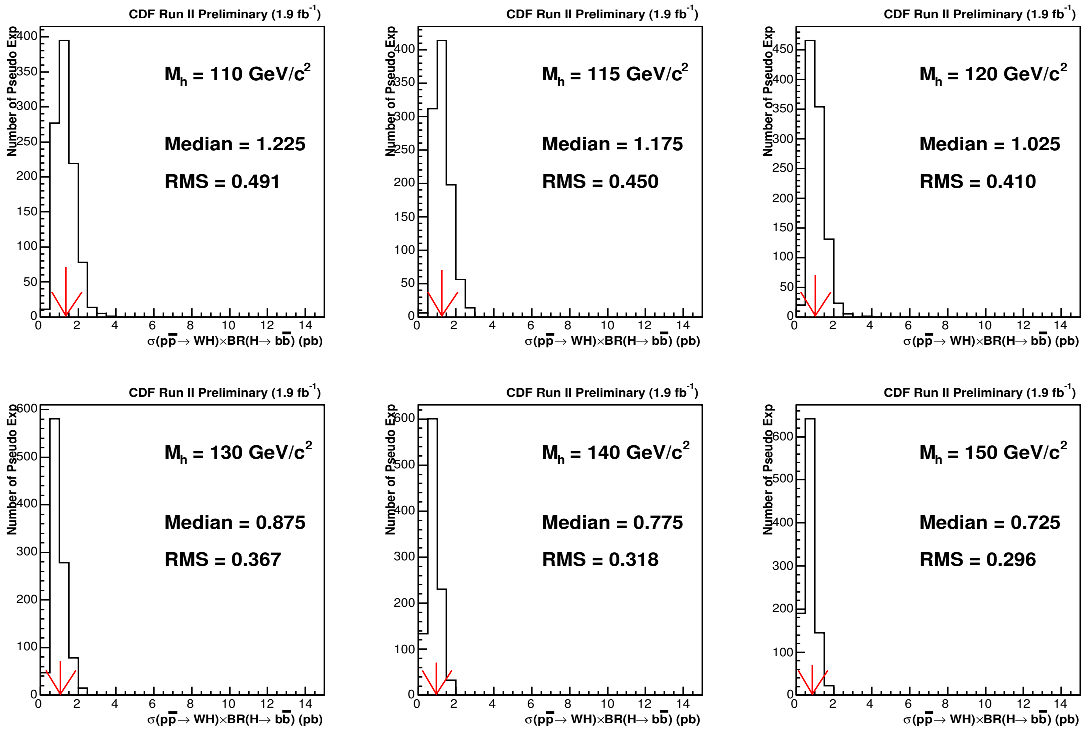

Figure 52: The results using NN output for the combination of 1tag and 2tag with one thousand pseudo experiments for each Higgs mass. The results show 95% C.L. upper limit for each pseudo experiment. The red arrow means the observed upper limit.

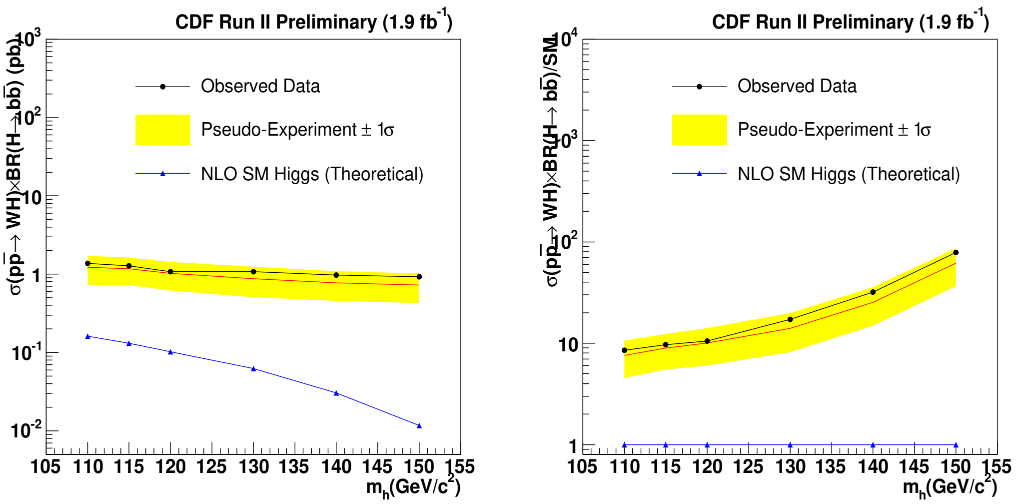

Figure 53: Observed limit calculated from NN shape. This plot shows double tight SECVTX and one tight SECVTX + jet probability combined results

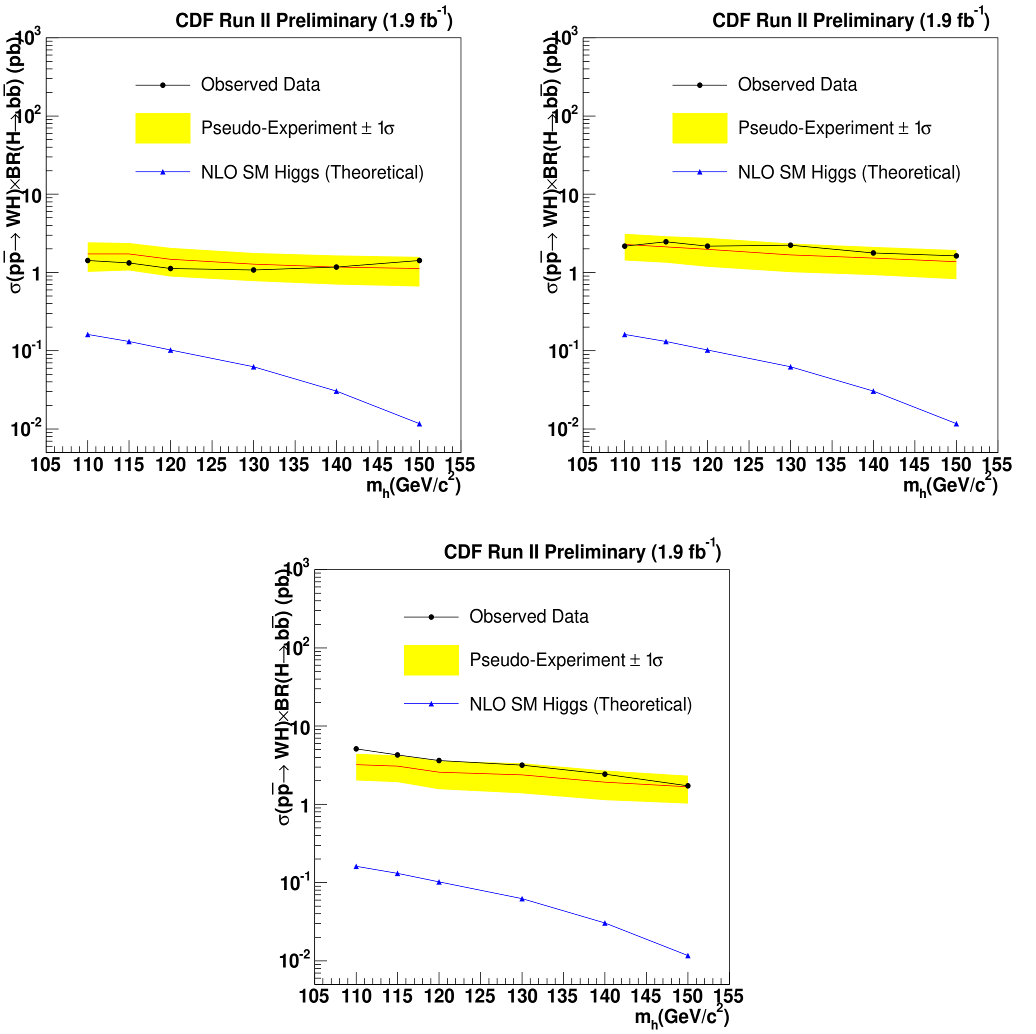

Figure 54: Observed limit calculated from NN shape for each tagging category

10 PHX Plug Electron

In this section we describe two independent analyses that use PHX plug electron to increase lepton acceptance for the WH search. The first analysis is mostly based on the standard single-top analysis [18] and the second analysis is using top-like selection, the same search strategies that used for the central lepton. At the end, we will choose one with the best search sensitivity based on the pseudo-experiments and combine it with the rest of WH results.

10.1 Selection of PHX Events

We require an electron triggered with the MET_PEM trigger and a Phoenix track (at least 3 r-ϕ hits in the silicon and no z or stereo signal). For missing transverse energy we demand a tighter cut with $\not{E}_T$ >25 GeV after level 5 correction. The events have to have two tight jets with $|\eta_{Detector}| < 2.8$ for the single-top type analysis or $|\eta_{Detector}| < 2.0$ for top-like analysis.
To reduce the fraction of QCD originating events, we apply the following cuts:

- $MET_{sig} > 2.0$
- For the first two leading jets $\not{E}_T > 45 - 30 \cdot |\Delta\phi|$, where $\Delta\phi$ is the azimuthal angle between $\vec{\not{E}}_T$ and the respective jet.
- If we have only one selected jet (control region), this requirement reduces to $\not{E}_T > 45 - 30 \cdot |\Delta\phi|$, where $\Delta\phi$ is the angle between $\vec{\not{E}}_T$ and the solely selected jet.

Here MET_{sig} is defined as:

$$MET_{sig} := \frac{\not{E}_T}{\sqrt{\sum_{jets} C_{JES}^2 \cos^2(\Delta\phi_{jet,MET}) + \cos^2(\Delta\phi_{vtx,corr})}} \tag{10}$$

Here C_{JES} is the level 5 jet energy correction factor; $\Delta\phi_{vtx,corr}$ is the azimuthal angle between corrected and uncorrected missing transverse energy.
The transverse W mass is calculated via:

$$M_{T,W} = \sqrt{2p_T^{lep}\not{E}_T - \vec{p}_T^{\,lep} \cdot \vec{\not{E}}_T}, \tag{11}$$

where p_T^{lep} is the transverse momentum of the charged lepton.
Due to the different shapes of the non-W and the other backgrounds in the missing transverse energy distribution, it is possible to fit the non-W model and the combined remaining Monte Carlo samples to the data to determine the fraction of QCD events in the observed data. Here the PHX Monte Carlo samples have to be weighted with the trigger turn-on curve [19]. The acceptance of the three trigger stages of the PHX trigger depends on the uncorrected missing transverse energy $\not{E}_T^{\mathrm{raw}}$ and the transverse momentum of the electron E_T^{ele}. For low values

the trigger has a reduced acceptance, which is not considered in the Monte Carlo samples. Therefore all Monte Carlo generated events are weighted with the following factor:

$$w(\eta) = \sum_{\text{period } i} f_i \cdot \frac{1}{1+e^{-\beta_1^i(\not{E}_T^{\text{raw}}-\alpha_1^i)}} \cdot \frac{1}{1+e^{-\beta_2^i(\eta)(E_T^{\text{ele}}-\alpha_2^i(\eta))}} \cdot \frac{1}{1+e^{-\beta_3^i(E_T^{\text{ele}}-\alpha_3^i)}} \qquad (12)$$

Here every factor models the turn-on curve of one of the three trigger levels (L1_MET15_L3 (1), L2_PEM20 (2) and L3_PEM20 (3)). The sum runs over the different periods of data acquisition (0d to mj), f_i is the luminosity fraction of period i. The turn-on parameters of period 0h are extrapolated to the 0d data range, for mi and mj the parametrization of period 0i is used. The parameters of the L2_PEM20 depend on η_{lep} and can be found in [19], the parameters for L1_MET15_L3 and L3_PEM20 are also taken from [19] and are listed in table 16.

	L1_MET15_L3	L3_PEM20
α^{0h}	14.79 GeV	21.46 GeV
β^{0h}	0.37 GeV^{-1}	0.42 GeV^{-1}
α^{0i}	14.00 GeV	20.91 GeV
β^{0i}	0.37 GeV^{-1}	1.66 GeV^{-1}

Table 16: parameters for the PHX turn-on curve

A likelihood fit to the $\not{E}_T$ distribution is performed. From this fit we can conclude the QCD fraction in the final selection by integrating the fitted distributions of the non-W model and the Monte Carlo samples above 25 GeV and determining the ratios of the integrals. The fit range includes the $\not{E}_T$ distribution from 15 to 100 GeV and one overflow bin for all events with $\not{E}_T >$100 GeV. In figure 55 the results of the fits for the sample with two selected jets are shown using the jet-electron sample as QCD model. The jet-electron model uses data, which have been selected with a jet trigger. We require events with a jet fulfilling $E_T > 20$ GeV and $0.05 < E_{HAD}/E_{EM} < 0.2$ as well as at least four reconstructed tracks. We hope to reject events with real electrons or muons and to keep only events consisting of QCD processes using this trigger. Since we need QCD events faking an electron or muon, we take this data sample and assign one jet per event to be a misidentified lepton. The charge and the flavor, i.e electron or muon, of this faked lepton is chosen randomly.
In addition the fits are also performed without including the QCD veto. As can be seen, it is impossible to describe the $\not{E}_T$ distribution without the QCD veto under the assumption, that the jet-electron sample models the QCD background correctly. From the bad agreement between data and model it is also unfeasible to determine the fraction of QCD events in the selected data. Applying the QCD veto, we find a good fit result and a describable non-W background.
The acceptance and the number of expected events for the W-Higgs process (see table 17) is calculated similarly to the explanation in section 5.1. The trigger efficiencies for the PHX trigger are taken from [19], the lepton identification/reconstruction scale factors has been

calculated in [20]. The background estimations for the two categories with one respectively two SECVTX b-tags are shown in tables 18 and 19.

As a cross check, we have performed the search with slight different event selection criteria as described above. The events have to have two tight jets with $|\eta_{Det}| < 2.0$ with $E_T > 20$ GeV after jet energy correction at L5 and both of them are required to be b-tagged by SECVTX-SECVTX or SECVTX-JetPrb. The final acceptance and expected number of events are shown in table 20. The data and expected backgrounds events are shown in table 21-24 for different btag categories (at least one SECVTX, one SECVTX tag w/ NNtag, SECVTX-SECVTX and SECVTX-JetPrb). Overall, there is a good agreement between two analyses.

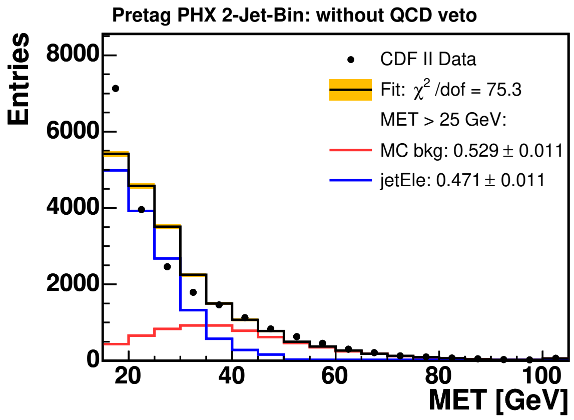

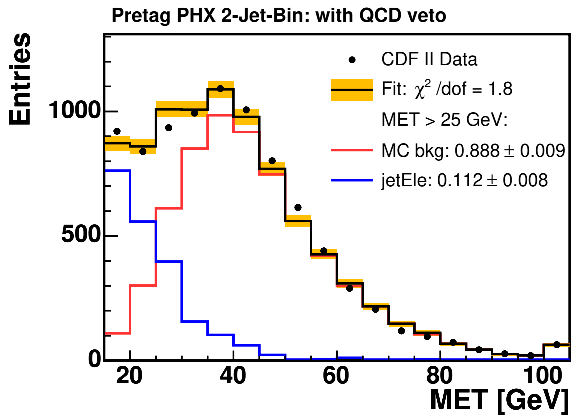

Figure 55: $\not{E}_T$ fits without (left) and with QCD veto (right) in the pretag sample with two tight jets

category	110 GeV	115 GeV	120 GeV	130 GeV
one tag	0.48	0.40	0.31	0.19
two tags	0.12	0.12	0.09	0.07

Table 17: Number of expected signal events in the 2-jet bin

Process	1jet	2jets	3jets	4jets	5jets
WW	2.1 ± 0.2	5.3 ± 0.6	1.5 ± 0.2	0.4 ± 0.0	0.1 ± 0.0
WZ	1.4 ± 0.1	2.6 ± 0.2	0.7 ± 0.1	0.1 ± 0.0	0.0 ± 0.0
ZZ	0.0 ± 0.0	0.0 ± 0.0	0.0 ± 0.0	0.0 ± 0.0	0.0 ± 0.0
TopLJ	0.6 ± 0.1	5.9 ± 1.2	16.1 ± 3.4	17.8 ± 3.7	4.9 ± 1.0
TopDil	0.6 ± 0.1	3.1 ± 0.6	2.3 ± 0.5	0.4 ± 0.1	0.1 ± 0.0
STopT	2.4 ± 0.4	5.2 ± 0.8	1.3 ± 0.2	0.2 ± 0.0	0.0 ± 0.0
STopS	0.8 ± 0.1	2.4 ± 0.3	0.7 ± 0.1	0.1 ± 0.0	0.0 ± 0.0
Z+jets	1.4 ± 0.2	1.1 ± 0.2	0.5 ± 0.1	0.1 ± 0.0	0.0 ± 0.0
Wbb	99.2 ± 35.0	64.1 ± 22.6	20.4 ± 7.2	4.2 ± 1.5	2.0 ± 0.7
Wcc/Wc	185.5 ± 66.8	71.9 ± 25.8	19.9 ± 7.2	3.9 ± 1.4	1.9 ± 0.7
Mistags	148.7 ± 19.9	55.3 ± 7.8	16.4 ± 2.6	3.5 ± 0.7	1.4 ± 0.3
Non-W	10.3 ± 4.1	12.3 ± 4.9	4.3 ± 1.7	1.7 ± 0.7	0.0 ± 0.0
Total Prediction	453.1 ± 103.6	229.5 ± 49.1	84.3 ± 15.1	32.5 ± 4.8	10.6 ± 1.8
Observed	468.0 ± 0.0	240.0 ± 0.0	89.0 ± 0.0	35.0 ± 0.0	11.0 ± 0.0

Table 18: background estimation for 1tag

Process	1jet	2jets	3jets	4jets	5jets
WW	0.0 ± 0.0	0.0 ± 0.0	0.0 ± 0.0	0.0 ± 0.0	0.0 ± 0.0
WZ	0.0 ± 0.0	0.6 ± 0.1	0.1 ± 0.0	0.0 ± 0.0	0.0 ± 0.0
ZZ	0.0 ± 0.0	0.0 ± 0.0	0.0 ± 0.0	0.0 ± 0.0	0.0 ± 0.0
TopLJ	0.0 ± 0.0	1.1 ± 0.2	4.6 ± 1.0	7.0 ± 1.6	2.1 ± 0.5
TopDil	0.0 ± 0.0	1.0 ± 0.2	0.9 ± 0.2	0.2 ± 0.0	0.0 ± 0.0
STopT	0.0 ± 0.0	0.2 ± 0.0	0.2 ± 0.0	0.1 ± 0.0	0.0 ± 0.0
STopS	0.0 ± 0.0	0.7 ± 0.1	0.2 ± 0.0	0.1 ± 0.0	0.0 ± 0.0
Z+jets	0.0 ± 0.0	0.0 ± 0.0	0.0 ± 0.0	0.0 ± 0.0	0.0 ± 0.0
Wbb	0.0 ± 0.0	7.9 ± 2.8	3.1 ± 1.1	0.8 ± 0.3	0.4 ± 0.1
Wcc/Wc	0.0 ± 0.0	1.0 ± 0.4	0.5 ± 0.2	0.2 ± 0.1	0.1 ± 0.0
Mistags	0.0 ± 0.0	0.2 ± 0.1	0.2 ± 0.0	0.1 ± 0.0	0.0 ± 0.0
Non-W	0.0 ± 0.8	0.2 ± 0.1	0.3 ± 0.1	0.1 ± 0.0	0.0 ± 0.0
Total Prediction	0.0 ± 0.0	12.9 ± 3.3	10.2 ± 1.7	8.5 ± 1.6	2.7 ± 0.5
Observed	0.0 ± 0.0	10.0 ± 0.0	11.0 ± 0.0	10.0 ± 0.0	4.0 ± 0.0

Table 19: background estimation for 2 or more tags

Higgs Mass (GeV)	110	115	120	130
At least one SECVTX b-tag				
ϵ (%)	0.186± 0.011	0.196± 0.011	0.198± 0.011	0.198± 0.011
Signal (Ev)	0.578± 0.033	0.493± 0.028	0.387± 0.022	0.237± 0.014
Exact one SECVTX b-tag w/ NN tag				
ϵ (%)	0.102± 0.004	0.099± 0.004	0.102± 0.004	0.099± 0.004
Signal (Ev)	0.317± 0.012	0.249± 0.009	0.199± 0.007	0.118± 0.004
Double SECVTX-SECVTX b-tag				
ϵ (%)	0.039± 0.003	0.047± 0.004	0.046± 0.004	0.049± 0.004
Signal (Ev)	0.121± 0.011	0.119± 0.010	0.090± 0.008	0.059± 0.005
Double SECVTX-JetPrb b-tag				
ϵ (%)	0.029± 0.003	0.032± 0.004	0.032± 0.003	0.031± 0.003
Signal (Ev)	0.090± 0.010	0.081± 0.009	0.062± 0.007	0.038± 0.004

Table 20: The acceptance and Number of expected signal events in the 2-jet bin with top-like selection.

Njet	1jet	2jet	3jet	>=4jet
Pretag Events	39942	5879	1010	202
Mistag	140.3±6.89	47.98±3.76	12.13±1.64	2.29±0.85
$Wb\bar{b}$	110.6±57.4	66.50±19.02	18.70±5.41	3.40±1.18
$Wc\bar{c}$	196.2±99.8	61.09±17.48	15.47±4.47	2.72±0.94
$t\bar{t}$(6.7pb)	1.52±0.23	12.28±1.81	25.52±3.75	34.01±4.99
Single top(s-ch)	1.05±0.15	3.03±0.42	0.87±0.12	0.21±0.03
Single top(t-ch)	4.26±0.60	4.40±0.62	1.15±0.16	0.26±0.04
WW	2.42±0.21	5.07±0.38	1.32±0.13	0.51±0.07
WZ	1.59±0.12	3.14±0.21	0.83±0.07	0.18±0.02
ZZ	0.01±0.00	0.03±0.01	0.01±0.00	0.01±0.00
$Z->\tau\tau$	0.86±0.11	0.56±0.07	0.22±0.03	0.06±0.01
nonW QCD	29.39±10.89	29.78±8.92	12.44±5.73	5.70±4.51
Total Bkg	488.2±115.9	233.9±27.7	88.66±9.94	49.35±6.95
WH signal (120 GeV)	Control region	0.39±0.02	Control region	Control region
Observed Events	487	232	94	54

Table 21: Background summary table of PHX for at least one tag category

Njet	1jet	2jet	3jet	>=4jet
Pretag Events	39942	5879	1010	202
Mistag	91.19±8.32	28.47±3.30	6.48±1.20	0.78±0.60
$Wb\bar{b}$	98.10±50.81	43.09±12.33	10.74±3.10	1.79±0.62
$Wc\bar{c}$	116.9±49.6	33.37±9.55	7.90±2.28	1.21±0.42
$t\bar{t}$(6.7pb)	1.36±0.20	7.17±1.00	12.30±1.71	13.89±1.93
Single top(s-ch)	0.96±0.13	1.53±0.20	0.41±0.05	0.09±0.01
Single top(t-ch)	3.88±0.51	3.54±0.47	0.73±0.10	0.12±0.02
WW	1.23±0.12	3.00±0.20	0.74±0.09	0.14±0.04
WZ	1.38±0.08	1.62±0.09	0.43±0.04	0.08±0.02
ZZ	0.01±0.00	0.02±0.00	0.01±0.00	0.00±0.00
$Z->\tau\tau$	0.43±0.05	0.24±0.03	0.11±0.01	0.03±0.00
nonW QCD	18.76±6.98	18.34±5.54	5.54±2.59	3.18±2.53
Total Bkg	334.2±71.8	140.4±16.9	45.39±5.09	21.31±3.33
WH signal (120 GeV)	Control region	0.20±0.01	Control region	Control region
Observed Events	299	136	48	25

Table 22: Background summary table of PHX for one tag w/ NNtag category

Njet	2jet	3jet	>=4jet
Pretag Events	5879	1010	202
Mistag	1.00±0.18	0.46±0.06	0.35±0.15
$Wb\bar{b}$	7.40±3.96	2.34±1.15	0.47±0.26
$Wc\bar{c}$	0.96±0.49	0.33±0.37	0.07± 0.03
$t\bar{t}$(6.7pb)	2.14±0.34	5.69±0.89	9.11± 1.43
Single top(s-ch)	0.69±0.10	0.22±0.03	0.06± 0.01
Single top(t-ch)	0.22±0.04	0.18±0.03	0.06± 0.01
WW	0.01±0.01	0.03±0.02	0.02± 0.01
WZ	0.58±0.06	0.12±0.02	0.04± 0.01
ZZ	0.00±0.00	0.00±0.00	0.00±0.00
$Z->\tau\tau$	0.00±0.00	0.00±0.00	0.00±0.00
nonW QCD	1.16±0.44	0.96±0.50	0.51±0.44
Total Bkg	14.18±4.03	10.32±1.58	10.67± 1.52
WH signal (120 GeV)	0.09±0.01	Control region	Control region
Observed Events	11	12	11

Table 23: Background summary table of PHX for double SECVTX tag category

Njet	2jet	3jet	>=4jet
Pretag Events	5879	1010	202
Mistag	3.18±0.49	1.71±0.33	0.74± 0.29
$Wb\bar{b}$	6.23±3.37	2.00±0.99	0.45±0.24
$Wc\bar{c}$	1.53±0.81	0.76±0.38	0.21± 0.11
$t\bar{t}$(6.7pb)	1.79±0.31	4.72±0.80	7.03± 1.19
Single top(s-ch)	0.51±0.08	0.16±0.03	0.04± 0.01
Single top(t-ch)	0.24±0.04	0.16±0.03	0.05± 0.01
WW	0.12±0.03	0.10±0.03	0.07± 0.02
WZ	0.42±0.05	0.13±0.02	0.03± 0.01
ZZ	0.01±0.00	0.00±0.00	0.00±0.00
$Z->\tau\tau$	0.01±0.00	0.01±0.00	0.01±0.00
nonW QCD	1.51±0.55	1.78±0.88	0.79±0.67
Total Bkg	15.54±3.56	11.53±1.63	9.43± 1.42
WH signal (120 GeV)	0.06±0.01	Control region	Control region
Observed Events	12	10	10

Table 24: Background summary table of PHX for one SECVTX tag + Jet Probability tag category

10.2 Neural Network Discriminant in PHX

To gain a variable, which discriminates the Higgs signal form the background, we train a neural network using the NeuroBayes® package [21].

1. $M_{b\bar{b}}$, the invariant mass of the reconstructed Higgs boson. For the W-Higgs process we expect all events to lie around the assumed mass of the Higgs boson. In events including top quarks the invariant mass of the two b quarks has a maximum at higher values, since the b quarks originates from heavy massive t quark decays, whereas for W+jets the distribution of this variable has a lower maximum than for Higgs events.
2. neuro-Tag 1, the output of the neural network flavor separator [22] for the jet with highest E_T. This variable is taken only into account if the jet with highest E_T has a secondary vertex b tag. The flavor separator distinguishes events with jets originating from b quark production from events with c or light quarks. For the Higgs the flavor separator can only divide mistag and $W + c/W + c\bar{c}$ events from the signal, $W + b\bar{b}$ and top quark production looks similar to the Higgs events in this variable.
3. neuro-Tag 2, the output of the neural network flavor separator for the jet with lowest E_T. This variable is taken only into account if the jet with lowest E_T has a secondary vertex b tag.
4. $\sum_{jets} E_{T,jet}$, the scalar sum of all tight jets.
5. $E_{T,b}$, the transverse energy of the reconstructed b quark four vector with the highest neural network b tagger output.
6. $P_{T,b}$, the transverse momentum of the quark with the highest neural network b tagger output.
7. M_{min}, the invariant mass of the jet with lowest energy (correction level 7).
8. M_{max}, the invariant mass of the jet with highest energy (correction level 7).
9. $P_{T,min}$, the transverse momentum of the jet with lowest energy.
10. $P_{T,W}$, the transverse momentum of the reconstructed W boson.
11. $Q \cdot \eta_{lep}$, the product of the charge and the pseudo rapidity of the lepton. Multiplying the pseudo rapidity with the lepton charge symmetrizes this distribution.
12. $\eta_{2^{nd}b}$, the pseudo rapidity of the b quark four vector of the jet with lowest neural network b tagger output (if both jets are b tagged) or respectively of the jet without b tag.
13. $\Delta\phi_{H,W}$, the azimuthal angle between the Higgs and the W boson.
14. $\Delta\phi_{MET,lep}$, the azimuthal angle between the missing transverse energy direction and the lepton vector.

15. M_{W^*}, the invariant mass of the reconstructed W boson before Higgs radiation.

16. $\not{E}_T \sin(\Delta\phi_{min})$, where $\Delta\phi_{min}$ is the angle between $\vec{\not{E}}_T$ and the closest object in the x-y-plane. This quantity is highly correlated to $\not{E}_T$, but it takes also the isolation of the neutrino into account and shows a slightly more significant discrimination than the $\not{E}_T$ solely.

17. $\Delta R_{b\bar{b}}$ the distance in the η-ϕ-plane of the two reconstructed quark vectors.

18. $M_{l\nu b}$, which corresponds to the invariant top mass if the we have a single top or top-antitop event.

19. $P_{T,H}$, the transverse momentum of the Higgs boson.

20. H_T, the scalar sum of the P_T of all jets, lepton and neutrino.

21. $\log(A)$, where A is the aplanarity which is given by $A := \frac{3}{2}Q_1$. Here Q_1 is the smallest eigenvalue of the sphericity tensor S_{ij}. The components of the sphericity tensor are given by:

$$S_{ij} := \frac{\sum_{k=1}^{N} p_i^k p_j^k}{\sum_{k=1}^{N} |p^k|^2} \tag{13}$$

where i and j denote the coordinates x, y and z, and the sum goes over all N particles of the event, i.e. in our case two jets, charged lepton and neutrino. The sphericity tensor describes an ellipsoid with the aplanarity as the smallest elongation in the direction of one of the three principle axes. Therefore the aplanarity indicates the flatness of the momentum distribution of an event.

We overall considered about 50 further variables, but we only took variables into account, which are described well by the background model in the b tagged as well as in the pretag sample and which provide a significant discrimination between signal and background. For the final selection of variables we use the automatic variable selection of the NeuroBayes® package. The chosen topology for all networks contains, besides the nodes for the selected variables, one bias node in the first layer. The second layer is filled with twelve nodes. We also trained networks with a different number of secondary nodes, but the training result was very stable under this variation. In the third and final layer we have one node, since we want the network only to deliver a probability for every event to be Higgs- or background-like.
The final used variables differ for each trained network. For the two networks trained to separate Higgs events with a mass of 120 GeV, the input variables selected by the automatic variable selection their impacts to the final output are listed in tables 25 and 26.
The outputs of the two neural networks for the different backgrounds as well as for the W-Higgs signal with m_H=120 GeV are shown in figures 56 and 57. The plots 58 to 70 show the comparison between data and background model for important network input variables in the tagged and in the pretag sample.

ranking	variable	correlation to target in%	in σ
1	$M_{b\bar{b}}$	52.9	62.8
2	neuro-Tag 1	18.9	22.4
3	$P_{T,min}$	16.6	19.8
4	neuro-Tag 2	12.5	14.9
5	$\sum_{jets} E_{T,jet}$	7.6	9.0
6	$\eta_{2^{nd}b}$	6.8	8.1
7	$\Delta R_{b\bar{b}}$	4.7	5.6
8	M_{max}	3.2	3.8
9	M_{min}	2.5	2.9
10	$P_{T,b}$	0.6	0.7
11	$E_{T,b}$	3.3	3.9
12	$\not{E}_T \sin(\Delta\phi_{min})$	3.3	3.9
13	$\log(A)$	2.8	3.4

Table 25: Input variables for the 1-tag network

ranking	variable	correlation to target in%	in σ
1	$M_{b\bar{b}}$	61.3	41.0
2	$P_{T,min}$	7.8	5.2
3	$\eta_{2^{nd}b}$	7.5	5.0
4	$\not{E}_T \sin(\Delta\phi_{min})$	7.1	4.8

Table 26: Input variables for the 2-tag network

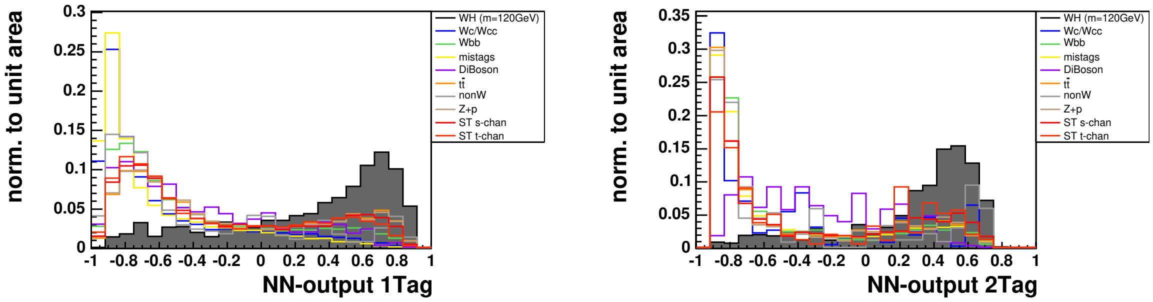

Figure 56: The neural network templates for the different processes

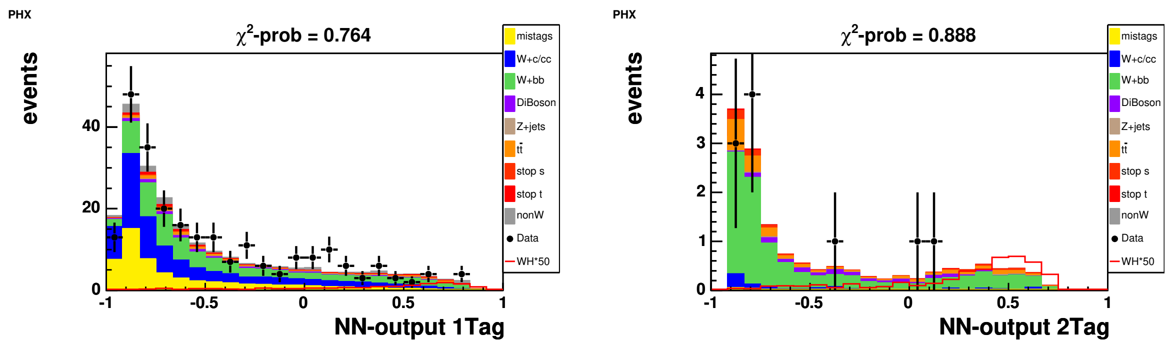

Figure 57: The output of the neural networks

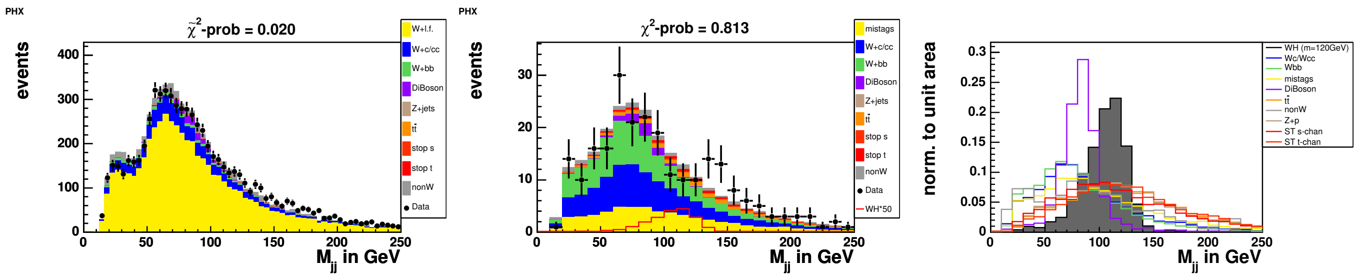

Figure 58: The invariant mass of the two quarks for the pretag (right) and tagged (center) sample and the shape comparison in the tagged sample (right)

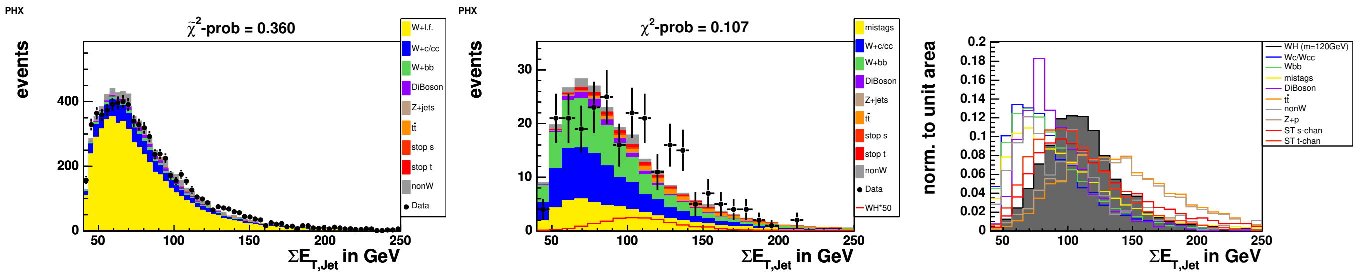

Figure 59: The scalar sum of the transverse energy of all jets

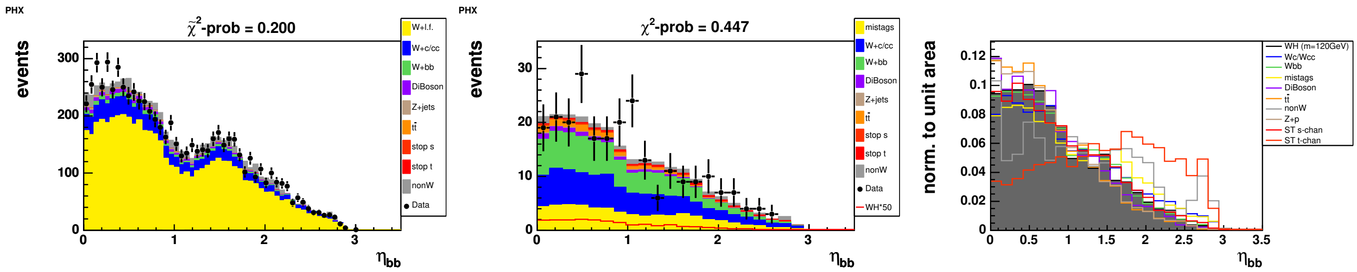

Figure 60: The pseudo rapidity of the 2^{nd} leading jet

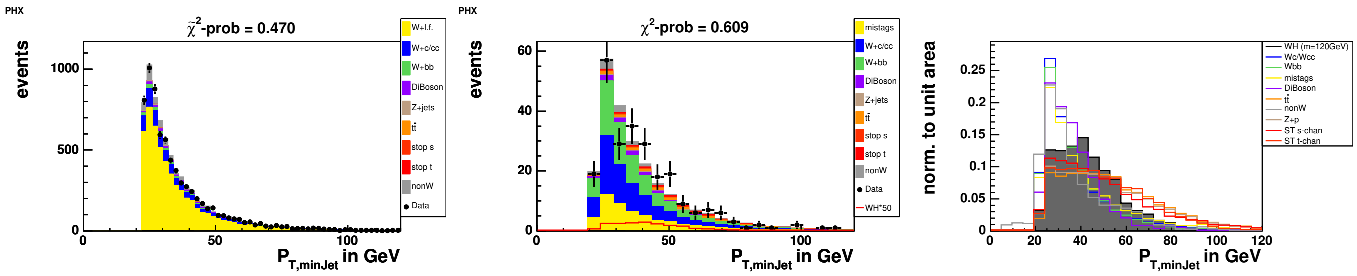

Figure 61: The transverse momentum of the jet with lowest energy

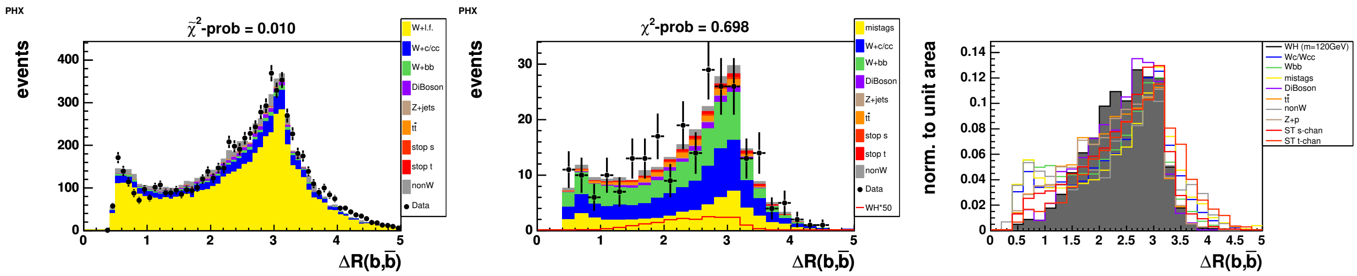

Figure 62: Distance in the ϕ-η-plane between the two jets

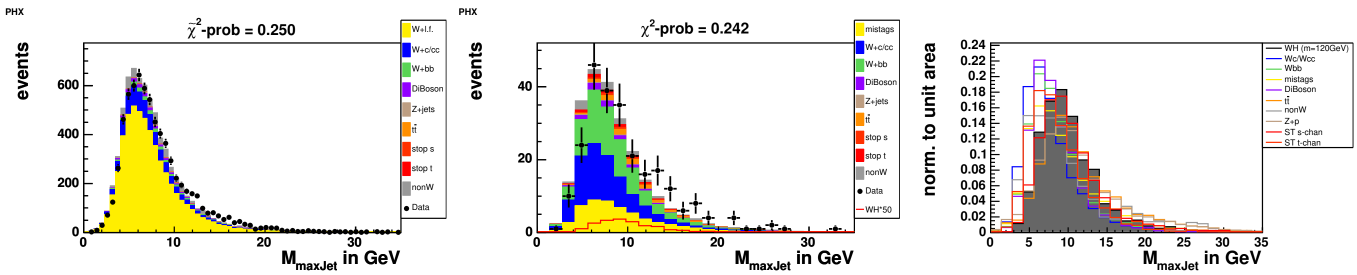

Figure 63: The mass of the jet with highest energy

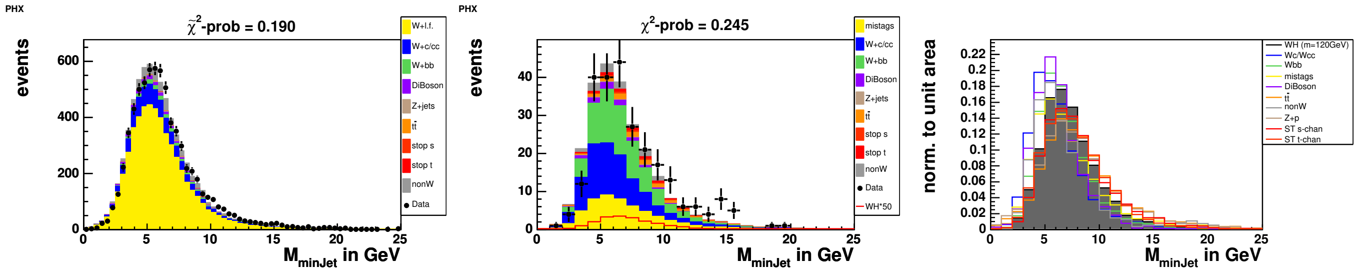

Figure 64: The mass of the jet with lowest energy

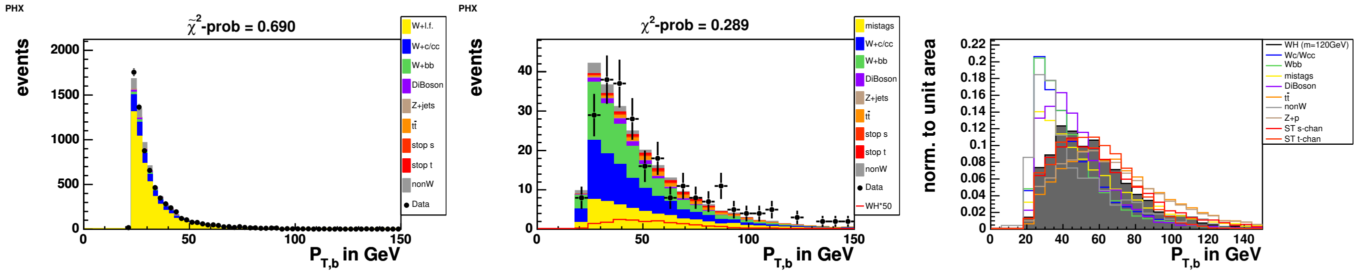

Figure 65: The transverse momentum of the b tagged jet (leading jet for the pretag and double tag samples)

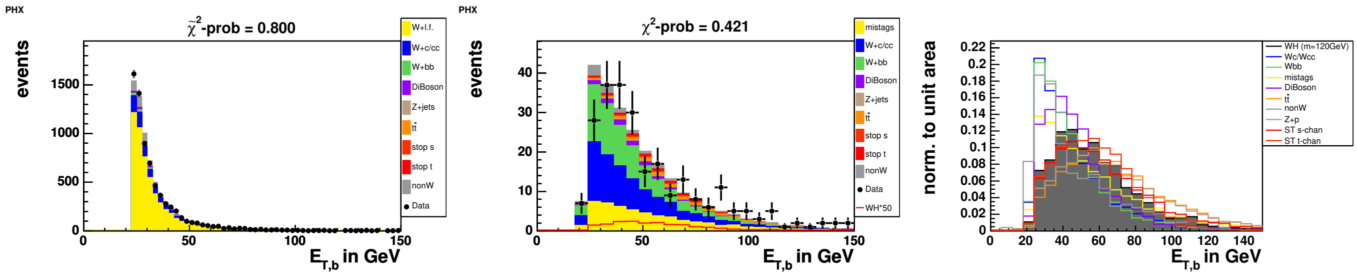

Figure 66: The transverse energy of the b tagged jet

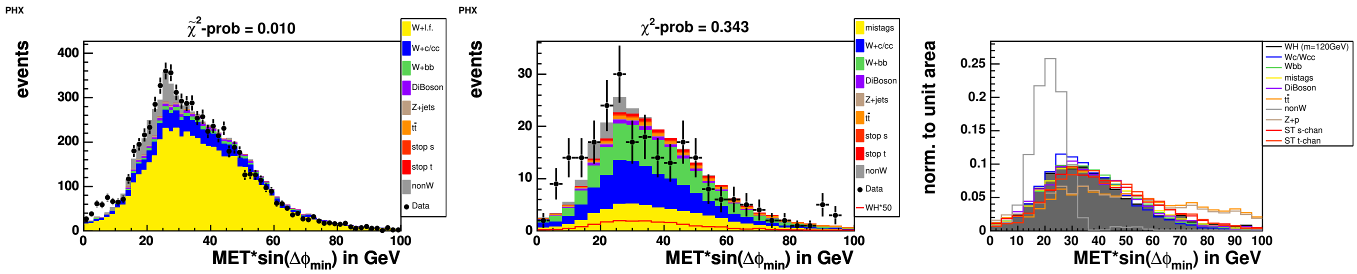

Figure 67: Product of missing transverse energy and the angle between $\vec{\not{E}}_T$ and the closest object in the x-y-plane

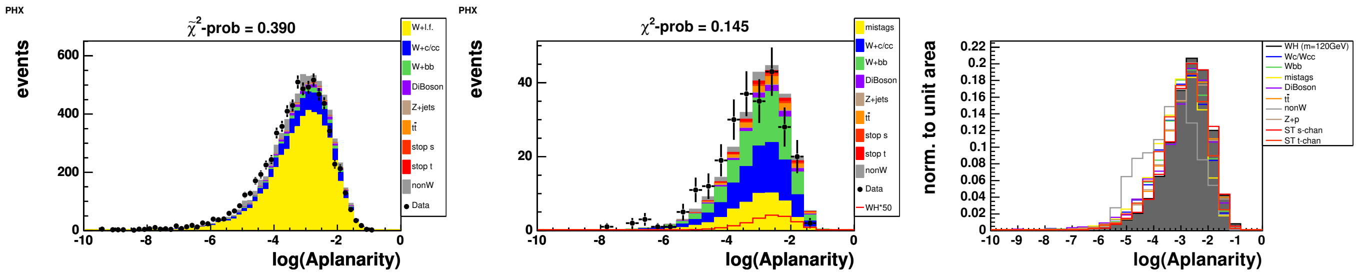

Figure 68: Logarithm of the aplanarity

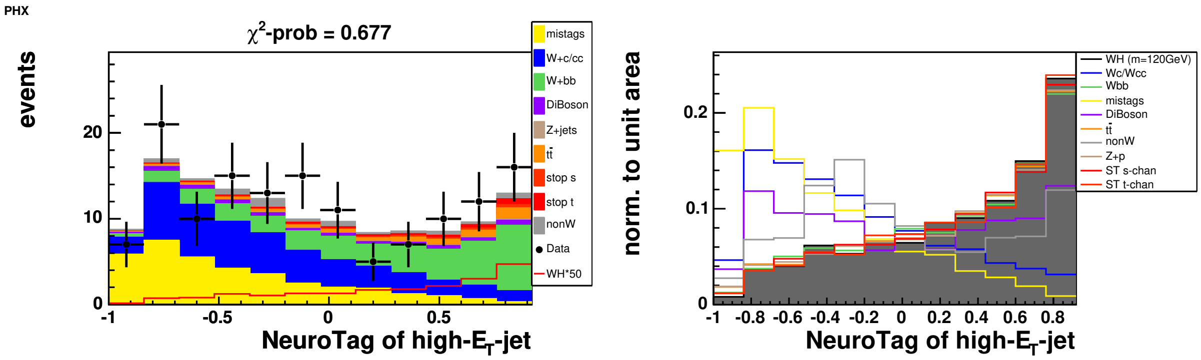

Figure 69: Output of the neural network flavor separator for the jet with highest E_T

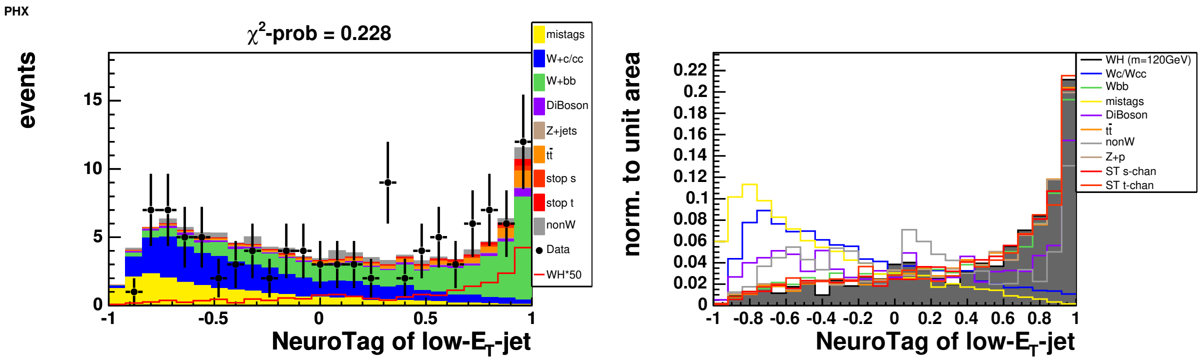

Figure 70: Output of the neural network flavor separator for the jet with lowest E_T

10.3 Neural Network Discriminant in PHX for top-like analysis

To further improve signal to background discrimination, we apply an artificial Neural Network (NN) trained on the kinematic variables to separate WH signal from backgrounds. Our Neural Network, which is the same Neural Network as central analysis, consists of 6 input variables, 11 hidden nodes and 1 output node. The 6 input variables are,

M_{jj+}**:** This variable is the invariant mass calculated from the two tight jets using Level-5 jet corrections. Furthermore, if there are additional loose jets present ($E_{T,L5} < 12$ GeV and $|\eta| < 2.4$), the loose jet that is closest to one of the two tight jets is included in this invariant mass calculation, if the separation between that loose jet and one of the tight jets is $\Delta R < 0.9$.

$\sum E_T$**(Loose Jets):** This variable is the scalar sum of the loose jet transverse energy (with Level-5 corrections).

p_T **Imbalance:** This variable expresses the difference between the scalar sum of the transverse momenta of all measured objects and the $\not\!\!E_T$. Specifically, it is calculated as $P_T(jet_1) + P_T(jet_2) + P_T(lep) - \not\!\!E_T$.

$M_{l\nu j}^{max}$**:** This is the invariant mass of the lepton, $\not\!\!E_T$, and one of the two jets, where the jet is chosen to give the maximum invariant mass. For this quantity, the p_z of the neutrino is ignored.

ΔR**(lepton-**ν_{max}**):** This is the ΔR separation between the lepton and the neutrino, where the p_z of the neutrino is taken from by choosing the solutions from the quadratic equations for the W mass constraint with the largest $|p_z|$.

$P_T(W + H)$**:** This is the total transverse momentum of the W plus two jets system, $P_T(\vec{lep} + \vec{\nu} + \vec{jet}_1 + \vec{jet}_2)$.

For detail, refer to the section 6.

10.4 Kinematic Shape in PHX

We check the kinematic shapes for each tagging categories. The W+jets shape is determined from ALPGEN Monte Carlo sample and is normalized to the data after subtracting other backgrounds at pretag stage. The non-W shape is derived from Anti-PHX Electron, which passes all the kinematic variables but fails at least two identification variables out of five them. We choose Had/Em, $Pem3x3FitTow$, $Pem3x3Chisq$, $Pes5by9U$ and $Pes5by9V$ as the identification variables. To estimate the non-W fraction, we perform a two-component fit (20 GeV to 100 GeV) to the $\not\!\!E_T$ distribution with the same QCD veto as stated Section 10.1. Figure 71 shows the results of fits with and without the QCD veto for 1-3 jet bin.

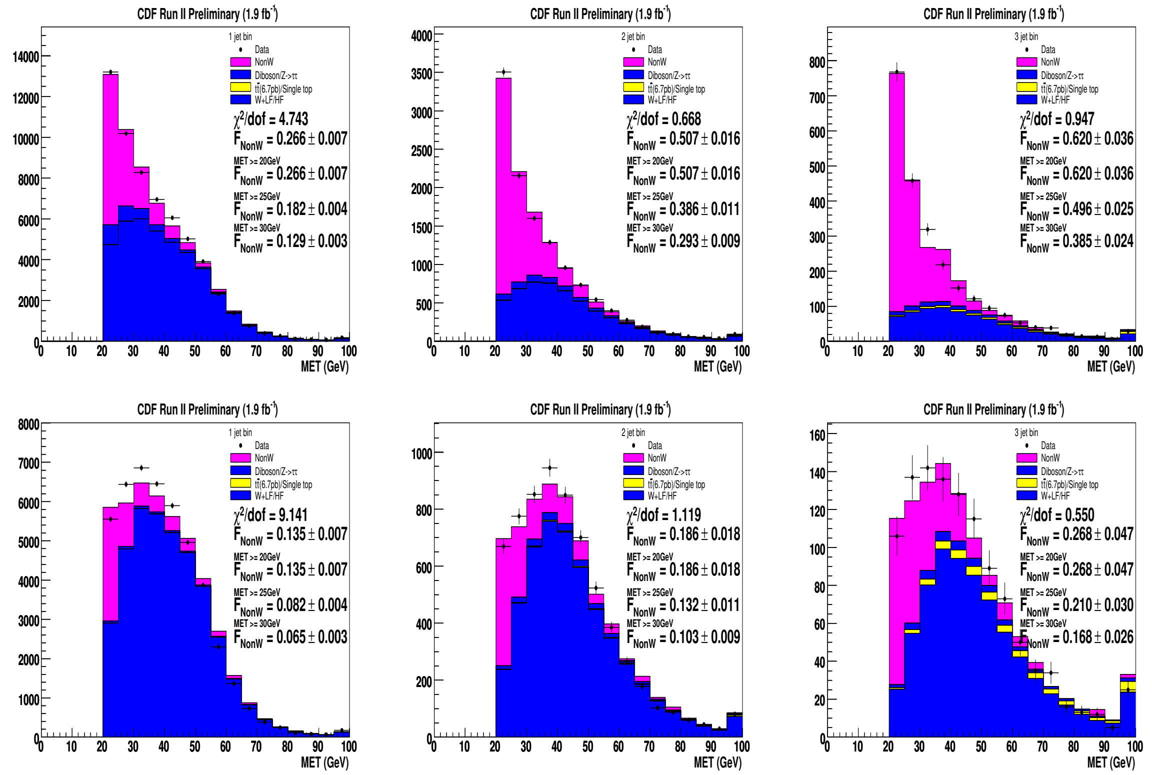

Figure 71: $\not\!\!E_T$ distribution fit without (top) and with (bottom) the QCD veto for 1-3 jet bin.

10.4.1 Pretag

Figure 72-78 show the pretag shapes of Lepton, Missing energy and two jets related variables. These shapes are W+2jet bin.

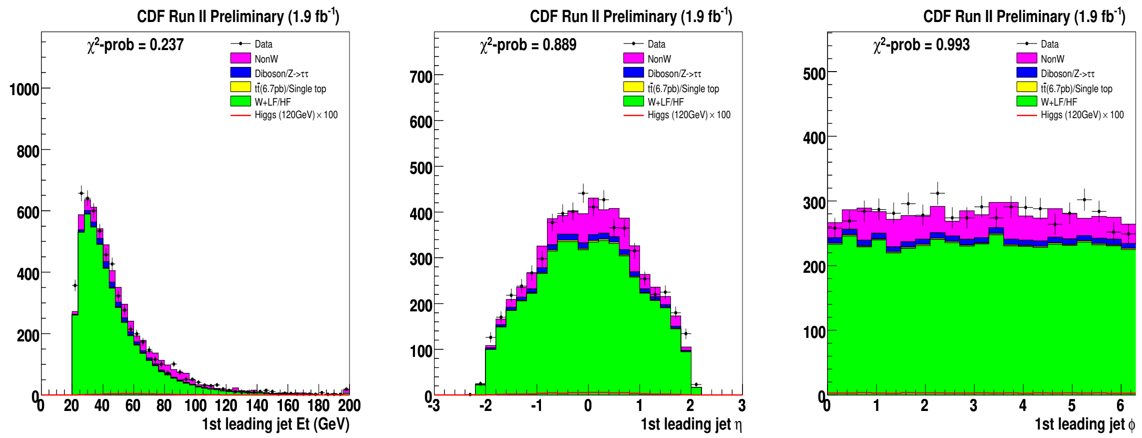

Figure 72: The first leading jet E_T, η and ϕ kinematic distributions in the pretag events.

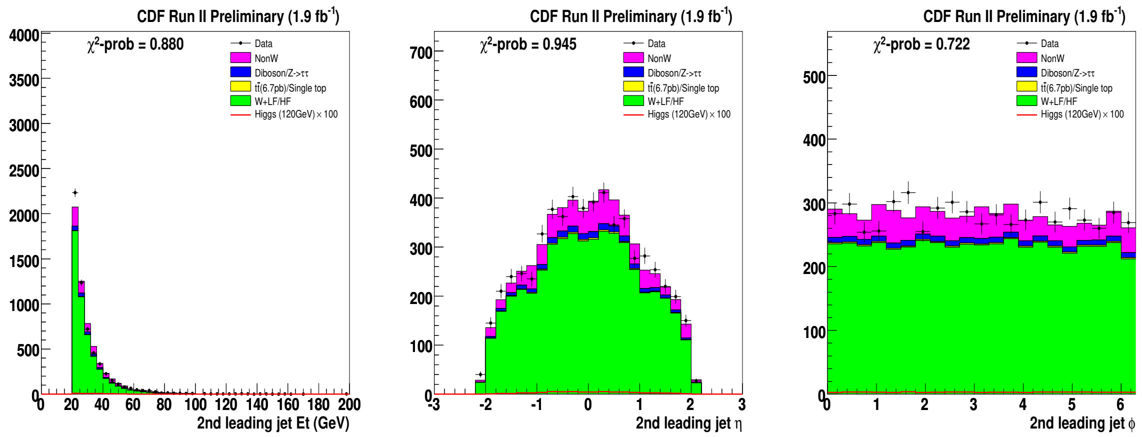

Figure 73: The second leading jet E_T, η and ϕ kinematic distributions in the pretag events.

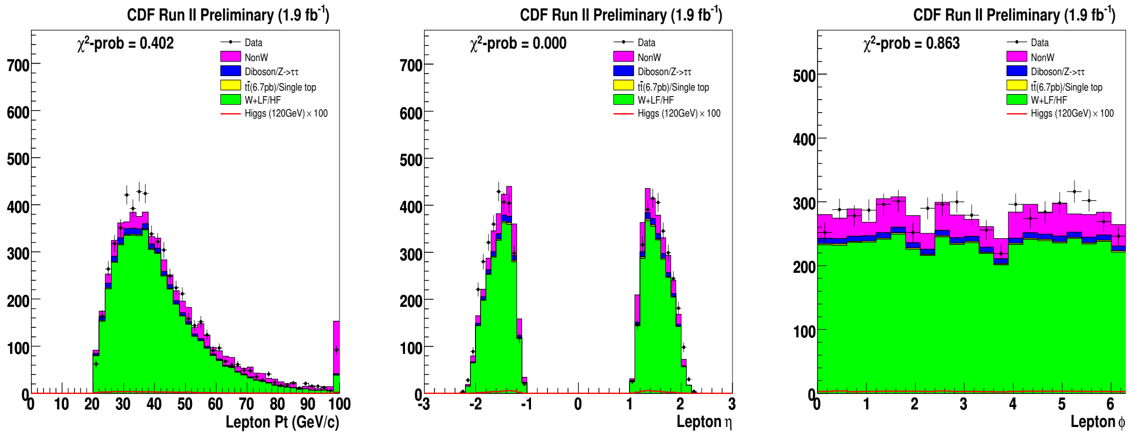

Figure 74: The lepton P_T, η and ϕ kinematic distributions in the pretag events.

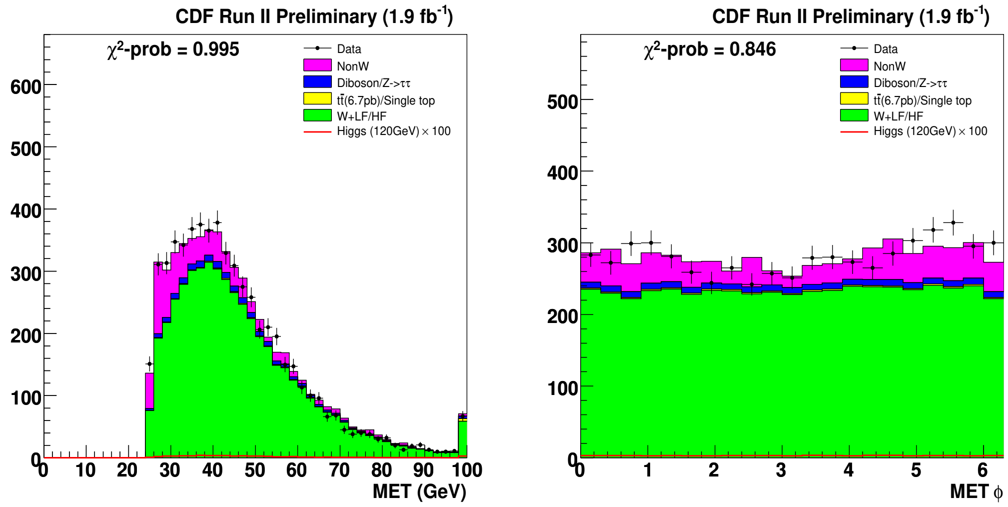

Figure 75: The $\not\!\!E_T$ and ϕ kinematic distributions in the pretag events.

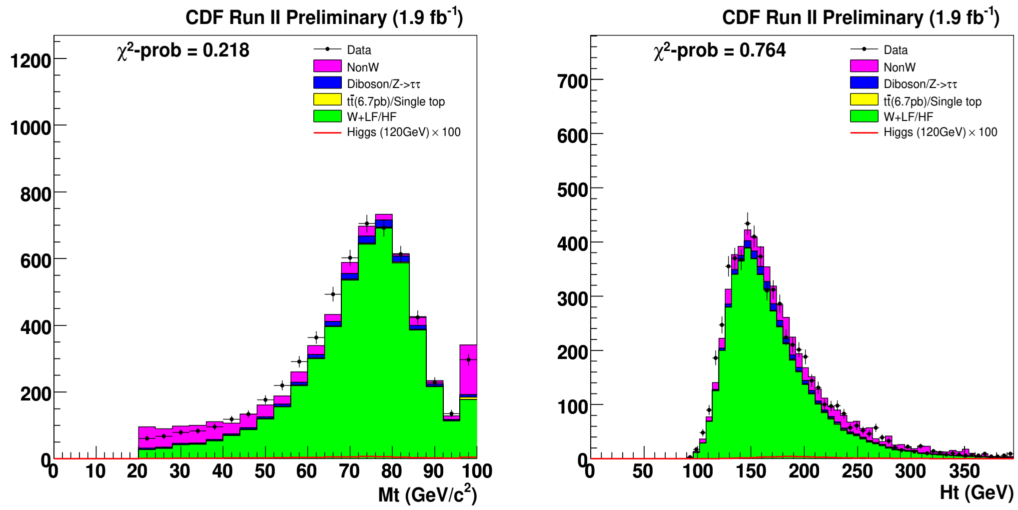

Figure 76: The reconstructed W transverse mass and Ht distributions in the pretag events.

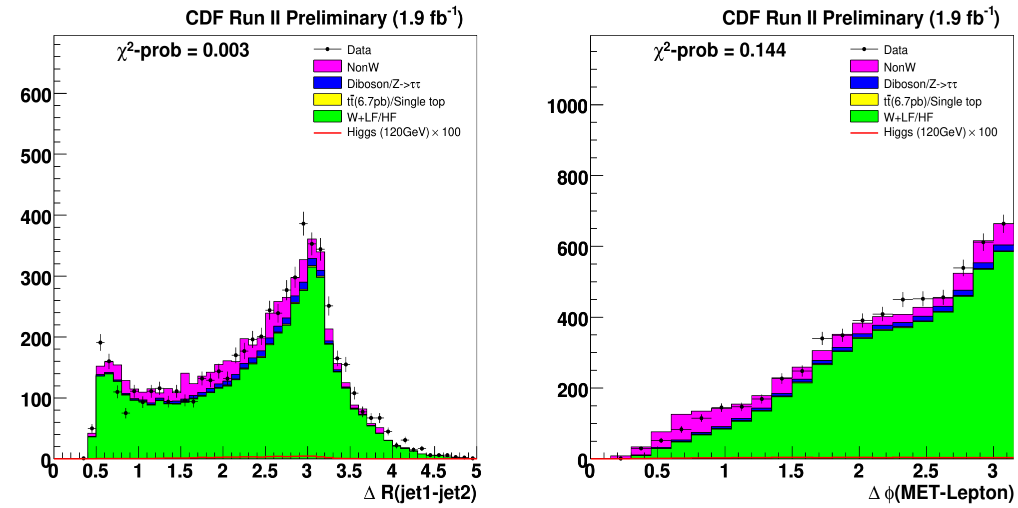

Figure 77: The observed and expected ΔR between dijet and $\Delta\phi$ between $\not\!\!E_T$ and lepton in the pretag events.

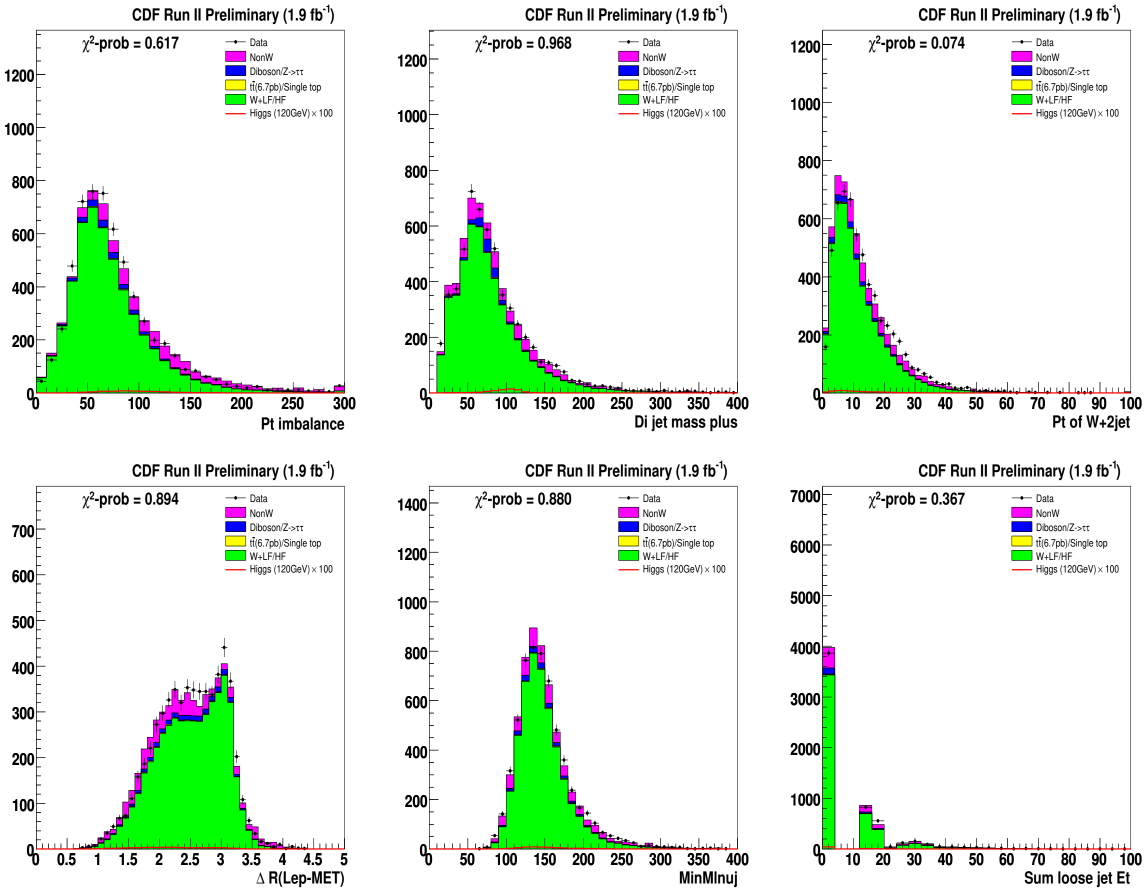

Figure 78: The NN input variables. P_T Imbalance, Dijet plus closest loose jet mass, $P_T(W+H)$,ΔR between $\not{E}_T$ and lepton, invariant mass of $W+1$jet system and sum of loose jet E_T kinematic distributions in the pretag events.

10.4.2 One tight SecVtx tag w/ NNtag

Figure 79-85 show the double SevVtx tag shapes of Lepton, Missing energy and two jets related variables. These shapes are W+2jet bin.

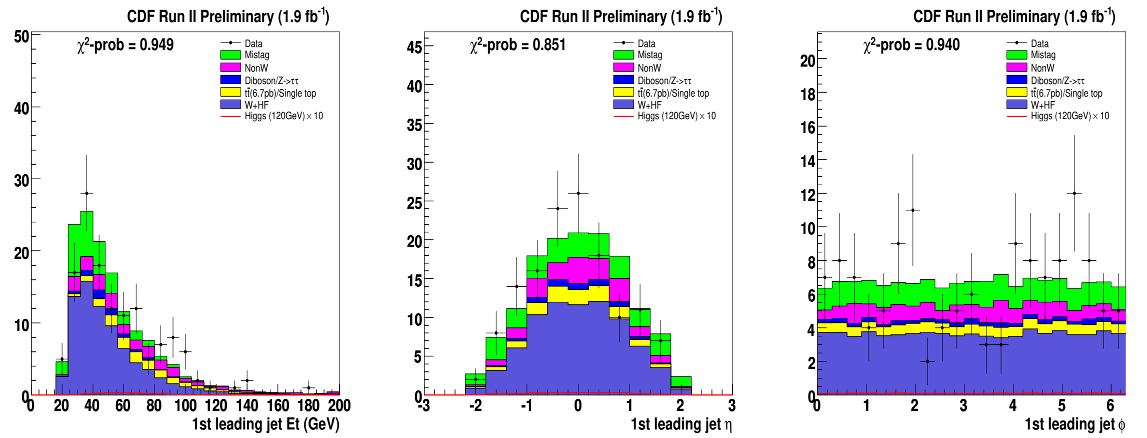

Figure 79: The first leading jet E_T, η and ϕ kinematic distributions in the one tight SecVtx tag w/ NNtag events.

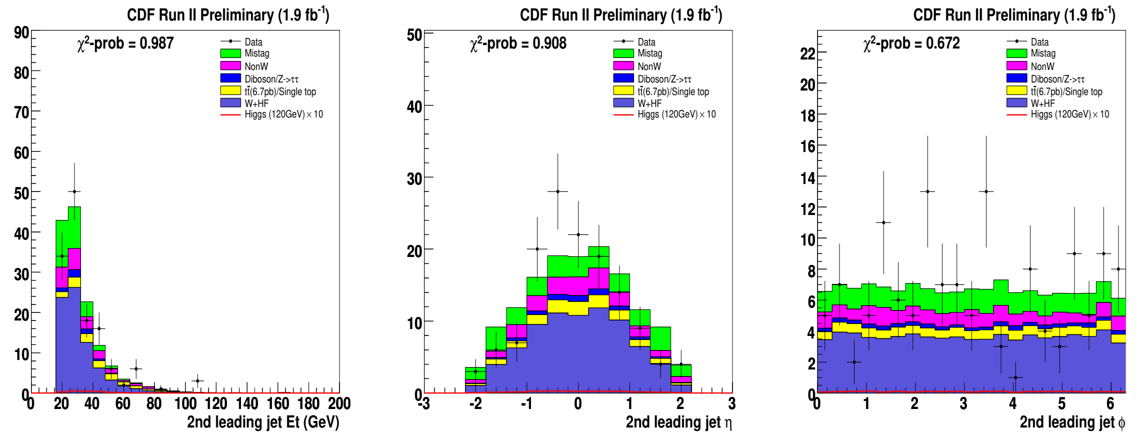

Figure 80: The second leading jet E_T, η and ϕ kinematic distributions in the one tight SecVtx tag w/ NNtag events.

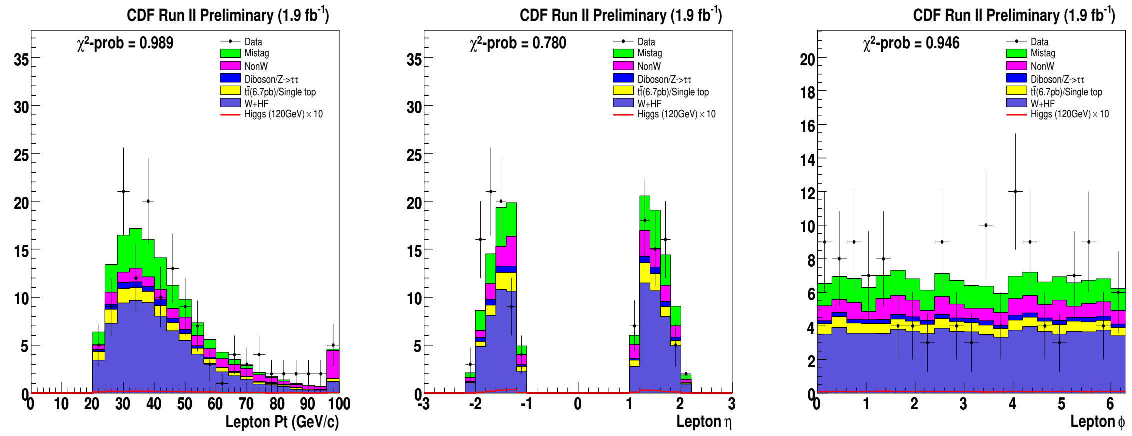

Figure 81: The lepton P_T, η and ϕ kinematic distributions in the one tight SecVtx tag w/ NNtag events.

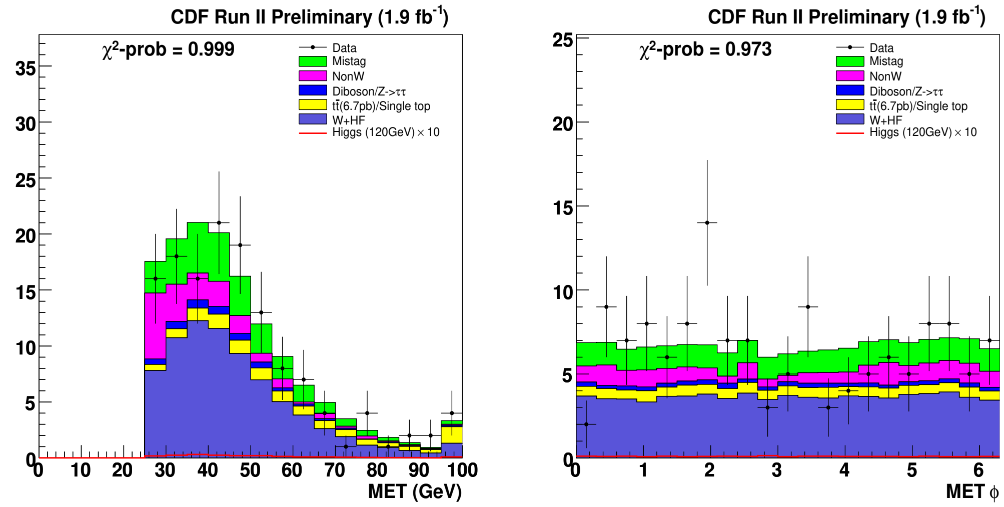

Figure 82: The $\not{E}_T$ and ϕ kinematic distributions in the one tight SecVtx tag w/ NNtag events.

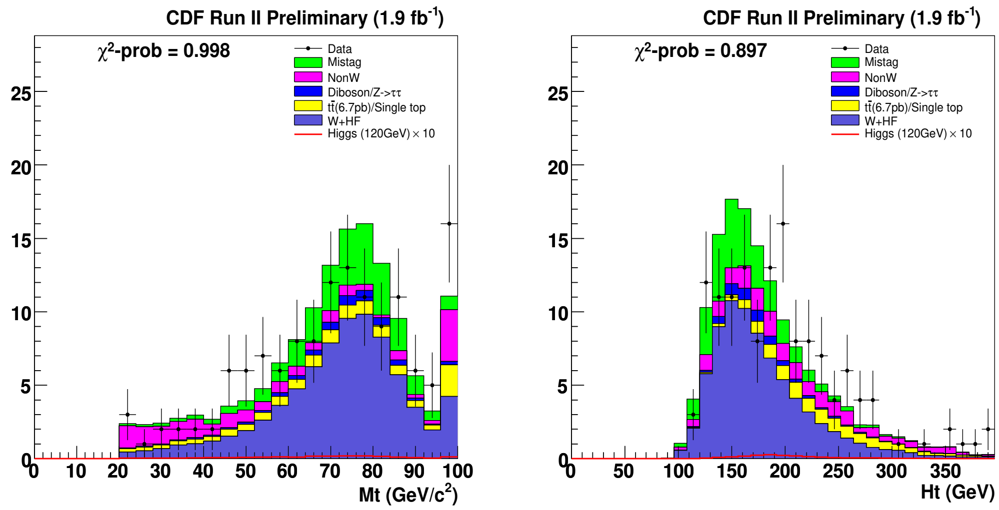

Figure 83: The reconstructed W transverse mass and Ht distributions in the one tight SecVtx tag w/ NNtag events.

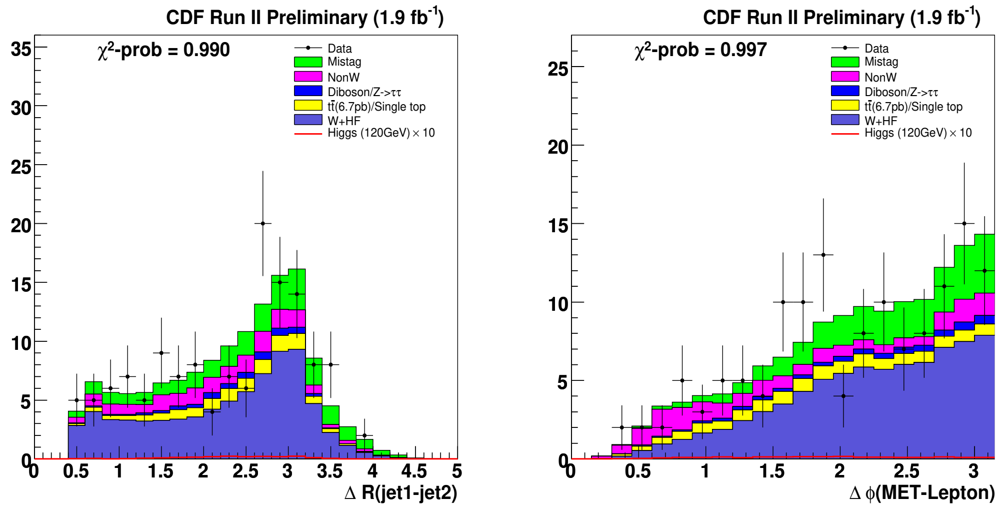

Figure 84: The observed and expected ΔR between dijet and $\Delta\phi$ between $\not{E}_T$ and lepton in the one tight SecVtx tag w/ NNtag events.

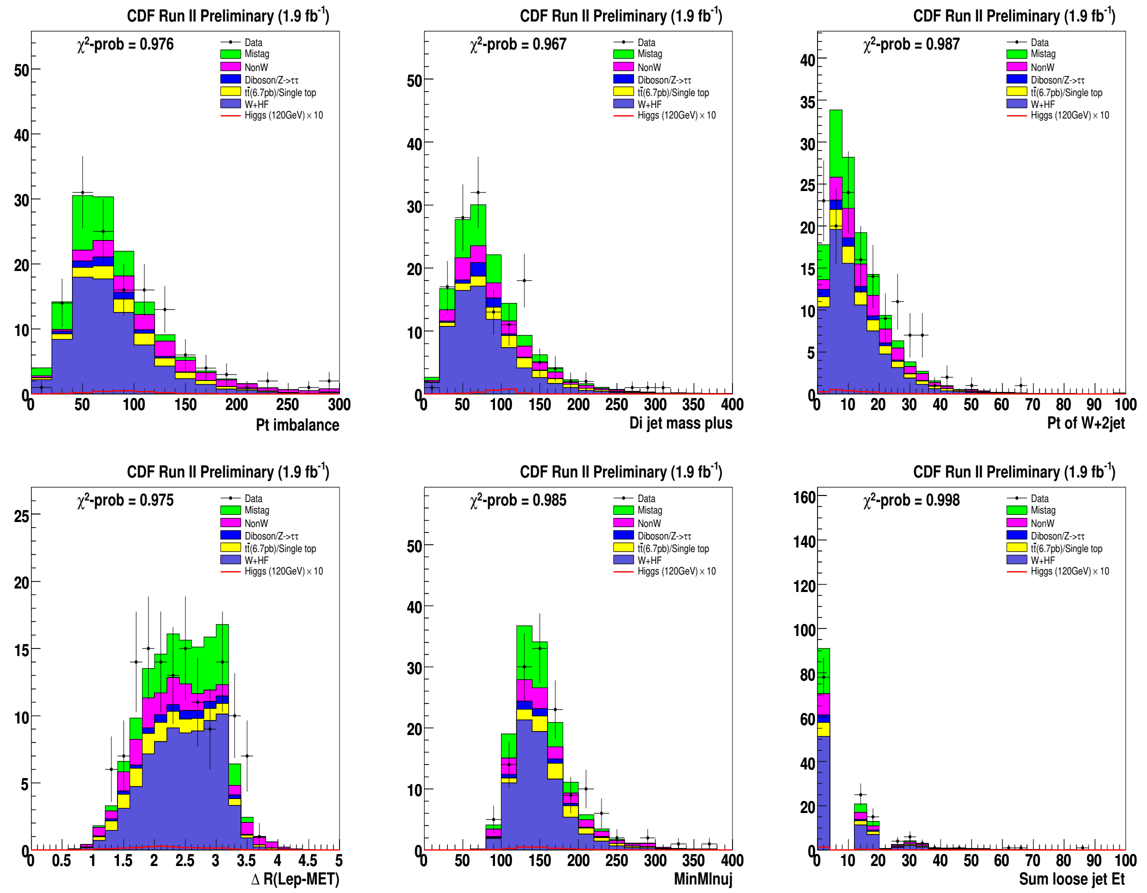

Figure 85: The NN input variables. P_T Imbalance, Dijet plus closest loose jet mass, $P_T(W+H)$,ΔR between $\not\!\!E_T$ and lepton, invariant mass of $W+1$jet system and sum of loose jet E_T kinematic distributions in the one tight SecVtx tag w/ NNtag events.

10.4.3 Double SecVtx tag

Figure 86-92 show the double SevVtx tag shapes of Lepton, Missing energy and two jets related variables. These shapes are W+2jet bin.

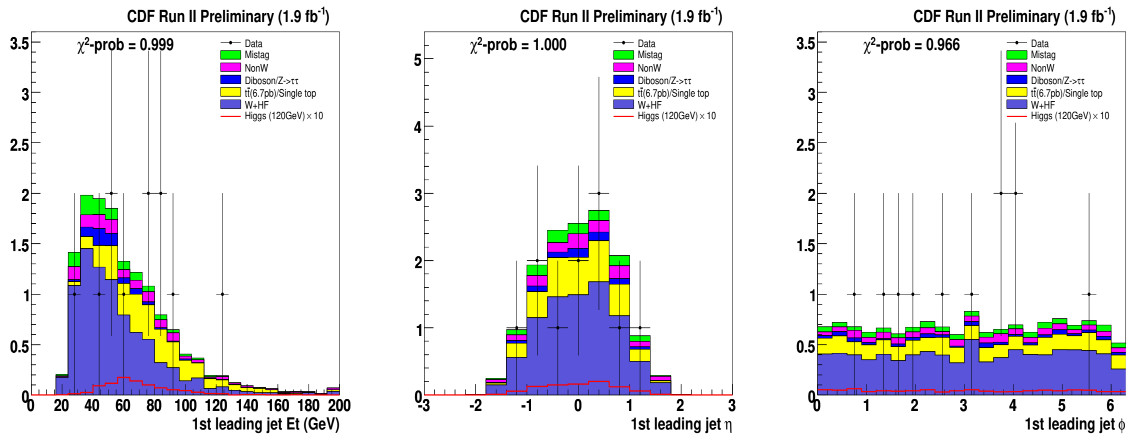

Figure 86: The first leading jet E_T, η and ϕ kinematic distributions in the double tight SecVtx tag events.

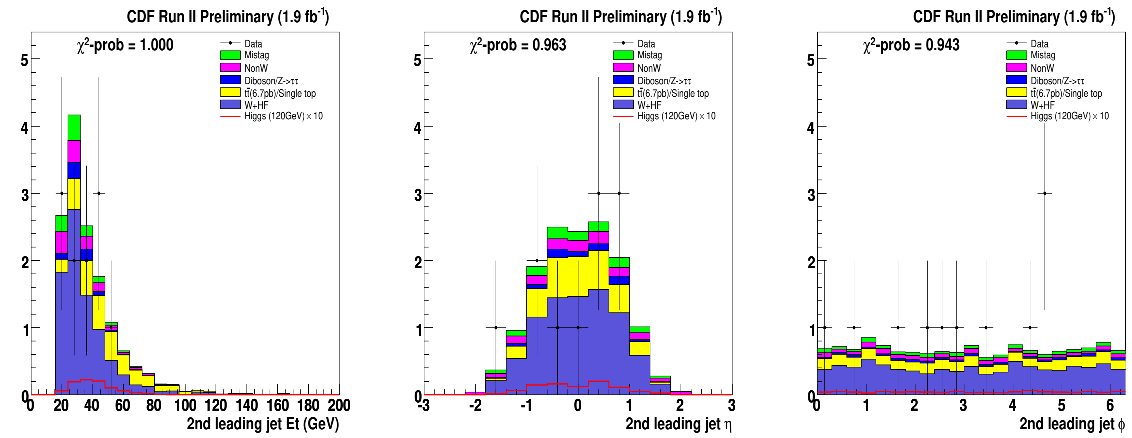

Figure 87: The second leading jet E_T, η and ϕ kinematic distributions in the double tight SecVtx tag events.

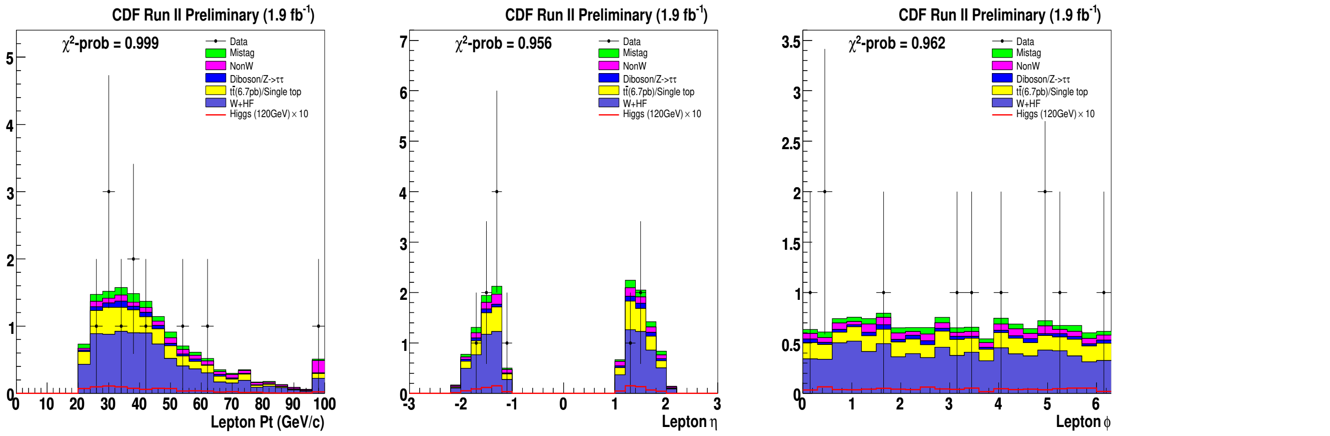

Figure 88: The lepton P_T, η and ϕ kinematic distributions in the double tight SecVtx tag events.

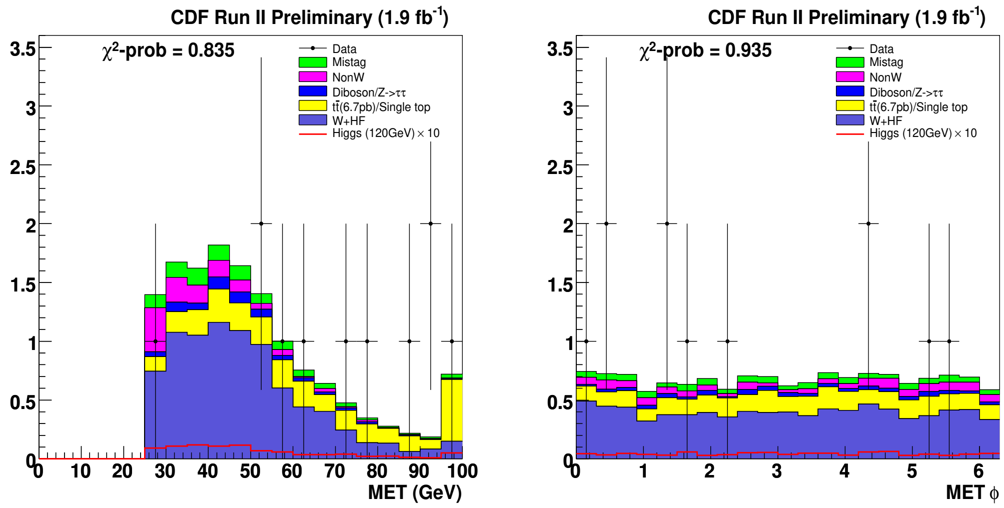

Figure 89: The $\not{E}_T$ and ϕ kinematic distributions in the double tight SecVtx tag events.

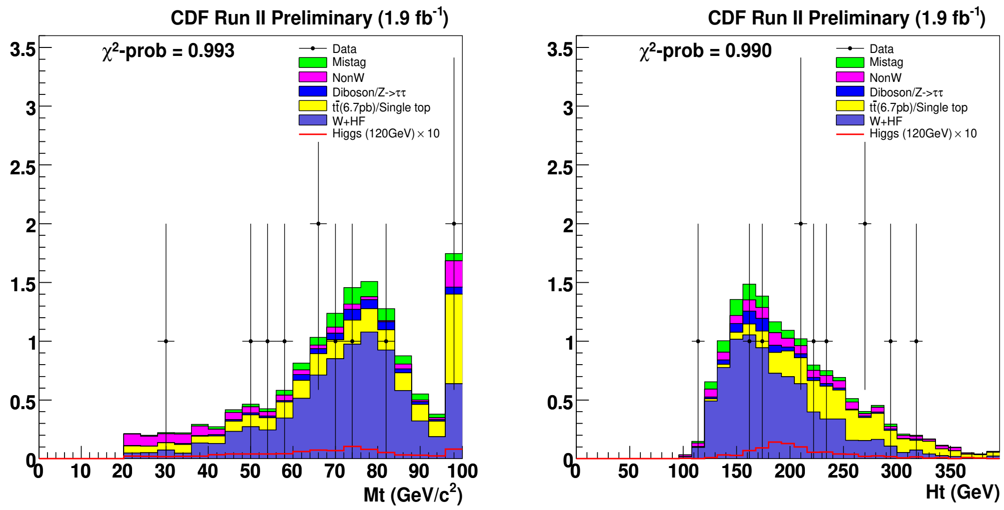

Figure 90: The reconstructed W transverse mass and Ht distributions in the double tight SecVtx tag events.

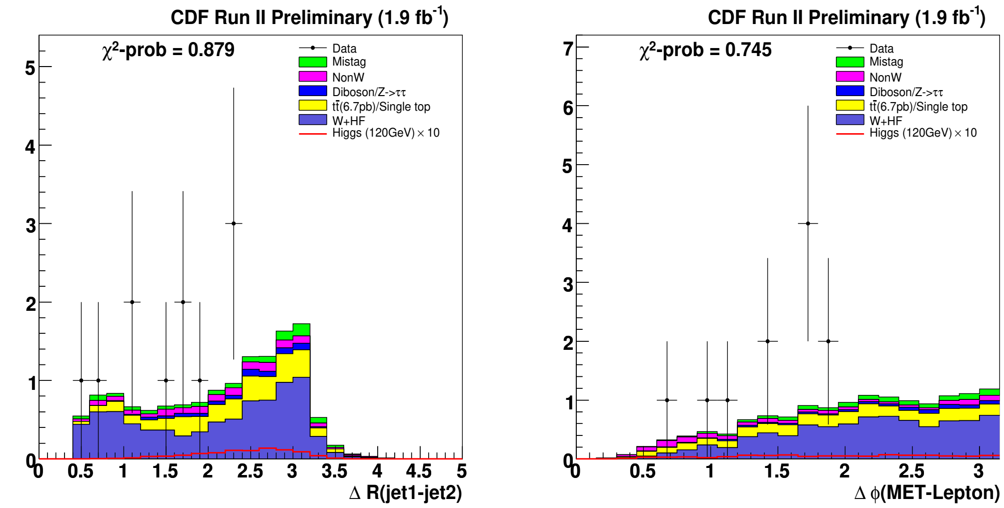

Figure 91: The observed and expected ΔR between dijet and $\Delta\phi$ between $\not\!\!E_T$ and lepton in the double tight SecVtx tag events.

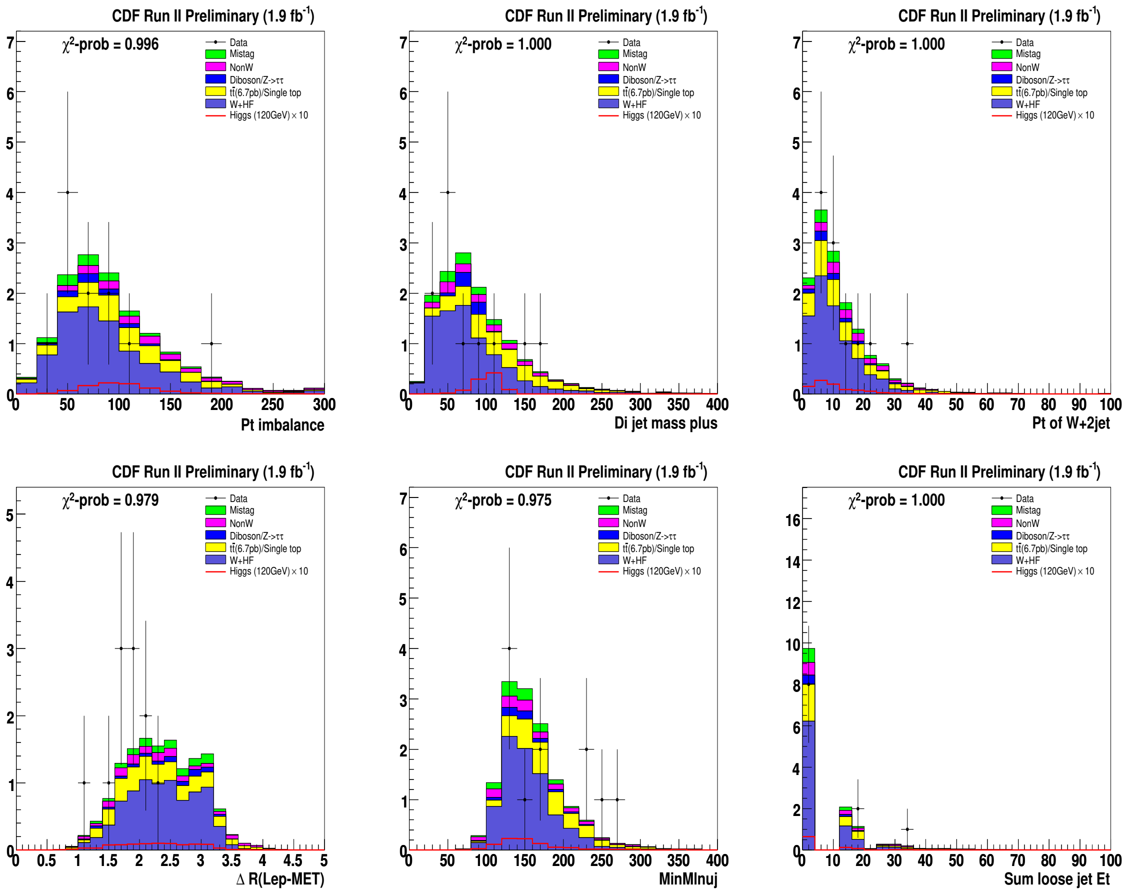

Figure 92: The NN input variables. P_T Imbalance, Dijet plus closest loose jet mass, $P_T(W+H)$,ΔR between $\not\!\!E_T$ and lepton, invariant mass of $W+1$jet system and sum of loose jet E_T kinematic distributions in the double tight SecVtx tag events.

10.4.4 One SecVtx tag and One jet probability tag

Figure 93-99 show the double SevVtx tag shapes of Lepton, Missing energy and two jets related variables. These shapes are W+2jet bin.

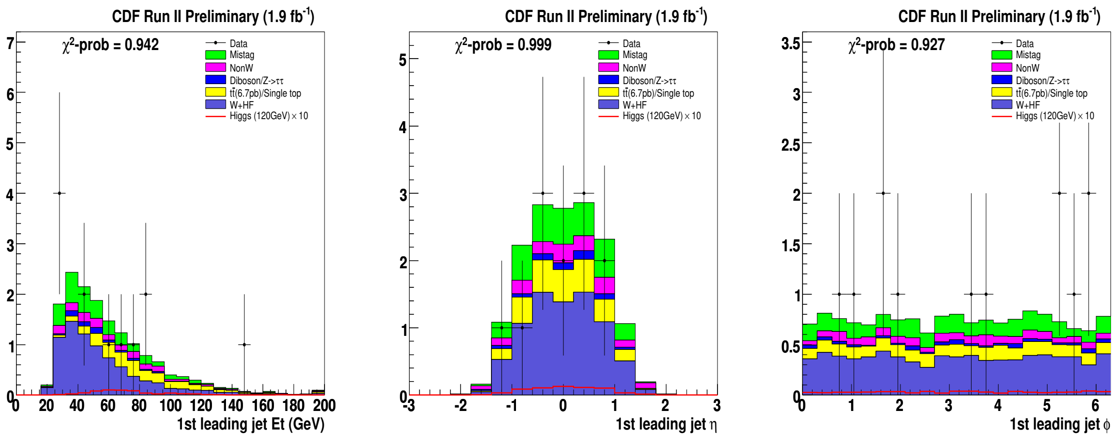

Figure 93: The first leading jet E_T, η and ϕ kinematic distributions in the one tight SecVtx tag and one jet probability tag events.

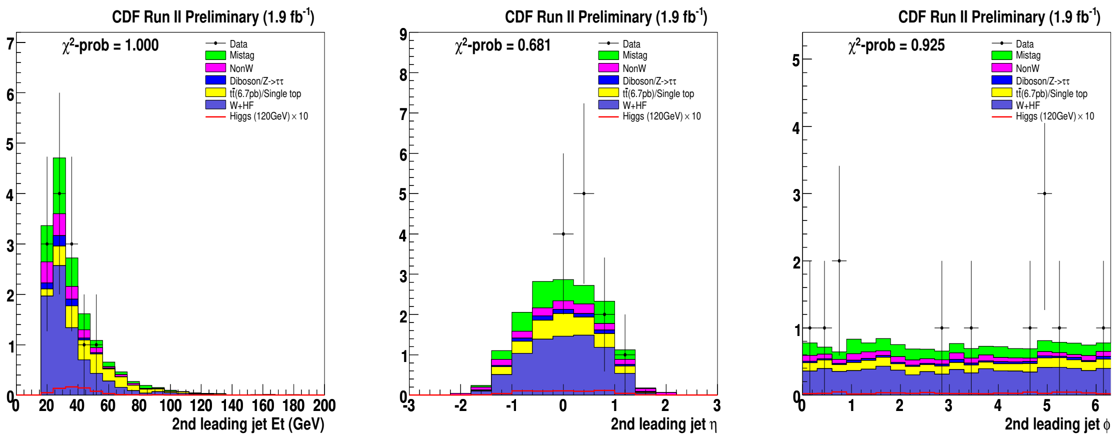

Figure 94: The second leading jet E_T, η and ϕ kinematic distributions in the one tight SecVtx tag and one jet probability tag events.

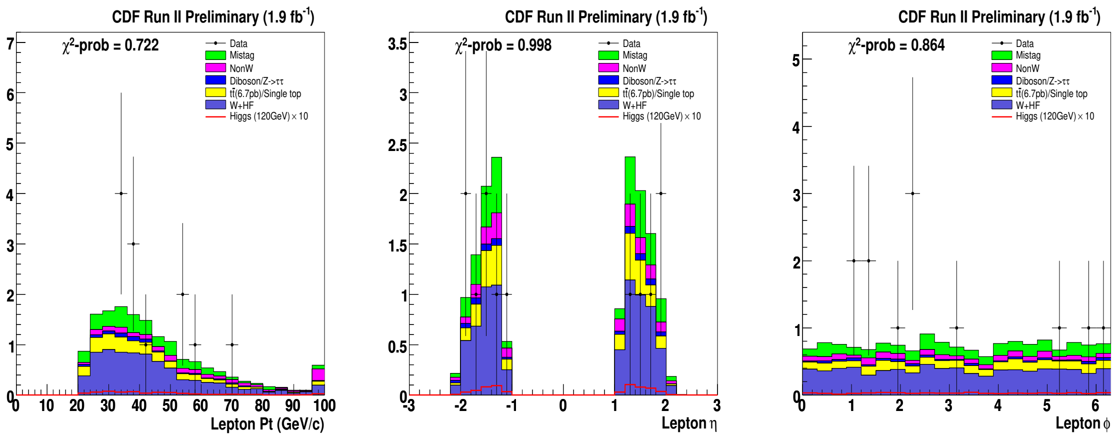

Figure 95: The lepton P_T, η and ϕ kinematic distributions in the one tight SecVtx tag and one jet probability tag events.

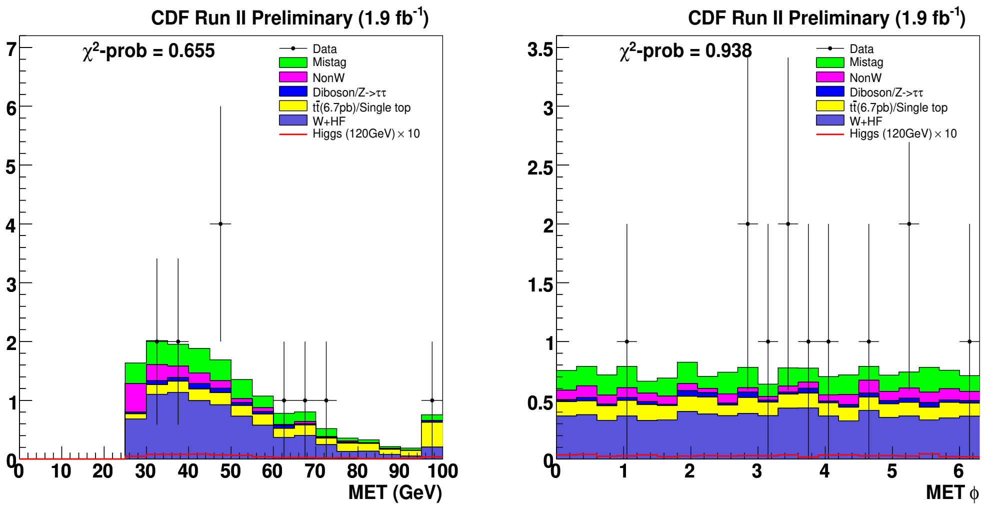

Figure 96: The $\not{E}_T$ and ϕ kinematic distributions in the one tight SecVtx tag and one jet probability tag events.

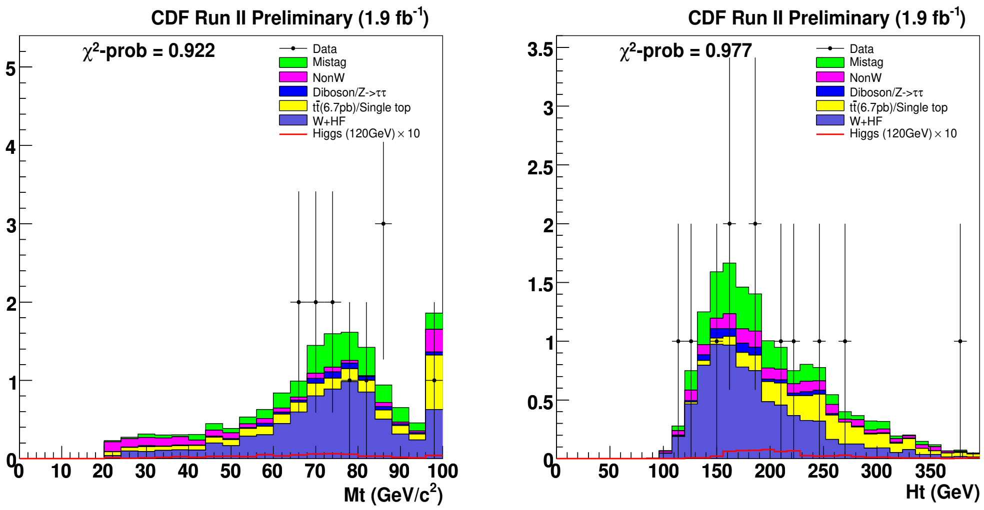

Figure 97: The reconstructed W transverse mass and Ht distributions in the one tight SecVtx tag and one jet probability tag events.

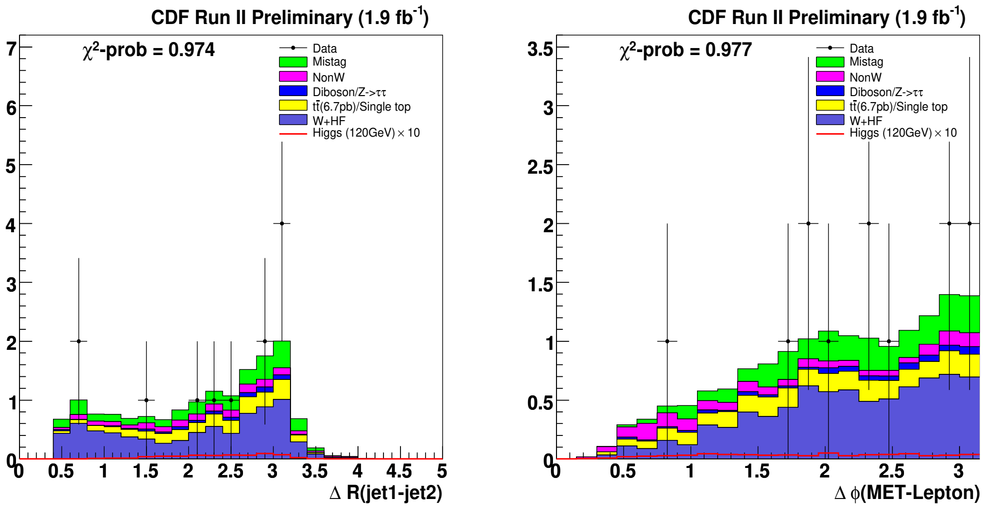

Figure 98: The observed and expected ΔR between dijet and $\Delta\phi$ between $\not\!\!E_T$ and lepton in the one tight SecVtx tag and one jet probability tag events.

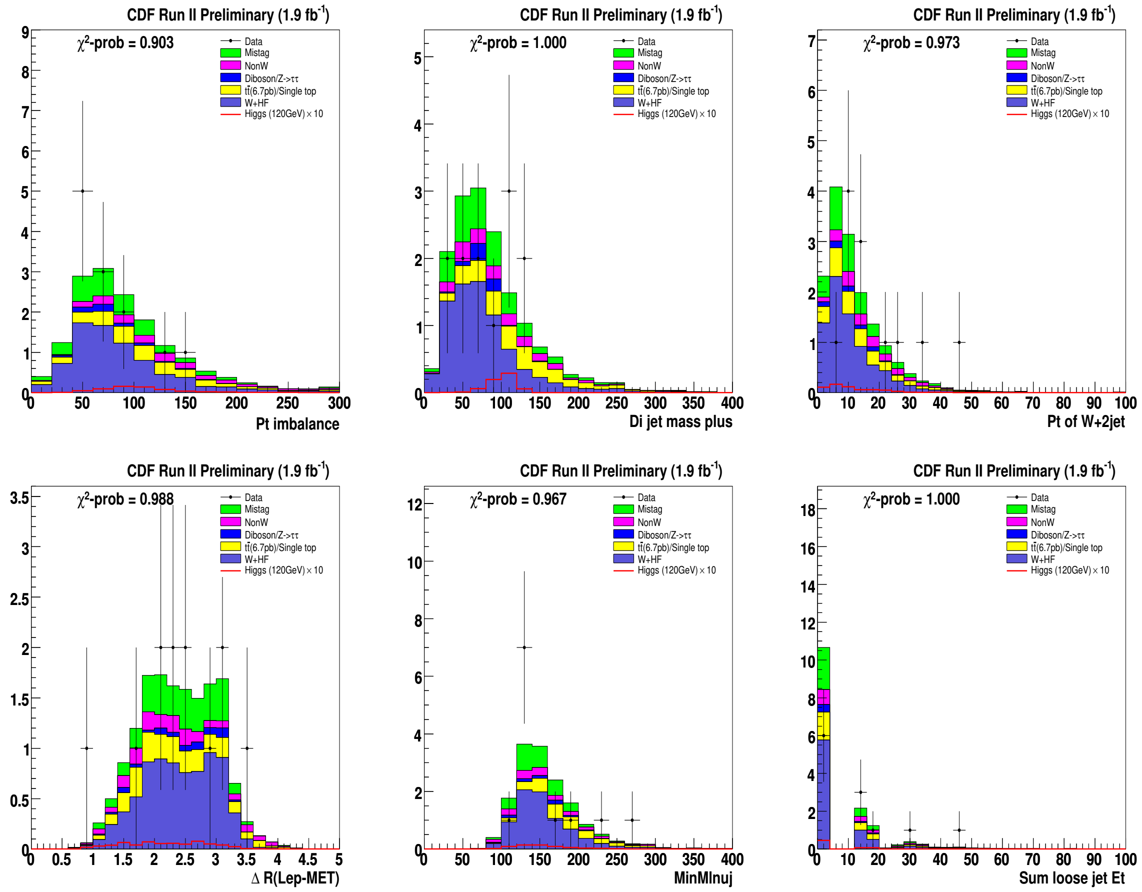

Figure 99: The NN input variables. P_T Imbalance, Dijet plus closest loose jet mass, $P_T(W+H)$,ΔR between $\not{E}_T$ and lepton, invariant mass of $W+1$jet system and sum of loose jet E_T kinematic distributions in the one tight SecVtx tag and one jet probability tag events.

10.5 Neural Network Discriminant Result

We show the results of NN discriminant for each tag categories (Pretag, ST w/ NNtag, ST+ST and ST+JP). Each backgrounds are normalized the same value of table 22 - 24.

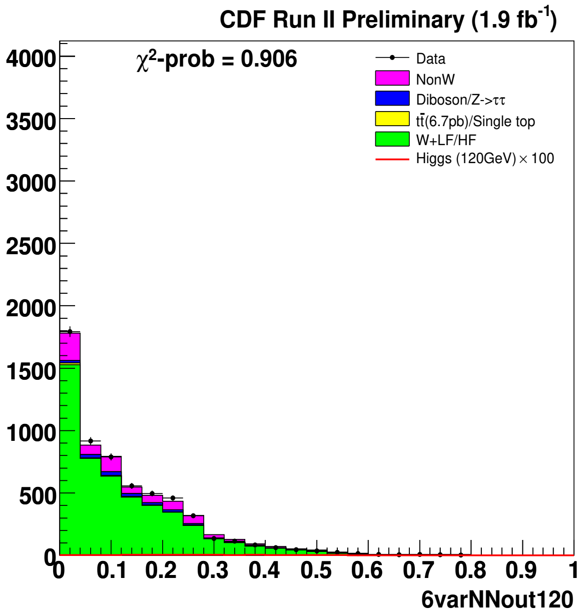

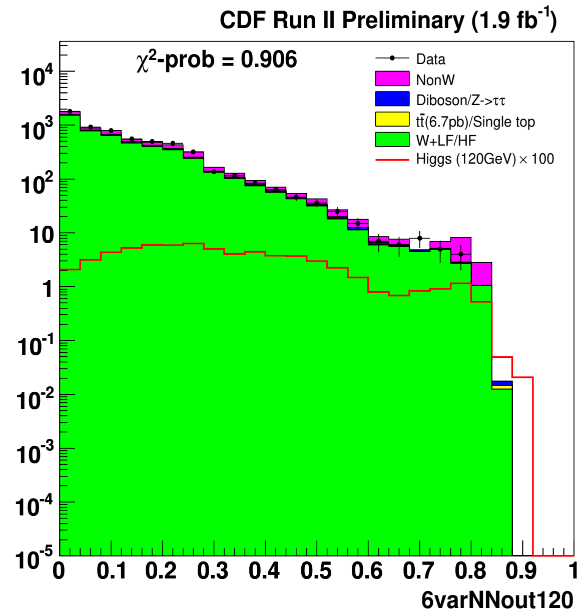

Figure 100: The NN output shape of the pretag category. Higgs signal ($120GeV/_{c^2}$) should produce high NN output values.

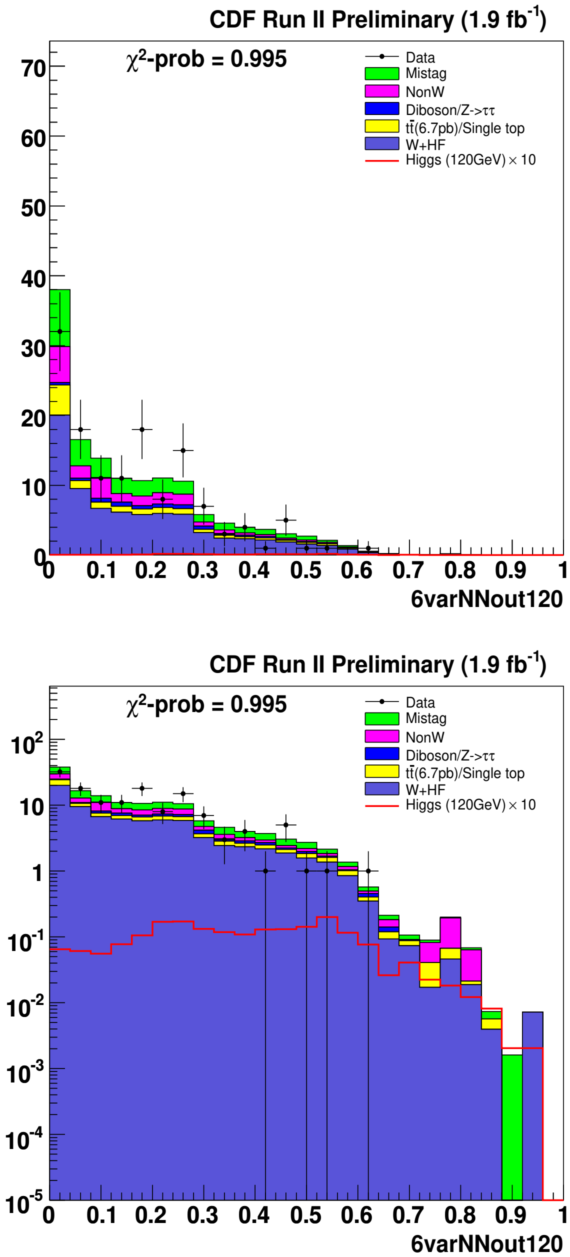

Figure 101: The NN output shape of the one tight SecVtx tag w/ NN tag category. Higgs signal ($120GeV/_{c^2}$) should produce high NN output values.

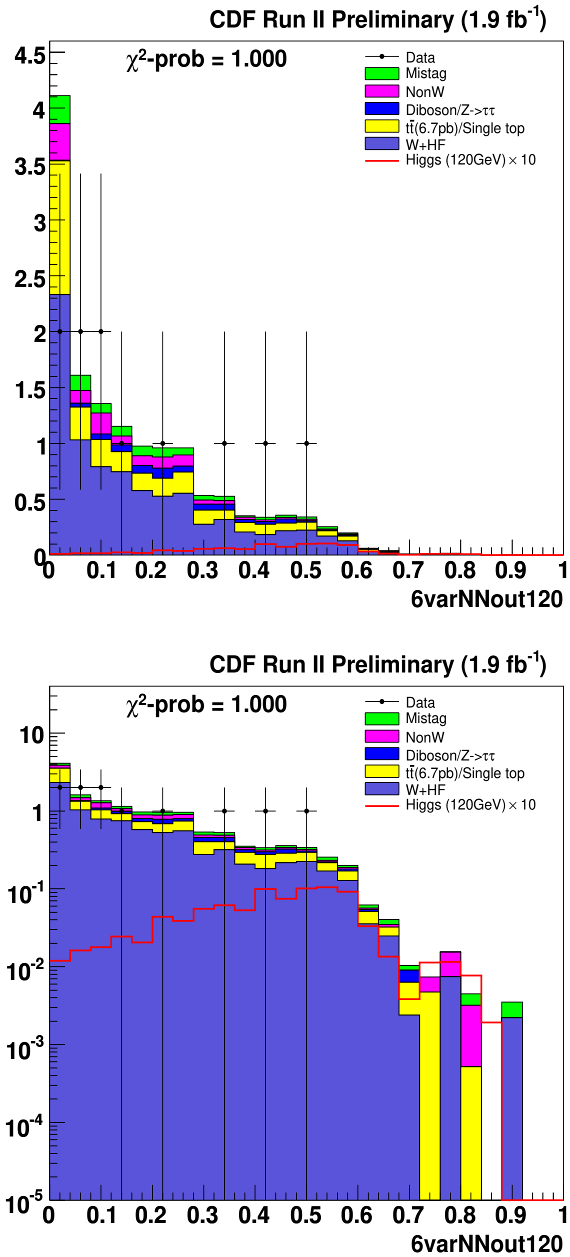

Figure 102: The NN output shape of the double tight SecVtx tag category. Higgs signal $(120GeV/_{c^2})$ should produce high NN output values.

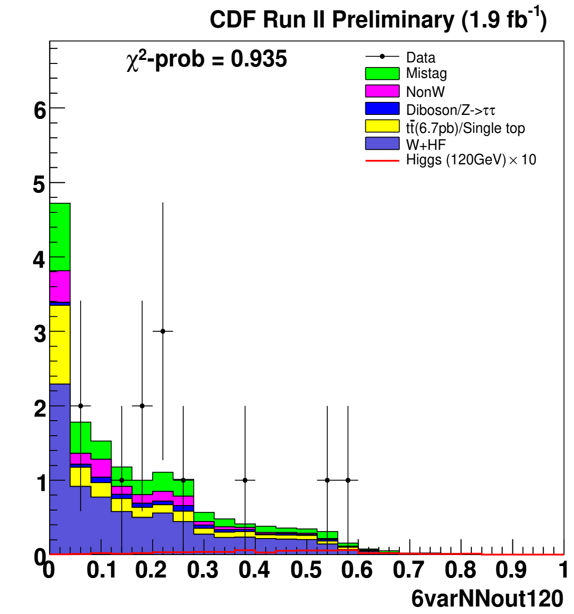

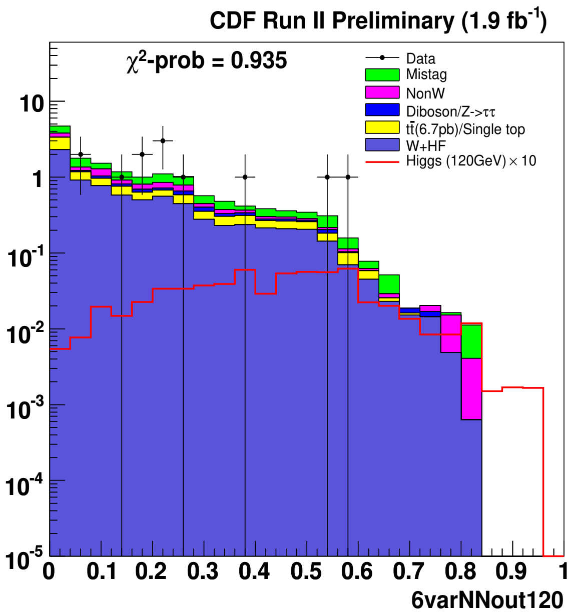

Figure 103: The NN output shape of the one tight SecVtx tag and ont jet probability tag category. Higgs signal ($120 GeV/_{c^2}$) should produce high NN output values.

10.6 Expected Limits

We use the Bayesian procedure to fit the NN output and extract the expected limit using pseudo-experiments based on the background expectations. Table 27 shows the average of 95% C.L. upper limit on the Higgs production over the Standard Model cross section from the two PHX analyzes for each mass. For a comparison purpose, we have included with and without systematic in the calculation that listed in Table 28. It's interesting to note that the best limit is obtained from single tag, instead of double tags where the statistic is limited. After combination, both analyzes give very similar expected limits. Figure 104 shows the expected limits for each individual tagging category and their combination in single-top and top like analyzes.

	No Systematic				With Systematic			
mH (GeV)	110	115	120	130	110	115	120	130
KA one tag	39.6	44.6	55.8	86.8	46.9	51.3	64.5	97.7
KA two tags	57.3	57.1	72.0	106.0	63.1	61.2	78.3	114.1
KA combined	30.8	32.4	40.9	61.4	35.2	37.1	46.3	69.0
STST	56.6	57.8	71.9	108.3	61.4	62.5	78.1	113.7
STJP	78.1	81.8	107.7	165.0	84.1	89.8	113.1	167.3
ST+NNtag	54.5	69.5	82.6	137.0	65.4	85.1	99.9	156.9
Combined	30.3	33.9	41.6	63.8	34.0	38.5	47.1	72.5

Table 27: The average of 95% C.L. upper limit on the Higgs production over the SM cross section from each category for each mass

Source (%)	KA Single	KA Doub	STST	STJP	ST+NNtag
Lum	6	6	6	6	6
btag	4.3	10	8	9	4.3
ID	2	2	2	2	2
JES	1	1	1	1	1
ISR/FSR	5	5	5	5	5
Mistag	14	14	18	16	12
QCD	40	40	40	40	30
W+HF	35	35	35	35	35
Top	20	20	15	15	15
Diboson	11	11	10	10	10

Table 28: The listed systematic that used in the phex analyzes

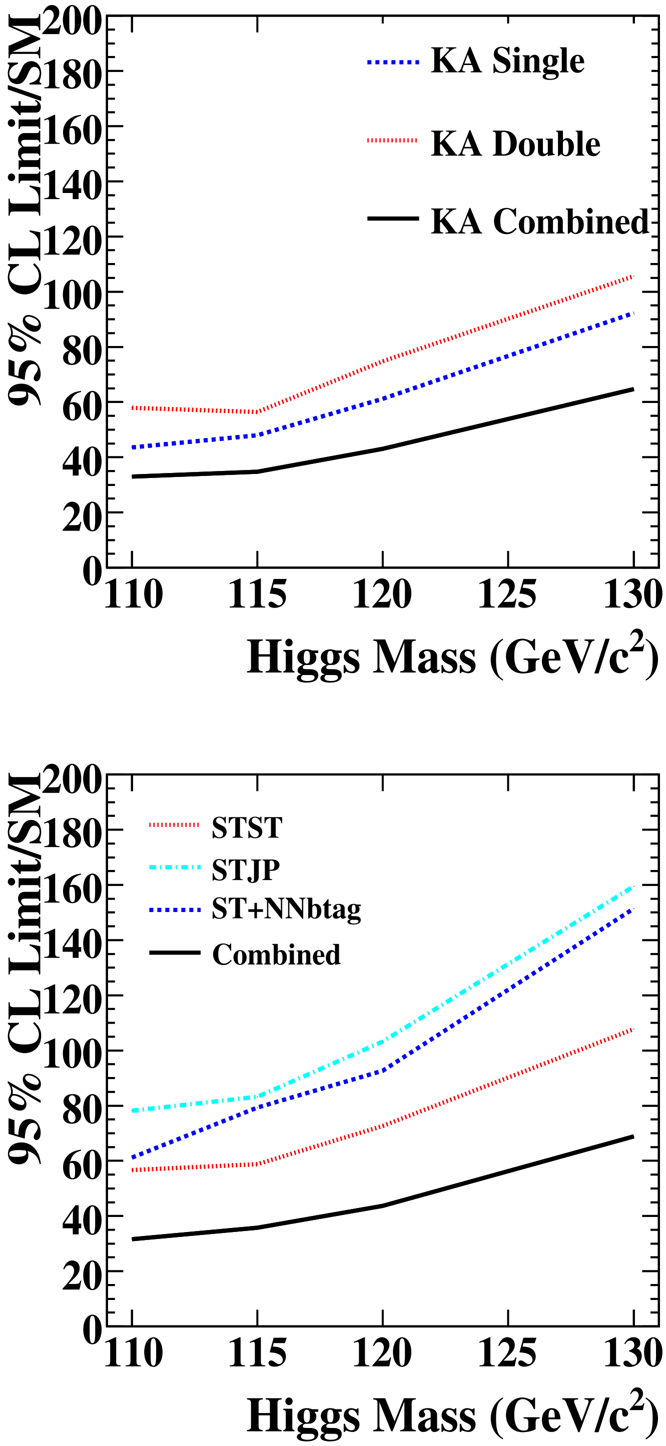

Figure 104: The 95% C.L. upper limit over SM expectation as function of Higgs masses for each individual tagging category and their combination in single-top (top) and top like (bottom) analyzes

10.7 Observed Limits

Figure 105 shows observed 95% C.L upper limit combined 1tag and 2tag. Our observed limit is resonable compared to pseudo experiment results. The observed upper limit for each mass point and category are shown in Table 29.

mH (GeV)	110	115	120	130
KA one tag	43.2	48.2	52.2	145.8
KA two tags	45.8	41.2	46.2	69.8
KA combined	27.8	27.8	28.2	69.8
STST	57.8	48.2	72.2	82.2
STJP	73.8	89.8	155.2	190.8
ST+NNbtag	37.8	52.8	69.2	184.2
combined	22.8	25.8	47.2	75.2

Table 29: The observed upper limit using NN shape fitfor each mass point and each category.

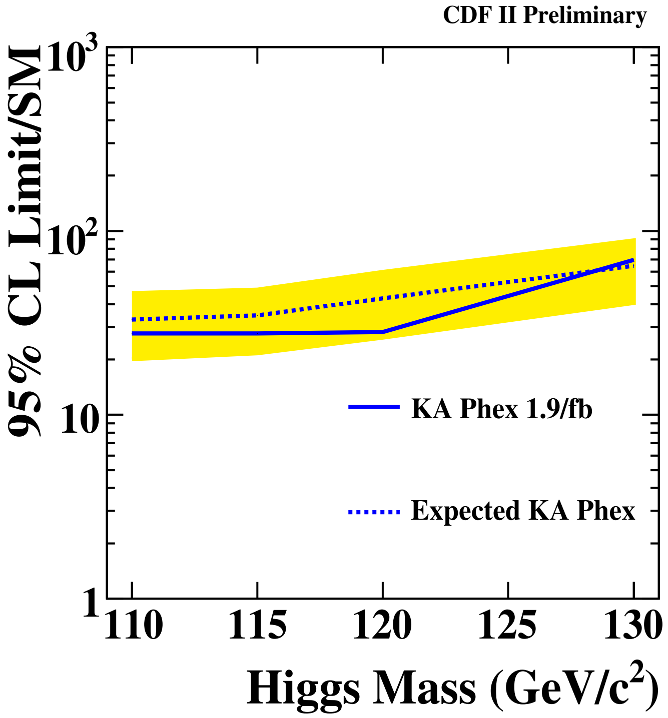

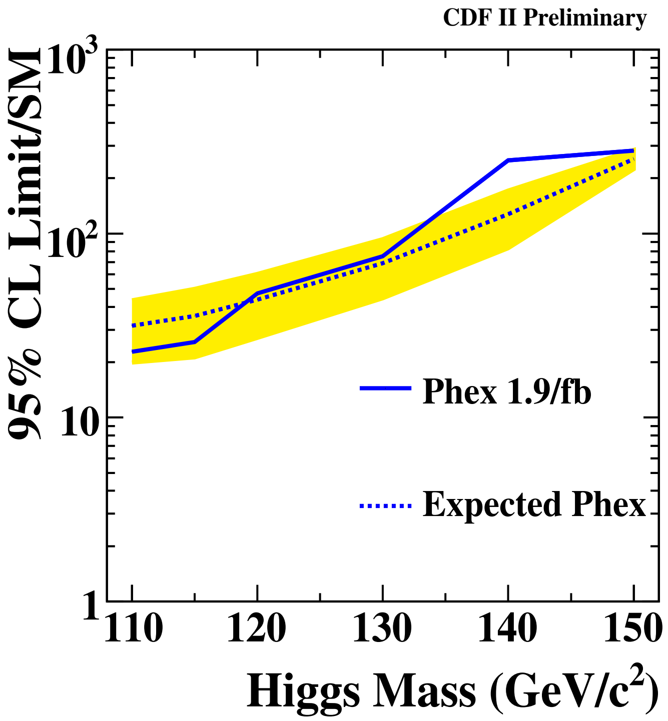

Figure 105: The observed 95% C.L. upper limit combined 1tag and 2tag in single-top (top) and top like (bottom) analyzes

10.8 Combination with the Central Leptons

Figure 106 shows distribution of the combined 95% C.L. upper limit results from one thousand pseudo-experiments. The medium of these distribution is quoted as the central value for the expected limit and the RMS provides the 1 σ uncertainty band. Figure 107 shows observed 95% C.L. limit combined Central and Phex for WH production cross section.

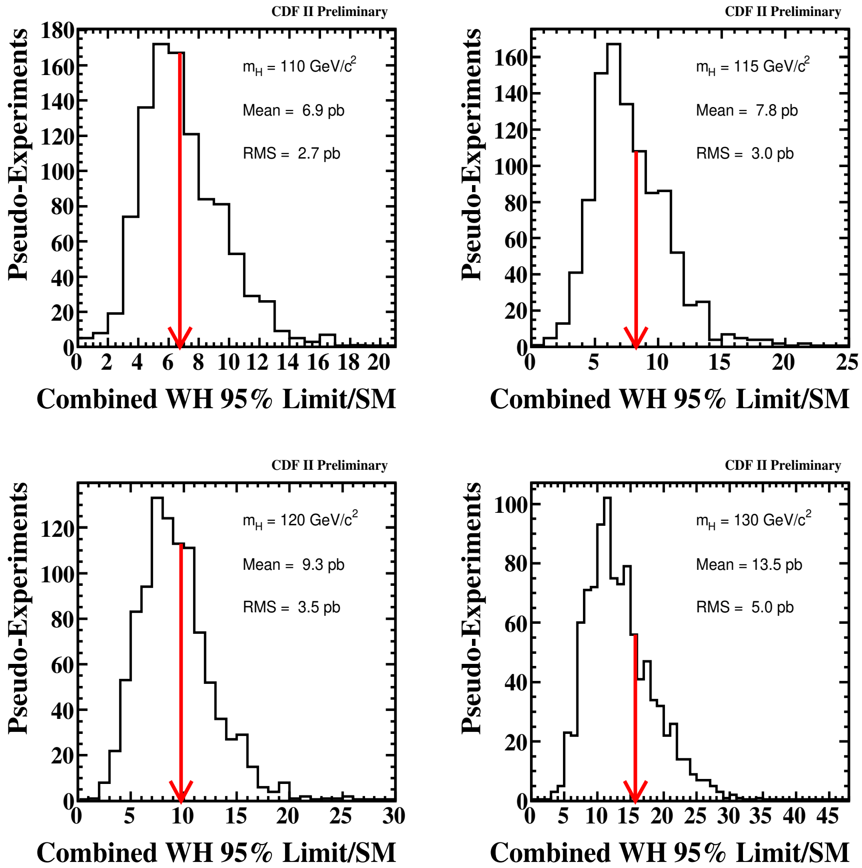

Figure 106: The combined 95% C.L. upper limit result from the one thousand pseudo-experiments. The red arrow means the observed upper limit.

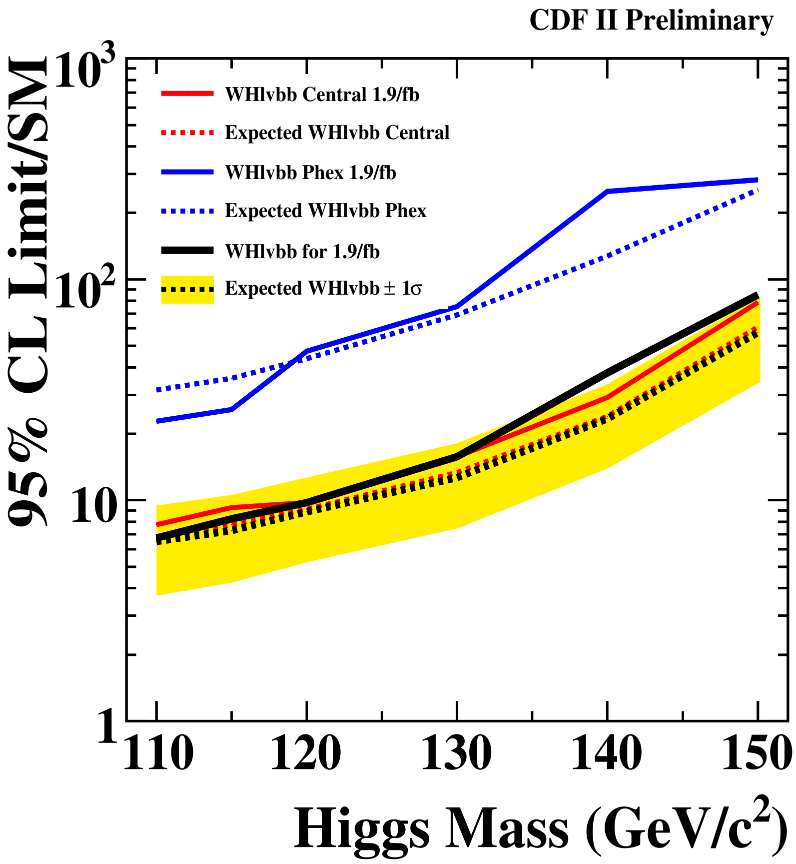

Figure 107: The observed 95% C.L. upper limit combined Central and Phex for WH production cross section.

mH (GeV)	110	115	120	130	140	150
Expected (Mediam)						
Central	6.8	7.8	9.1	13.4	24.0	60.8
Phex	31.6	35.7	43.7	68.9	127.3	254.6
Combined	6.5	7.3	8.9	12.6	23.4	57.6
Observed						
Central	7.8	9.2	9.8	15.8	29.2	78.8
Phex	22.8	25.8	47.2	75.2	250.2	282.8
Combined	6.8	8.2	9.8	15.8	37.8	85.2

Table 30: The combination result of WH Central and Phex.

11 Conclusions

We have presented the results of a search for the Standard Model Higgs boson via associated WH production and decay to $b\bar{b}$. This analysis is studied one SECVTX tagged events and two double btagged events. We find that for the dataset corresponding to integrated luminosity of 1.9fb^{-1} , the observed data for each tagged events agrees with the SM background predictions within the systematic uncertainties. Therefore we set upper limit on the Higgs production cross section using 1tagged and 2tagged events. The observed limit using the neural network output distribution is $\sigma(p\bar{p} \to W^{\pm}H) \times BR(H \to b\bar{b})$ ranging from 1.4pb (for m_h = 110 GeV/c^2) to 0.9pb (for m_h = 150 GeV/c^2) at 95% confidence level.

References

[1] T. Masubuchi et al., “earch for Higgs Boson Production in Association with W Boson with 1.7fb-1”, CDF Note 8916

[2] Frankli, Grinstein, Guimaraes da Costa, Lannon, Schwarz, Sherman and Taffard, “Method 2 Backgrounds for 1.12/fb Lepton+Jets Analysis, CDF Note 8766

[3] H.Bachacou, P.Lujan, M.McFarlane, W.Yao, Advanced Heavy Flavor Tagging Using a Neural Network, CDF Note 7742

[4] Y. Kusakabe et al., “Search for Standard Model Higgs Boson Production in Association with W$^{\pm}$ Boson at CDF with $\int \mathcal{L}dt$ = 695 pb^{-1}, CDF Note 8194

[5] Y. Kusakabe et al., “Search for Standard Model Higgs Boson Production in Association with a W$^{\pm}$ Boson at CDF with $\int \mathcal{L}dt$ = 1.0 fb^{-1}, CDF Note 8355

[6] Franklin, Grinstein Sherman, “Measurement of the Top Pair Cross Section in Lepton+Jets in 1.12/fb, CDF Note 8768

[7] S. Grinstein, D. Sherman, “SecVtx Scale Factors and Mistag Matrices for the 2007 Summer Conferences”, CDF Note 8910

[8] Grintein, Guimaraes da Costa, Shrman, “SecVtx Mistag Asymmetry for Winter 2007”, CDF Note 8626

[9] Ford Garberson, Enrique Palencia, “Jet Probability B-Tag Efficiency Measurement Using Muon Transverse Momemtum for 1.2 fb^{-1} ”, CDF Note 8882

[10] http://www.physics.ucdavis.esu/ conway/research/higgs/higgs.html

[11] http://ncdf70.fnal.gov:8001/PerfIDia/PerfIDia.html

[12] Han, Boisvert, “Trigger Efficiencies for the High Et Central Electron in the Gen6 data”, CDF Note 8629

[13] Hare, Halkiadakis, Spreitzer, “Electron ID Efficiency and Scale Factors for Winter 2007 Analyses”, CDF Note 8614

[14] Grundler, Lovas, Taffard, “High-Pt muons recommended cuts and efficiencies for Winter 2007”, CDF Note 8618

[15] http://www-cdf.fnal.gov/internal/physics/joint_physics/index.html

[16] H. Bachacou, C. Feretti, J. Nielse, W.Yao, “Heavy Flavor contributions to the SECVTX-tagged W+Jets sample” CDF note 7007

[17] J. Efron et al., “Improved search for ZH to llbb in 1 fb-1”, CDF Note 8704.

[18] D. Hirschbühl, J. Lück, Th. Müller, A. Papaikonomou, Th. Peiffer, M. Renz, S. Richter, I. Schall, J. Wagner-Kuhr, W. Wagner, “Search for single top-quark production with neural networks using 1.92 fb-1”, CDF Note 9107

[19] Bo-Young Han, Eva Halkiadakis, “MET PEM trigger efficiency for Pheonix electrons”, CDF Note 7940

[20] D. Hare, E. Halkiadakis, T. Spreitzer, “ Electron ID Efficiency and Scale Factors for Winter 2007 Analyses” CDF Note 8614

[21] Michael Feindt, “A Neural Bayesian Estimator for Conditional Probability Densities”, physics/0402093

[22] T. Chwalek, M. Feindt, D. Hirschbuehl, T. Müller, M. Renz, S. Richter, W. Wagner, “ Documentation of the updated Neural Network b Tagger used for Single-Top Analyses”, CDF Note 8903